

Consequences of cracks on ship structural integrity

An investigation of hull girder ultimate strength and crack propagation on ship structures

Master's Thesis in the International Master's Programme Naval Architecture and Ocean Engineering

DA WU AND QIAOJIAN YE

Department of Shipping and Marine Technology
Division of Marine Technology
CHALMERS UNIVERSITY OF TECHNOLOGY
Göteborg, Sweden 2015
Master's thesis X-15/328

MASTER'S THESIS IN THE INTERNATIONAL MASTER'S PROGRAMME IN
NAVAL ARCHITECTURE AND OCEAN ENGINEERING

Consequences of cracks on ship structural integrity

An investigation of hull girder ultimate strength and crack propagation on ship
structures

DA WU AND QIAOJIAN YE

Department of Shipping and Marine Technology
Division of Marine Technology
CHALMERS UNIVERSITY OF TECHNOLOGY
Göteborg, Sweden 2015

Consequences of cracks on ship structural integrity
An investigation of hull girder ultimate strength and crack propagation on ship
structures
DA WU AND QIAOJIAN YE

© DA WU AND QIAOJIAN YE, 2015

Master's Thesis X-15/328
ISSN 1652-8557
Department of Shipping and Marine Technology
Division of Marine Technology
Chalmers University of Technology
SE-412 96 Göteborg
Sweden
Telephone: + 46 (0)31-772 1000

Cover:
The presence of ultimate strength curve and fracture analysis model with partial results.

Printed by Chalmers Reproservice
Göteborg, Sweden 2015

Consequences of cracks on ship structural integrity

An investigation of hull girder ultimate strength and crack propagation on ship structures

Master's Thesis in the International Master's Programme in Naval Architecture and Ocean Engineering

DA WU AND QIAOJIAN YE

Department of Shipping and Marine Technology

Division of Marine

Chalmers University of Technology

ABSTRACT

The ship structural integrity plays a significant role in ship structural safety and environmental protection. There are four types of limit states in ship design, serviceability limit states (SLS), ultimate limit states (ULS), fatigue limit states (FLS), and accidental limit states (ALS). This thesis will address two of these limit state assessment, namely ULS and FLS.

In the ULS analysis, the incremental iterative approach is applied to estimate the ultimate strength of a ship's hull girder. In this method, some factors which can affect the accuracy and calculation time and are further studied in the project. The analysis for buckling of a deck plate was carried out using both finite element method (FEM) and Common Structure Rules (CSR) for the accuracy and reliability comparison.

For the FLS study the effect of fatigue cracks presence in ships on her structural safety and serviceability is investigated. A great number of survey report the existence of crack on structural components among the commercial ship fleets. Owing to the fact that it is not possible to repair all cracks immediately after they have been identified when the ship is on the sea, it is essential to predict the crack propagation speed under different operation conditions and encountered weather environment. At the same time the reduction of the ultimate strength of the hull girder due to the presentation of crack can be used as a criterion to evaluate the status of the ship's structural safety. Consequently, the approach to solve the problem is divided into two parts, 1) evaluation of the ultimate strength and 2) crack propagation simulation. In the crack propagation simulation part, analytical handbook method, conventional finite element methods and extended finite element methods are used. Besides, both two dimensional and three dimensional geometries were considered. The stress intensity factors were extracted and used in Paris law to simulate the crack growth speed in the FRANC2D / 3D analysis; likewise the direct cyclic approach in ABAQUS was used in XFEM based fatigue analysis to plot the cycle number versus crack length curve. The results show that the crack propagation speed in 2-D case is faster than 3-D case under the same loads. If making a comparison between FRANC3D and ABAQUS analysis, the XFEM gives a more realistic result with much slower crack propagation speed.

On this account, the results can be used as a reference for simplified the problem and provide a quantification of difference between different crack simulation methods in solving marine structural integrity problems. What is more, it provides a route to build a fast crack propagation prediction method in ship structures.

Key words: buckling; crack propagation; FEM; fracture mechanics; progressive collapse analysis; ultimate strength; XFEM

Contents

ABSTRACT	I
CONTENTS	III
PREFACE	V
NOTATIONS	VII
1 INTRODUCTION	1
1.1 Background	1
1.2 Objectives	3
1.3 Limitations	3
1.4 Thesis outline	3
2 ULTIMATE STRENGTH	5
2.1 Methods of ultimate strength analysis	5
2.2 Incremental iterative approach	6
2.2.1 Calculation procedure	6
2.2.2 Assumptions	9
2.2.3 Definition of structure elements	9
2.2.4 Factors to consider in buckling analysis	10
3 FRACTURE MECHANICS THEORY AND METHODS	15
3.1 Fracture mechanics literature review	15
3.2 Fatigue crack growth models	18
3.2.1 Crack growth direction	19
3.2.2 Crack growth magnitude	20
3.3 Finite element methods (FEM)	21
3.3.1 Finite Elements with Quarter Points (FEQP) method	21
3.3.2 Mixed mode critical energy release rate	22
3.3.3 Virtual Crack Closure Technique (VCCT)	22
3.3.4 Extended finite element method (XFEM)	23
3.3.5 Phantom node approach	25
3.3.6 Level set method	25
4 ULTIMATE STRENGTH AND BUCKLING ANALYSIS	29
4.1 Ultimate strength analysis	29
4.1.1 Types of Elements	30
4.1.2 Load-end shortening curve	30
4.1.3 Result of ultimate strength	37
4.2 Buckling analysis	39
4.2.1 Boundary conditions and Load	39
4.2.2 Result of buckling analysis	42

5	CRACK PROPAGATION ESTIMATION IN FRANC2D/3D	45
5.1	Introduction of FRANC2D and FRANC3D	45
5.2	Estimation in FRANC2D	45
5.2.1	Analysis procedures and models	45
5.2.2	Results in FRANC2D analysis	48
5.3	Estimation in FRANC3D	50
5.3.1	Analysis procedures and models	50
5.3.2	Results in FRANC3D analysis	54
6	CRACK PROPAGATION ESTIMATION IN ABAQUS (XFEM)	61
6.1	Analysis procedures and models	61
6.2	Results in ABAQUS analysis	67
7	CONCLUSION	73
8	FUTURE WORKS	77
	REFERENCES	78
	APPENDIX A	81
	APPENDIX B	92

Preface

This thesis is a part of the requirements for the master's degree in Naval Architecture and Ocean Engineering at Chalmers University of Technology, Göteborg, and has been carried out at the Division of Marine Technology, Department of Shipping and Marine Technology, Chalmers University of Technology between January and June of 2015.

We are very grateful to all the gentlemen who supported and helped us on this project. We would like to express our gratitude to our supervisor, Dr. Wengang Mao, for his technical guidance, availability to answer questions, and patience throughout our graduation. Without his support, this would not have been possible.

We also want to thank our co-supervisor, Dr. Jonas Ringsberg, whose technical expertise in marine structure is invaluable.

In addition, we would like to show our appreciation to PhD. student, Shunhan Yang, for her assistance on ANSYS.

Thanks to Omar Ibrahim in Process Optimization Corporation for his support on the FRANC2D/3D software.

Göteborg June 2015

Da Wu, Qiaojian Ye

Notations

β_E	Plating slenderness ratio corresponding to $\bar{\epsilon}$
δ_{ij}	Kronecker delta
$\bar{\epsilon}$	Relative strain ratio
σ_0	Specified minimum yield point of material
σ_{C1}	Beam-column buckling stress of longitudinal corresponding to $\bar{\epsilon}$
σ_{C2}	Torsional-flexural buckling stress of longitudinal corresponding to $\bar{\epsilon}$
σ_{C3}	Local buckling stress of longitudinal corresponding to $\bar{\epsilon}$
σ_{CA}	Critical buckling stress of longitudinal in axial compression
σ_{CA}^E	Critical buckling stress of longitudinal corresponding to $\bar{\epsilon}$
σ_{CL}^E	Critical local buckling stress of a stiffener corresponding to $\bar{\epsilon}$
σ_{CP}^E	Critical buckling strength of an unstiffened plate corresponding to $\bar{\epsilon}$
σ_{CT}	Critical torsional-flexural buckling stress
σ_{CT}^E	Critical torsional-flexural buckling stress of a stiffener corresponding to $\bar{\epsilon}$
$\sigma_{E(C)}$	Euler's buckling stress of longitudinal
σ_{EF}	Euler's buckling stress of flange
σ_{EL}	Elastic local buckling stress, which is the smaller value of σ_{EW} and σ_{EF}
σ_{ET}	Elastic torsional-flexural buckling stress
σ_{EW}	Euler's buckling stress of web
σ_{Ex}	Elastic buckling stress of plating in longitudinal direction
σ_{UP}^E	Ultimate strength of an unstiffened plate corresponding to $\bar{\epsilon}$
σ_{Ux}	Ultimate strength in the longitudinal direction
σ_{cL}	Critical buckling stress for associated plating corresponding to n-half waves
ΔK	Stress intensity range
$\overline{\Delta K}$	Equivalent stress intensity range
Γ	Contour surrounding the crack tip
Γ	Warping constant
\mathcal{G}	Linear elastic energy release rate
β	Plating slenderness ratio
ν	Poisson's ratio
ω	Angular frequency
ϕ, ψ	Level set functions
A_e	Effective sectional area of longitudinal
A_s	Sectional area of longitudinal
E	Young's modulus
F	Force
G	Shear modulus
$\mathcal{G}_I, \mathcal{G}_{II}, \mathcal{G}_{III}$	Mode dependent energy release rates
$\mathcal{G}_{Ic}, \mathcal{G}_{IIc}, \mathcal{G}_{IIIc}$	Mode dependent critical energy release rates
\mathcal{G}_c	Critical linear elastic energy release rate
\mathcal{G}_{pl}	Energy release rate at Paris limit
\mathcal{G}_{th}	Threshold energy release rate
K	Stress intensity factor (in Section 3)

K	St. Venant torsion constant (in Section 4)
K_I, K_{II}, K_{III}	Mode dependent stress intensity factors
$K_{Ic}, K_{IIc}, K_{IIIc}$	Mode dependent stress intensity factors
K_c	Critical stress intensity factor
K_{max}, K_{min}	Maximum and minimum stress intensity factor
K_{th}	Threshold stress intensity factor
N	Fatigue cycles
P_r	Proportional linear elastic limit of structure, 0.6 for steel
a	Crack length
a_i	Initial half crack length
c_1, c_2, c_3, c_4	Coefficients for ABAQUS' crack growth model
l	Length of plate
r, θ	Axes in a polar coordinate system
s	Longitudinal spacing
s_e	Effective width of plating
s_e^E	Effective width of plating corresponding to $\bar{\epsilon}$
t	Plate thickness
ALS	Accidental Limit States
CAE	ABAQUS' Complete ABAQUS Environment
FE	Finite Element
FEM	Finite Element Method
FEQP	Finite Elements with Quarter Points
FLS	Fatigue Limit States
INP	ABAQUS' analysis input file extension
LEFM	Linear Elastic Fracture Mechanics
LSM	Level Set Method
MD	Maximum Difference
MERR	Maximum Energy Release Rate
MTS	Maximum Tangential Stress
NA	Neutral Axis
ODB	ABAQUS' output database file extension
RMSD	Root Mean Square Difference
SIF	Stress Intensity Factor
SLS	Serviceability Limit States
TMCP	Thermo-Mechanically Controlled Processed
ULS	Ultimate Limit States
VCCT	Virtual Crack Closure Technique
XFEM	eXtended Finite Element Method

1 Introduction

1.1 Background

There are four types of limit states in ship design, serviceability limit states (SLS), ultimate limit states (ULS), fatigue limit states (FLS), and accidental limit states (ALS). These four limit states are key factors used to keep the ship structure in safe status (only ULS and FLS is considered in this thesis). The ship structural integrity analysis is essential in a ship's design stage to ensure the ship structural safety, which will be indirectly benefit to sea environmental protection. For instance, the large oil tanker, the failure of hull structure could cause serious environmental pollution and ecological damage. According to the statistics data from ITOPF (International Tanker Owners Pollution Federation) (ITOPF, 2015), the oil spill pollution can be sorted by the spilled oil quantity, less than 7 ton, between 7 to 700 ton and greater than 700 ton. The ITOPF classifies three spill types at different operation conditions. When the spilled oil quantity is less than 7 ton, there are 12% of the accidents are result from the structure failure in totally 7864 accidents. In contrast the spilled oil quantity that is larger than 7 but less than 700 ton, 53% of the totally 1355 accidents are caused by structure failure. However, when the spilled oil exceed 700 ton, 75% of the accidents are caused by the damage of ship structural integrity. On that account, compared with other factors which can lead to oil spill, the failure of ship structural integrity is the most important reason. Because the structure failure always makes much more serious consequences, and it is deserved to pay more attention in the ship structural integrity studies.

For some ships with serious cracks observed onboard, ports authorities may have great concerns to approve the entrances of such ships due to the associated risks connected with the cracks. These ships need to be repaired in port, but nobody knows when and where the ship will collapse due to the crack and how the crack would influent the ultimate strength of ship. As a common sense, ships always take thousands tons of fuel oil, lubricating oil and million tons of cargo oil, which would lead to serious pollution and environmental issues, especially in a narrow area around ports. For port agencies, they are unwilling to undertake the risk of pollution. However, ship owners hope to have a place to repair the fleets as soon as possible. So there is an obvious contradiction to be resolved.

To solve this contradiction, two things need to be taken into account. Firstly, the ultimate strength of ship structure need to be estimated. That is the application of ULS. It is necessary to estimate the ultimate strength before crack happening, and it provides the possibility to evaluate the strength reduction due to cracks. Secondly, the crack propagation need to be analyzed to investigate the influence of cracks.

The hull girder strength is the most important strength in a ship structure. Besides the hull girder ultimate strength is related to the relationship between applied bending moment and corresponding curvature as shown in Figure 1.1. It is a value that can prove the ship structure is strong enough to take impact bending load in certain weather condition. In design processes, the linear elastic analysis is simple and fast, but it only shows the results in a limit stress range which cannot present the real material behavior and geometrical characteristics of ship structures. So an alternative method is applied instead to estimate the ultimate strength of ship structures in this thesis project.

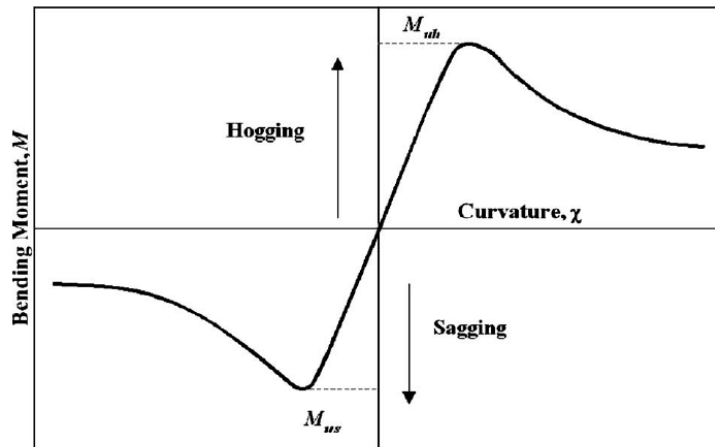


Figure 1.1 General relationship between bending moment and curvature (Sun et al, 2005).

The aforementioned ULS is only considered under the intact structure conditions. However it has been found that there were, on average, 86 structural cracks per ship at any inspection on the commercial ships in the United States in 1980s (Jordan and Cochran, 1978). The existence of fatigue cracks in structural components plays a significant role of a ship's safety.

An estimation on the costs of failure due to crack and fracture has been done in 1983, concluding that \$119 billion per year in 1982 dollars. Except for the loss of financial, the loss of human life and injury due to the fracture failure is unacceptable also. Although the stress in the structure is below the yielding or failure stress level, the crack can grow catastrophically if the length of the crack approaches to a critical value (Roylance, 2001). This phenomenon becomes common when the high-strength materials are used, owing to cracks can modify the local stress to an area that the elastic analysis cannot cover. Since 1950s the high-strength steel has been widely used in ship building, especially in these couple of decades, the invention of Thermo-Mechanically Controlled Processed (TMCP) highly reduces the cost and threshold of facilitating the high-strength steel usage. Nevertheless, in recent decades, many ships have been found crack and fracture accidents within two years after delivered from yards. Moreover, some of these tragedy happened in a calm water harbor. The survey reports show that these crack initialized at the corner of hatch coaming, then propagated along the main deck and end around the water line through the strake plates. When the vessels are navigating on the sea, the loads from wave and cargo tend to do a cyclic change, the fatigue and fracture problems then are popped out and cannot be ignored. Considering the whole ship consists with thousands of structural components, which will withstand aforementioned loads, any imperfection of material from the steel mill, the inappropriate fabrication from yards and the residual stress due to assembling and welding will be zoomed out dramatically on the whole vessel. Once cracks initialized, before being found out in the regular survey, they must will propagate under the cyclic loading. In order to estimate the safety window of the structure strength capability, a time estimation should be carried out before the catastrophe happens. The fracture part of this thesis discussed herein is designed to give a judgment on the way to simulate the crack propagation speed based on the current existing commercial software programs.

1.2 Objectives

The overall objective of the thesis project is to establish a formal methodological procedure for structural integrity analysis of marine structures. Here it is referred to the ultimate strength assessment and crack propagation predication. To achieve such an ambition objective in a so short time period, the thesis project has been refined to carry out the following tasks.

First for the ultimate assessment, though finite element method is accurate and intuitive, it is time-consuming in modelling and calculation. Incremental iterative approach can save a lot of time. MATLAB is applied to deduce the relationship between bending moment and curvature using incremental iterative approach. Due to ultimate strength has close relation with buckling strength, a buckling model should be analyzed to prove the load-end shortening curve has feasibility in real condition.

The other important focus is to address the reliability and uncertainties of various methods which are state-of-the-art and widely applied for fatigue crack propagation. As the second part, from the fracture mechanics point of view, the primary goals of this thesis are to model crack propagation and estimate the crack growth speed on a certain ship structure component. Different methods and codes designed to predict the crack growth speed on both 2-D and 3-D problems are implemented in this thesis. By incorporating with different fracture mechanics code programs, a benchmark will be given following with an optimized procedure to analysis the fatigue fracture life on the naval structure.

1.3 Limitations

In the ultimate strength calculation, there is only one mid-ship cross section applied in this analysis, consequently the ultimate strength of one cross section cannot represent the entire ship structure. The material in this analysis is elasto-plastic behavior and the section is regarded as a soft region between two stiffened adjacent transverse frames. To simplify the calculation, the cross section of study region remains plane during the analysis when an incremental bending moment was applied on the structure. All the calculation is based on new build ship, in other word it means if some old ship with imperfection in structure, the feasibility of all the methods need to be checked in the future work.

The fracture analysis in this thesis focuses on the crack propagation and limited in the linear elastic fracture mechanics. Basically a pure Mode I dominated condition is assumed herein. The homogeneous, isotropic material is used in the thesis. The Paris law model is selected with the parameters lies on the standards BS 7910 (BSI, 2000) to simulate the crack growth rates.

1.4 Thesis outline

This thesis begins in Chapter 2 and 3 with a review of fundamental knowledge – hull girder ultimate strength and fracture mechanics. Chapter 4 includes the analysis of ultimate strength and buckling. In ultimate strength analysis, it includes the relationship between bending moment and curvature, as well as the relationship between neutral axis position and curvature. In buckling analysis, the load-end shortening curve is proved. Chapter 5 demonstrates the procedure to model the crack in FRANC2D and

FRANC3D. Then the fracture propagation will be implement in ABAQUS without user defined subroutines and compared to the aforementioned methods in Chapter 6. Finally, conclusions are made in Chapter 7, following with Chapter 8 where an introduction about the future works will be given. Additional data, result, and codes can be found in the Appendices.

2 Ultimate strength

The hull girder strength is the most basic strength in a ship structure. The hull girder ultimate strength is related to the relationship between applied bending moment and corresponding curvature. The maximum bending moment capacity shows the hull girder ultimate strength (Wang et al, 2011). There are several different methodologies to determine the hull girder ultimate strength capacity, such as nonlinear finite element method, Smith's method, idealized structure unit method and incremental iterative approach. All of them are able to perform progressive collapse analysis. In this thesis, the incremental iterative approach is applied to calculate the ultimate strength.

2.1 Methods of ultimate strength analysis

There are many different methods existed in the industry practice for the ultimate strength analysis of ship structure, seen as Fig.2.1. Caldwell is the first person who started to calculate the ultimate hull girder strength (Yao, 2003). He regarded no strength reduction beyond the ultimate strength in yielding and buckling behavior. In his method, stiffened panels were idealized with equivalent thickness. He took the influence of buckling into consideration when he calculated the fully plastic bending moment of the cross-section. The yielding stress was multiplied by a strength reduction factor without an accurate magnitude at that time when calculate the buckled part. But in this method, the maximum capacity is overestimated due to the uncertain reduction factor.

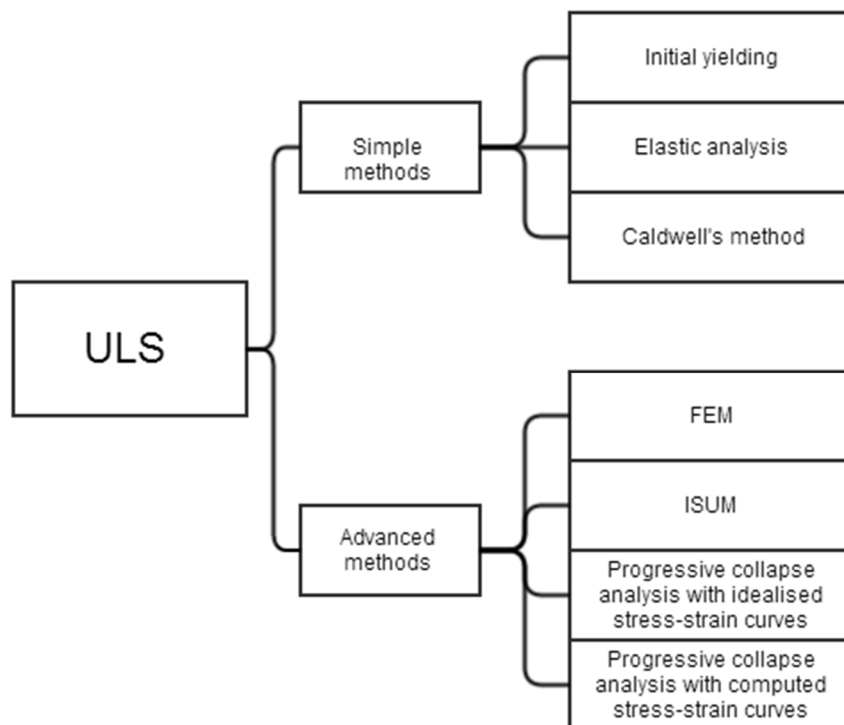


Figure 2.1 Different methods for calculating the ultimate strength.

After Caldwell, the strength reduction factor was determined by more accurate method, such as Smith's method. It is an advanced method compared with Caldwell's method. This method divides the cross-section into individual stiffener and plating elements.

The assumption is that all the elements follow the beam theory, a plane cross-section remains plane. The behavior of elements follows the average stress-average strain relationship, without interaction between adjacent elements. The bending moment is applied with respect to instantaneous neutral axis of the cross-section at every incremental step so that no axial force exist. Although the Smith's method is an advanced method, the accuracy of the results depends on the average stress-average strain relationship.

Another alternative method to perform progressive collapse analysis is the idealized structure unit method (ISUM), which was suggested by Ueda (Yao, 2003). It is based on a matrix formulation, which is similar to the conventional finite element analysis (Wang et al, 2011). However, in this method, the definitions of elements are particular. In ISUM modeling, support members (or beam-columns), rectangular plates and stiffened panels are regarded as ISUM units. These structure members are at same size scale as themselves, shown as in Fig.2.2.

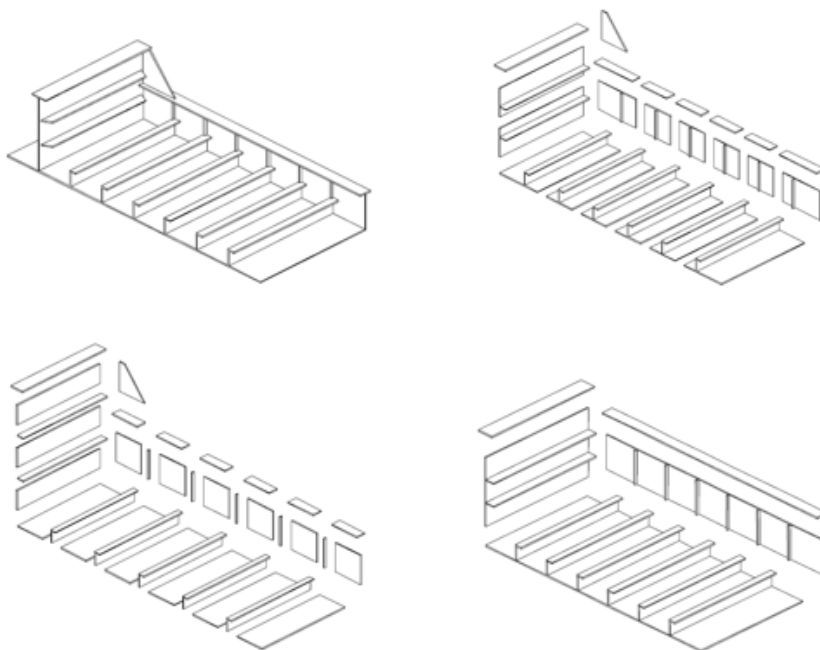


Figure 2.2 Four main types of structure elements definition in ISUM method (Paik et al, 2002).

Although FEM analysis is flexible and convenience in modeling structures, it is still complicated and time-consuming. Another widely accepted method is the Incremental iterative approach, which is based on Smith method described by Wang et al (2011). This method simplified the complex calculation and save a lot of time in the estimation of ultimate hull girder strength. It has some similarities with the two aforementioned methods and it will be applied in this thesis to estimate the ultimate strength of ship structure.

2.2 Incremental iterative approach

2.2.1 Calculation procedure

Firstly, it is required to calculate the initial curvature when one element or some elements start to yield and buckle. The initial curvature value is applied to start the

iterative calculation with add an incremental value of curvature. The step size Δk of the curvature should be $k_F/300$, where k_F is the expected maximum required curvature. In some conditions, in order to simplify the calculation, the initial curvature in the first step can be also taken as Δk . The initial neutral axis position should be determined at the same time, as well as the distance from each element to this neutral axis.

$$\chi = \chi + \Delta k \quad (2.1)$$

The strain of each structural element can be calculated by the product of curvature and distance at recent NA.

$$\varepsilon_i = \chi \cdot z_i \quad (2.2)$$

The stress relevant to the strain can be calculated through the relationship between stress and strain in $\sigma - \varepsilon$ load-end shortening curve, which will be derived in 4.1.2.

These stress values are used in the calculation of the total force on the cross-section. The stress σ_i is positive when the element under compression, or negative instead in tension condition. If the neutral axis is at a correct position, the force value should be no larger than δ , which is very close to 0. And the value of δ is a limitation of the accuracy of calculation.

$$|\sum \sigma_i \cdot A_i| \leq \delta \quad (2.3)$$

Then the corresponding bending moment can be calculated if the force value satisfies the criterion. Besides the relationship between curvature and bending moment can be established as Equation 2.4.

$$M = \sum \sigma_i \cdot A_i \cdot z_i \quad (2.4)$$

In contrast, if the force value exceeds the critical value δ , the position of neutral axis need to be adjusted. In hogging condition, the structural elements above neutral axis are under tension and the structural elements beneath neutral axis are under compression. In other word, the stress value is positive in upper elements and negative in lower elements. If the force value is positive, the position of neutral axis should be move upwards, otherwise downwards and vice versa in sagging condition.

The incremental step size for the neutral axis adjustment should be no larger than 0.0001 m. Although the smaller value will give accurate results, it takes longer time to iterate. It is necessary to repeat the force calculation with the updated position of neutral axis until the equilibrium is satisfied. After recording the bending moment value corresponding to the curvature, add an increment of curvature to find out next corresponding bending moment. Figure 2.3 illustrates the flow chart of this method.

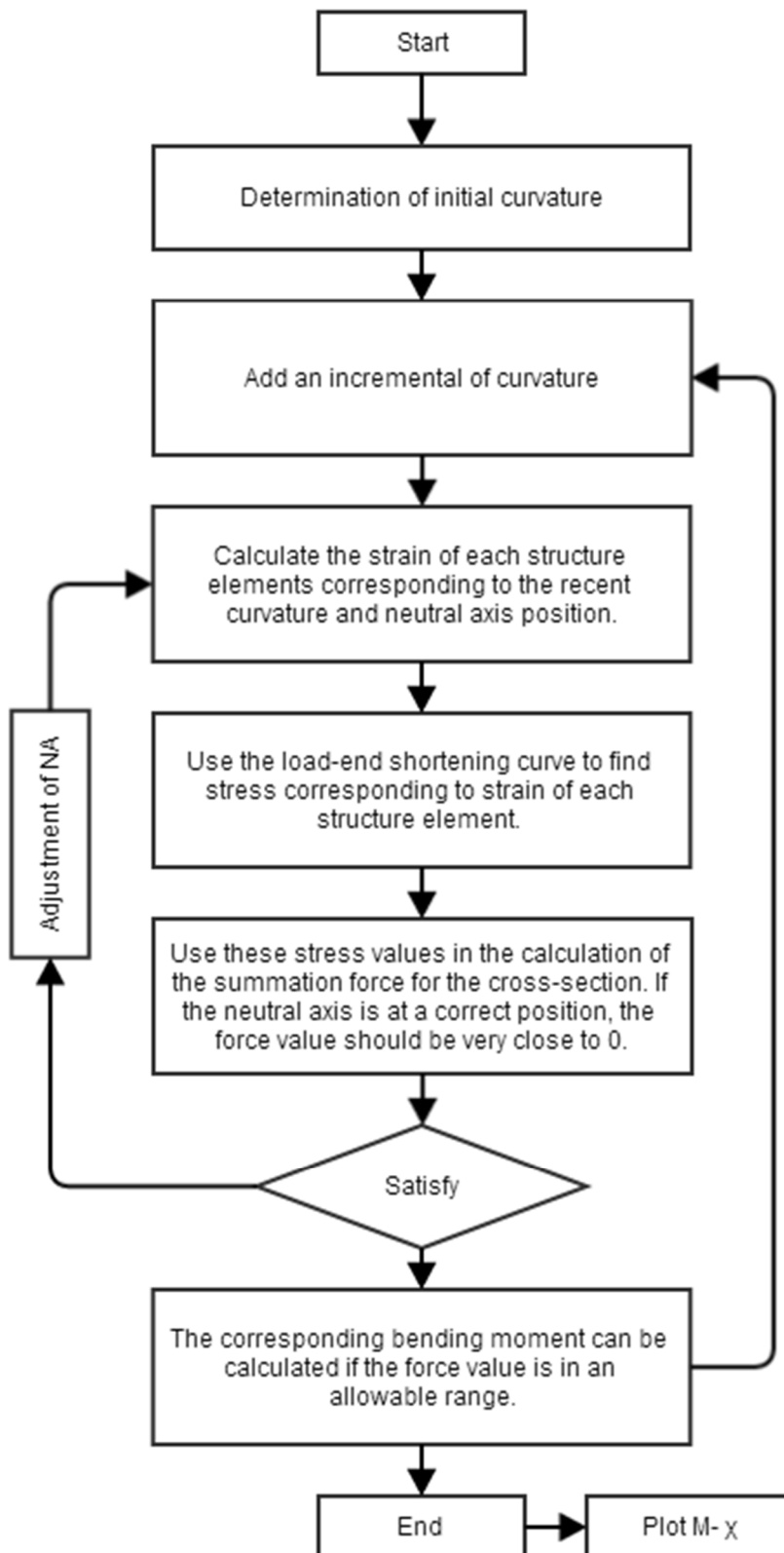


Figure 2.3 Calculation procedure for incremental iterative approach.

2.2.2 Assumptions

When Incremental Iterative Approach is applied, following assumptions and limitations need to be set.

1. The section studied in the ultimate strength calculation is regarded as a soft region between two stiffened adjacent transverse frames, shown in Figure 2.4.
2. The moment of inertia of transvers main support members must satisfy Equation 2.5.

$$I_G/i_0 \geq 0.2 \left(\frac{B}{l}\right)^3 \left(\frac{B}{s}\right) \quad (2.5)$$

3. The cross section of study region must remain plane during the analysis when an incremental bending moment is applied on the structure.
4. The material behavior of steel in the structure is regarded as elasto-plastic. The stress-strain relationship can be found in ‘load-end shortening curve’ in section 4.1.2.
5. The stress in each element corresponding to each curvature can be obtain in load-end shortening curve. Due to there are more than one type of buckling mode, a minimum value is selected for the ultimate strength calculation at a same strain or curvature.
6. The interaction between each elements is neglected.

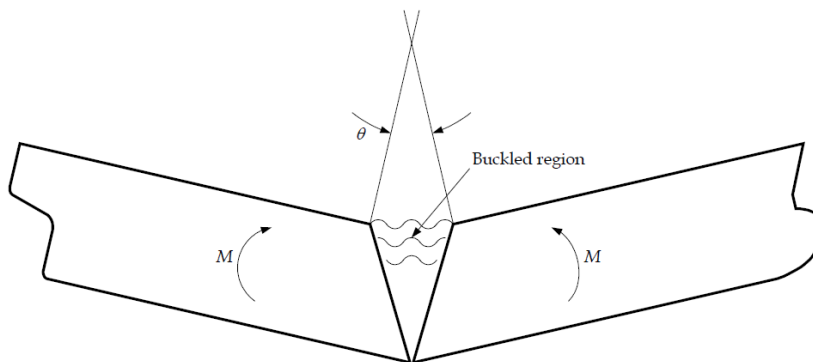
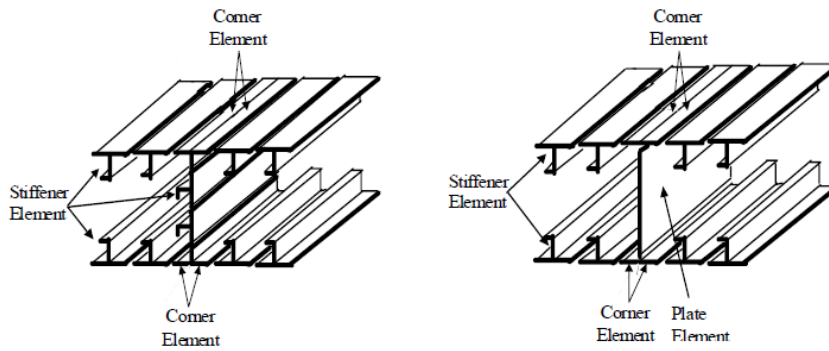


Figure 2.4 A soft region between two stiffened adjacent transverse frames (ABS, 2012).

2.2.3 Definition of structure elements

It is similar to Smith's method and ISUM, the cross-section need to be divided into different structure elements. There are three main types, plate elements, stiffened elements and cornered elements. Examples of individual structure are illustrated in Figure 2.5.



Girder with web stiffeners

Girder without web stiffeners

Figure 2.5 Definition of structure elements (Sun and Wang, 2005).

2.2.4 Factors to consider in buckling analysis

Buckling is a condition that structure starts to collapse and strength reduction. In section 4.1.2, the load-end shortening curves show the relationship of stress-strain. During compression, when the load exceed a limitation, relationship of stress-strain is non-linear, which means the occurrence of buckling. The limitation of load leading to buckling is the buckling capacity. In most condition, buckling capacity, which is the foundation of ultimate strength capacity estimation, is lower than the material yielding stress. The ultimate strength will appear when the summation of each element stress gets a peak.

In buckling analysis, there are several factors, which relate to the accuracy of result, need to be considered. Material behavior, geometrical imperfections, boundary conditions and simultaneous acting loads are included.

2.2.4.1 Material behavior

In buckling analysis, material should be regarded as inelastic non-linear behavior material (ABS, 2012). Because there is no buckling in elastic and elastic-perfectly plastic material, which is illustrated in the material behaviors Figure 2.6. To gain a result close to actual behavior, the element material was regarded as bi-linear isotropic elasto-plastic material. The material properties include material yield strength, Young's modules, and tangent modules. For high tensile strength steels with plastic behavior, the tangent modules is 1000Mpa.

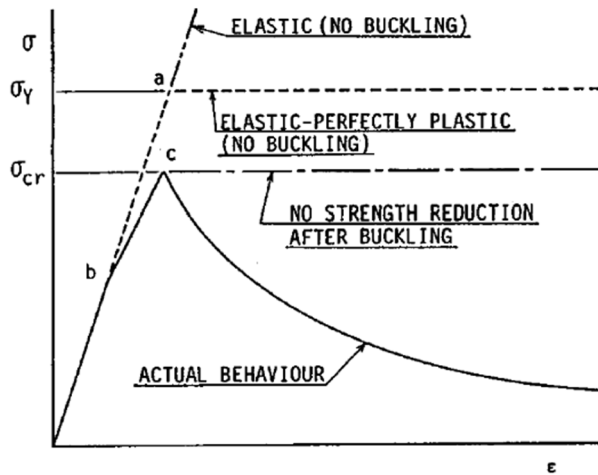


Figure 2.6 There is no buckling in elastic and elastic-perfectly plastic material (Yao, 2003).

2.2.4.2 Geometrical imperfections

The geometrical imperfections can be also called initial deflections. It is necessary to be consider in buckling analysis. The initial deflection has two main properties need to be determined before the buckling analysis, which are shape and maximum value of initial deflection.

The shape of initial deflection is determined through the most critical failure mode. In general, the lowest buckling eigen-modes will be applied (ABS, 2012). However, as a result of combination loads and the slenderness of plate, the critical failure mode would be one of buckling eigen-modes different from the lowest one, shown in Figure 2.7.

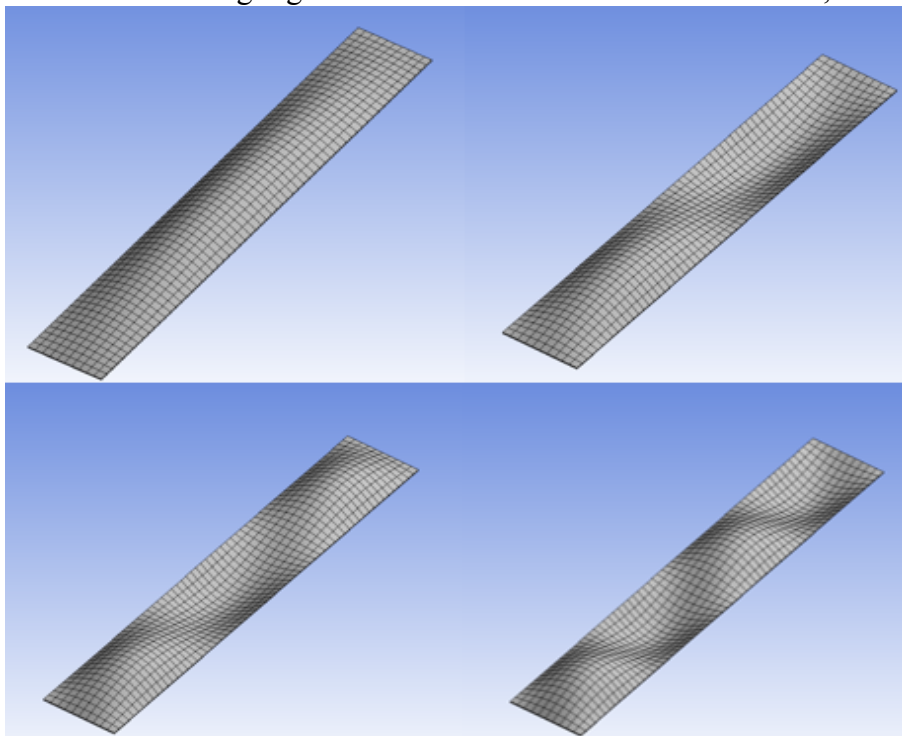


Figure 2.7 Different buckling eigenvalue modes.

The maximum value of initial deflections can be found in IACS Shipbuilding and Quality Repair Standard (Paik et al, 2008). In order to simplify the analysis, the

maximum value of initial deflections and total deflections can be calculated by the following equation:

$$\omega_0 = \frac{b}{200} \quad (2.6)$$

$$\omega = \omega_0 \sin\left(\frac{m\pi x}{a}\right) \sin\left(\frac{\pi y}{b}\right) \quad (2.7)$$

where a is the length of plate, b is the space of longitudinal, ω_0 is the maximum value of initial deflections, m is half wave numbers. In any condition, the initial deflection cannot be greater than the maximum value.

2.2.4.3 Plate model

There are two main types of plate models in the analysis, which are one-bay and two-bay plate models (Paik et al, 2008). In one-bay plate model, in Figure 2.8, the length is the space between transvers floors and width is the space between stiffeners. For two-bay plate model, the analysis region is the area inside the red dash line in Figure 2.9. The size of the plate is $(1/2+1+1/2)$ times the size of one-bay plate.

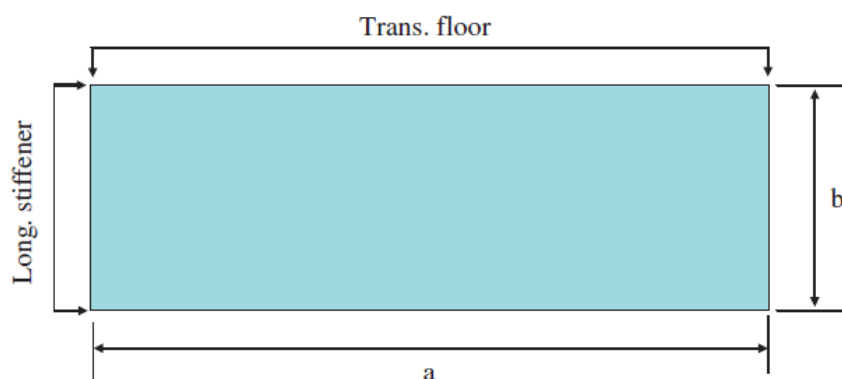


Figure 2.8 One-bay plate model (Paik et al, 2008).

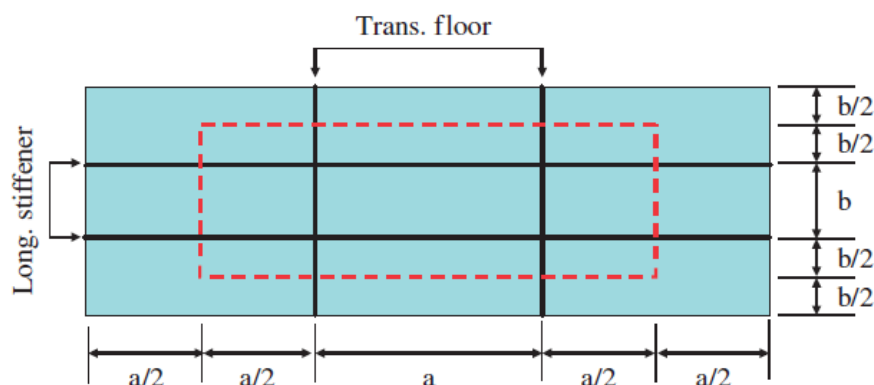


Figure 2.9 Two-bay plate model (Paik et al, 2008).

2.2.4.4 Boundary conditions

The boundary conditions can represent the actual response of the structures (ABS, 2012). There are two main types of boundary conditions, free edge plate and continuous plate. Such as the bottom and deck plate, the edges should be regarded as simply support or clamped, but can be free to move in-plane and forced to remain straight. However, some other edges of structure element such as stringer web panel should be considered as free. The rotational restraint is only considered in the analysis involving the interactive effects between plate and stiffener.

Free edge plate condition is for the structure that has weak in-plane support along one or more edges. While continuous plate condition is for the structure that has in-plane support around the entire structure. The panel edges in both of them perpendicular to the stiffeners are regarded as simply supported and the edges which are parallel to stiffeners should have rotational support. Furthermore, free edges in both of them can move inward. However, in free edge plate condition, if the ends of stiffeners are attached to adjacent structure, they should be regarded as supported sideways, otherwise they are simply supported. In continuous plate condition, the ends of stiffeners should be regarded as supported sideways.

For unstiffened plate, panel edges are simply supported. Free edges are free to move in-plane and continuous should remain straight.

2.2.4.5 Acting loads

The acting loads in the analysis includes biaxial in-plane compression and lateral pressure (ABS, 2012). In software analysis, to ensure the stability of plate, the axial load should act on one edge. The opposite edge to the acting load should be no translation. The lateral pressure should be applied first to create the deformed shape. Then the lateral pressure should be kept constant to enforce deflections in different patterns. Finally, to realize the geometrical imperfection, a very small force should be applied on the plate surface. Otherwise, there will be no buckling take place on the plate.

2.2.4.6 Element size of nonlinear finite element models

The element size of nonlinear finite element model should be small enough to describe the buckling deflections accurately (ABS, 2012). In general, the element size depends on the complexity of the geometry, acting loads and the element types. In any condition, the maximum size of element should be one fifth of a half-buckling wave length.

3 Fracture mechanics theory and methods

This chapter introduces the fundamental knowledge on the fracture mechanics used for crack propagation prediction in this thesis. It starts with the literature reviewing of linear elastic fracture mechanics then the theories about the mixed crack mode and fatigue crack growth modes will be explained. The finite element method, both of conventional and extended FE methods, are also described later.

3.1 Fracture mechanics literature review

Fracture mechanics is the field of solid mechanics that deals with the behavior of cracked bodies subjected to stresses and strains. In order to investigate the material behavior during fracture, two approaches can be considered: 1) stress intensity approach and 2) energy-balance approach. The first approach states the stress state in vicinity of the crack tip directly, and has been widely used in the engineering solutions (Roylance, 2001). Three types of cracks, mode I, II and III, have been decided by literature as shown in Figure 3.1.

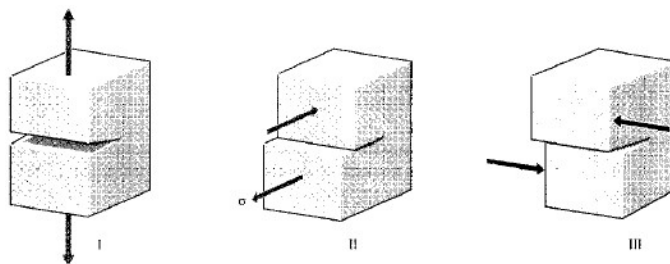


Figure 3.1 The crack modes I) Mode I, II) Mode II and III) Mode III (Roylance, 2001).

Mode I is a normal-opening mode, while mode II and III are shear sliding modes. K_I , K_{II} and K_{III} are the parameters known as the stress intensity factor. The I, II and III subscripts denote the crack opening modes. These three factors demonstrate the stress states near the crack tip. The factor $r^{1/2}$, in Equation 3.2, represents the singularity of the stress distribution in vicinity of the crack tip; the stress rises up to infinity when the r approaches to zero. Likewise the angular θ is another dependence. The factor K is in terms of the dependence on the specimen geometry F , far field applied stress σ and the crack length a , as shown in Equation 3.1. The critical stress intensity factor, K_{IC} , argues that the material can sustain crack tip stresses. The related failure stress, σ_f , can be expressed by crack length a and the fracture toughness as Equation 3.3 shown. The stress intensity factor is used as a measurement in the linear elastic fracture mechanics (LEFM), which assumes small deformations and minimal yielding around the crack tip.

$$K = F\sigma\sqrt{\pi a} \quad (3.1)$$

$$\begin{aligned} \sigma_x &= \frac{K_I}{\sqrt{2\pi r}} \cos \frac{\theta}{2} \left(1 - \sin \frac{\theta}{2} \sin \frac{3\theta}{2} \right) + \dots \\ \sigma_y &= \frac{K_I}{\sqrt{2\pi r}} \cos \frac{\theta}{2} \left(+ \sin \frac{\theta}{2} \sin \frac{3\theta}{2} \right) + \dots \end{aligned} \quad (3.2)$$

$$\begin{aligned} \tau_{xy} &= \frac{K_I}{\sqrt{2\pi r}} \cos \frac{\theta}{2} \cos \frac{3\theta}{2} \sin \frac{\theta}{2} \dots \\ \sigma_f &= \frac{K_{IC}}{\alpha\sqrt{\pi a}} \end{aligned} \quad (3.3)$$

An alternative method based on energy-balance approach provides the insight to the fracture process. As aforementioned, the stresses approach infinity at the perfectly sharp crack, even when the applied loads is small. However, the physical observation shows that the material generally trends to blunt the crack tip. Griffith (1920), who was aware of Inglis' work on developing a fundamental approach to predicting fracture strengths, suggested an energy-balance approach instead of limiting at the crack-tip stresses directly.

The strain energy will release if the crack grows to a certain length a then a area of materials that are conjunction with the free surfaces will unload, as shown in Figure 3.2. According to the Inglis solution, Griffith proposed the solution how to calculate the released energy.

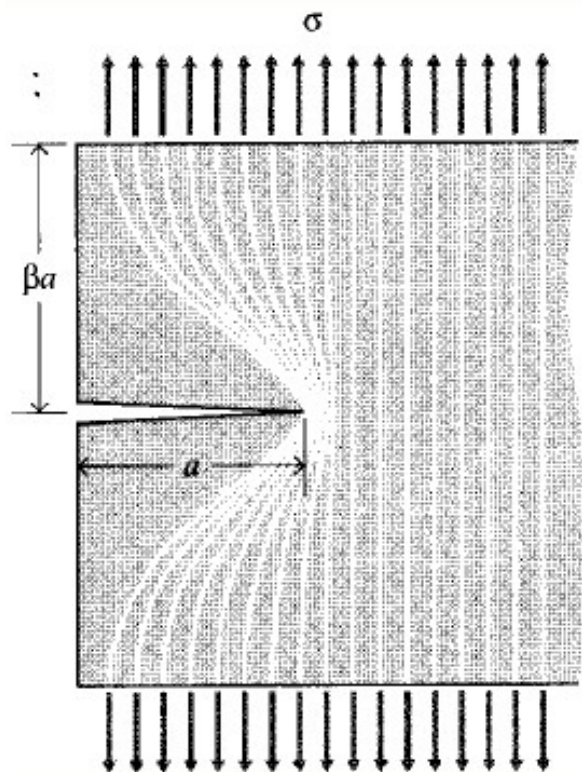


Figure 3.2 The concept of strain energy release rate (Roylance, 2001).

As illustrated in Figure 3.2, the total strain energy U released can be expressed as Equation 3.4:

$$U = -\frac{\sigma^2}{2E} \cdot \pi a^2 \quad (3.4)$$

This strain energy is liberated as crack grows. During the process of crack forming, bonds will be separated away, and materials will absorb the energy that are released. The surface energy S is expressed as $S = 2\gamma a$, where the factor 2 means two broken surfaces and γ is the surface energy (J/m^2). Then the total energy associated with the crack growth is the sum of the material absorbed energy plus the liberated strain energy as illustrated in Figure 3.3.

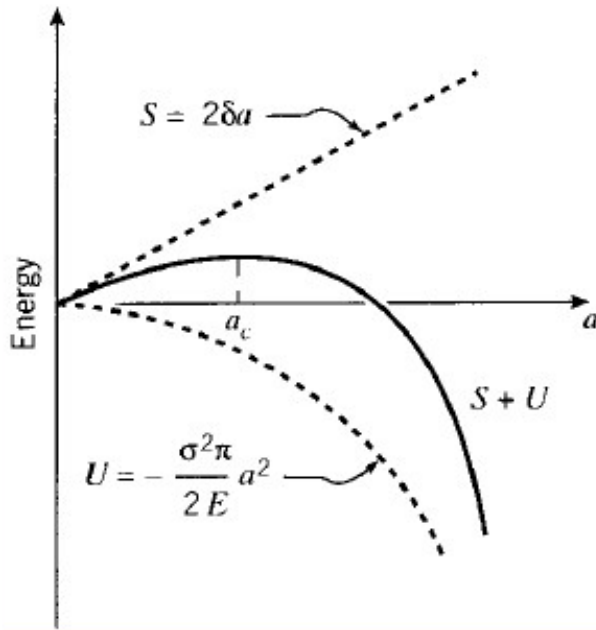


Figure 3.3 Total energy associated with the crack growth (Roylance, 2001).

Equation 3.5a represents the relation between the derivation of the summation of energy ($S + U$) and zero, it will give the critical crack length. Beyond the critical crack length a_c , the crack growth turns to catastrophic.

$$\frac{\partial(S+U)}{\partial a} = 2\gamma - \frac{\sigma_f^2}{E} \pi a = 0 \quad (3.5a)$$

Solving the above equation, the failure stress associated with the critical crack length can be deduced to

$$\sigma_f = \sqrt{\frac{2E\gamma}{\pi a}} \quad (3.5b)$$

For a ductile material the plastic flow around the crack tip is significant, on this account most of the liberated strain energy was absorbed by energy dissipation in terms of the plastic deformation. Irwin (1948) and Orowan (1949) reported that the catastrophic fracture occurs when the strain energy is released at a rate, critical strain energy release rate, named as \mathcal{G}_c , which can be written as:

$$\sigma_f = \sqrt{\frac{E\mathcal{G}_c}{\pi a}} \quad (3.6)$$

The critical strain energy release rate \mathcal{G}_c , the far field stress σ_f and the crack length a illustrate the interrelation of aspects of the fracture process. The strain release rate can be determined as Equation 3.7:

$$\mathcal{G} = \frac{\partial U}{\partial a} \quad (3.7)$$

Comparing the Equation 3.3 and 3.6, the strain energy release rate can be written related with the stress intensity factor as Equation 3.8:

$$\sqrt{\frac{E\mathcal{G}_c}{\pi a}} = \frac{K_{IC}}{\sqrt{\pi a}} \quad (3.8)$$

Rewriting the above expression as:

$$\mathcal{G} = \frac{K^2}{\bar{E}} \quad (3.9)$$

$$\bar{E} = \begin{cases} \bar{E}, & \text{for plane stress} \\ \frac{E}{1-\nu^2}, & \text{for plane strain} \end{cases} \quad (3.10)$$

Anderson (1995) and Rice (1968) reported a method, J-integral, to calculate the strain energy release rate by using a line integral around the crack tip as illustrated in Equation 3.11 and Figure 3.4. In this expression, W is the strain energy density, δ_{1j} is the Kronecker delta, n_j is the outward normal to the contour, u_i is the displacement and Γ is a contour surrounding the crack tip. For the homogenous and isotropic materials in LEFM, a relation between J-integral and stress intensity factor K was proposed by Shih and Asaro (1988), Equation 3.12 gives the aforementioned relation, where E is the Young's modulus and G is the shear modulus.

$$J = \int_{\Gamma} \left(W \delta_{1j} - \sigma_{ij} \frac{\partial u_i}{\partial x_1} \right) n_j d\Gamma \quad (3.11)$$

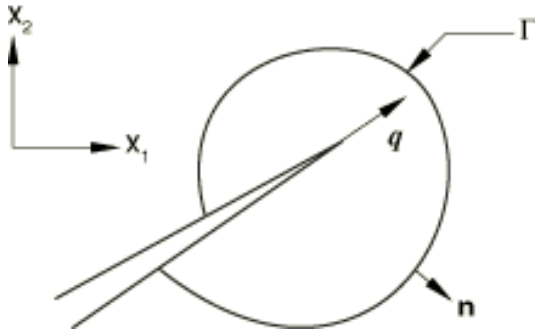


Figure 3.4 A two-dimensional contour integral approach. (Dassault, 2014b)

$$J = \mathcal{G} = \frac{1}{E} (K_I^2 + K_{II}^2) + \frac{1}{2G} K_{III}^2 \quad (3.12)$$

3.2 Fatigue crack growth models

Cracks tend to grow under a cyclic loading. In 1961, Paris *et al.* (1961) described that the fatigue crack growth rate, da/dN , was related to the stress intensity range, $\Delta K = K_{max} - K_{min}$. The da/dN versus ΔK curve is shown in Figure 3.5 on a log-log plot, which can be divided into three regions: region I, region II and region III.

In the region I, also known as threshold region, the curve asymptotically reaches the threshold value, ΔK_{th} . This is the limitation of cracks propagation will start. In other word, the crack will not grow if the stress intensity range below the threshold value. The slope of the curve is approximately constant in the intermediate region and defined as notation m . Paris and Erdogan (1963) suggested a relation between da/dN and stress intensity range as expressed in Equation 3.13, where C and m are empirically determined material constants.

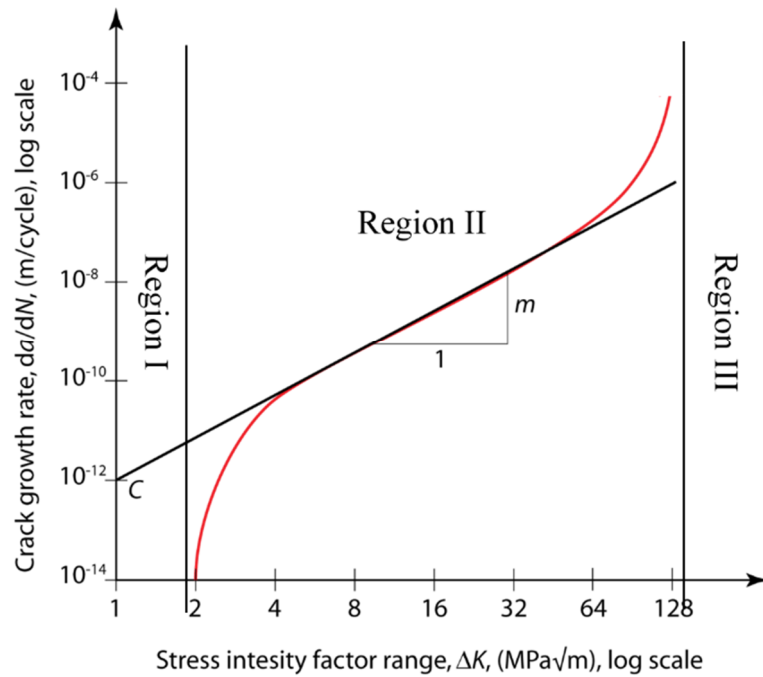


Figure 3.5 Crack growth rate versus stress intensity factor range curve.

$$\frac{da}{dN} = C(\Delta K)^m \quad (3.13)$$

The above equation is also known as Paris law. Walker (1970) modified this relation by considering the stress ratio, $R = \sigma_{min}/\sigma_{max}$, as expressed in Equation 3.14, where C_0 , m , and γ are empirically determined data.

$$\frac{da}{dN} = \frac{C_0}{(1-R)^{m(1-\gamma)}} (\Delta K)^m \quad (3.14)$$

The last region in Figure 3.5 is the unstable region. The curve becomes steep and the crack grows rapidly prior to final failure. The K_{max} asymptotically approaches the fracture toughness, K_c . The influence of nonlinear properties become significant due to the large scale of yielding, in other words, the LFM cannot be used in this region. Forman *et al.* (1967) gave a model-Forman equation-to demonstrate the behavior in this region.

3.2.1 Crack growth direction

The crack growth can be divided as two disciplines: 1) growth direction and 2) growth magnitude. Mixed-mode I and II crack growth has been studied for many years, different models have been established to predict the crack direction. Three of them are described herein: the maximum tangential stress criterion, the maximum energy release rate criterion and the zero K_{II} criterion.

The maximum tangential stress criterion (MTS) states that the extension angle of the crack growth is perpendicular to the maximum tangential stress at the crack tip. Equation 3.15 was reported as a parametric equation to describe this relation by Erdogan and Sih (1963):

$$\theta = \cos^{-1} \left(\frac{3K_{II}^2 + \sqrt{K_I^4 + 8K_I^2 K_{II}^2}}{K_I^2 + 9K_{II}^2} \right) \quad (3.15)$$

The θ in above equation represents the propagation angle, this relation is determined by setting shear stress $\tau = 0$, in the meanwhile, $\partial\sigma_\theta/\partial\theta = 0$. Some literature gives the maximum tangential stress, σ_θ can be denoted as Equation 3.16.

$$\sigma_\theta = \frac{1}{\sqrt{2\pi r}} \cos^2 \frac{\theta}{2} \left[K_I \cos \frac{\theta}{2} - 3K_{II} \sin \frac{\theta}{2} \right] \quad (3.16)$$

For materials with isotropic properties, the tangential stress is related to the mode I stress intensity factor K_I^r , which is expressed in Equation 3.17; and a numerical algorithm is used to find the angle that maximizes K_I^r .

$$K_I^r(\theta) = \sigma_\theta \sqrt{w\pi r} = \cos \frac{\theta}{2} \left[K_I \cos^2 \frac{\theta}{2} - \frac{3}{2} K_{II} \sin \theta \right] \quad (3.17)$$

The maximum energy release rate criterion (MERR) is proposed by Hussain *et al.* (1974) and developed from Griffith and Irwin's work. This theory states that the crack will extent at an angle, θ , which maximizes the energy release rate, \mathcal{G} . The MERR assumes $K_{III} = 0$ and it has been proven working well in a mixed mode I – II condition.

The last theory assume that the crack extension occurs in a direction where $K_{II} = 0$ for isotropic and homogeneous materials (Cotterell and Rice, 1980). Cotterell and Rice analyzed the curved and kinked cracks and suggested that the MTS and MERR models meet the $K_{II} = 0$ criterion once the crack has extended. However, this study has not been verified by any experimental data yet.

Aforementioned models will result in slight difference. The MTS model will be used in this thesis.

3.2.2 Crack growth magnitude

Aforementioned Equation 3.13 demonstrates the interrelationship between crack growth magnitude and applied load cycles. It is obvious that the stress intensity range, ΔK , determines the crack growth magnitude per cycle. In single mode problems, the stress intensity range can be defined by the maximum and minimum SIFs for each mode in one cycle as:

$$\Delta K_I = \Delta K_{I,max} - \Delta K_{I,min} \quad (3.18)$$

$$\Delta K_{II} = \Delta K_{II,max} - \Delta K_{II,min}$$

$$\Delta K_{III} = \Delta K_{III,max} - \Delta K_{III,min}$$

Moreover for the cases of mixed mode loading, an equivalent stress intensity factor is required to apply the Paris law. Tanaka (1974) reported the equivalent SIF can be expressed as Equation 3.19 within model I –II.

$$\Delta K_{eq} = \sqrt[4]{\Delta K_I^4 + 8\Delta K_{II}^4} \quad (3.19)$$

Rhee and Salama (1987) suggested that the equivalent SIF can be conducted from the energy release rete, which is illustrated in Equation 3.20

$$\Delta K_{eq} = \sqrt{\Delta K_I^2 + \Delta K_{II}^2} \quad (3.20)$$

As a result, the Paris Law can be modified as Equation 3.21 by using equivalent stress intensity factor, ΔK_{eq} .

$$\frac{da}{dN} = C_p (\Delta K_{eq})^{m_p} \quad (3.21)$$

3.3 Finite element methods (FEM)

3.3.1 Finite Elements with Quarter Points (FEQP) method

The conventional finite elements method (FEM) has been developed since 1851. FEM has been widely used in dealing with continuous field problems, such as stress and strain analysis, fluid flow, heat transfer and electrical and magnetic fields. Nevertheless it shows difficulty to solve discontinuous field problems with prohibitively expensive computation to obtain accurate solutions. When the FEM is applied in solving fracture problems, many reports have stated that it is unattainable that the stress singularity at the crack tip from linear elements. Alternately, energy release rate and contour integral for J and K were analyzed to represent the behavior at the crack tip.

In order to solve the stress singularity issues, the triangular crack tip element by Byskov (1970), and circular element by Wilson (1973) together with the rectangular elements by Hardy (1974) were developed to describe the crack tip. These special elements are characterized as specialized crack tip elements.

In spite of that, it is still not convenience to setup the model for fracture problems. In 1975, Henshell and Shaw (1975) reported a method to use quadratic elements instead of specialized elements. Henshell and Shaw moved the mid-side nodes of quadratic elements adjacent to the crack tip to their quarter portion location to represent the $1/\sqrt{r}$ stress singularity. This methods is known as Finite Elements with Quarter Points (FEQP). Around the crack tip, a concentric meshing scheme is followed as depicted in Figure 3.6 and the typical process of this method proceeds as Figure 3.7. Because the explicit crack propagation is not possible, the mesh should be generated at each crack increment, which is known as re-meshing, which was proposed by Nicolas *et al.* (1999), to attain accurate results. In response to the deficiency of meshing using FEQP, Virtual Crack Closure Technique was developed by Rybicki and Kanninen (1977) in 1977.

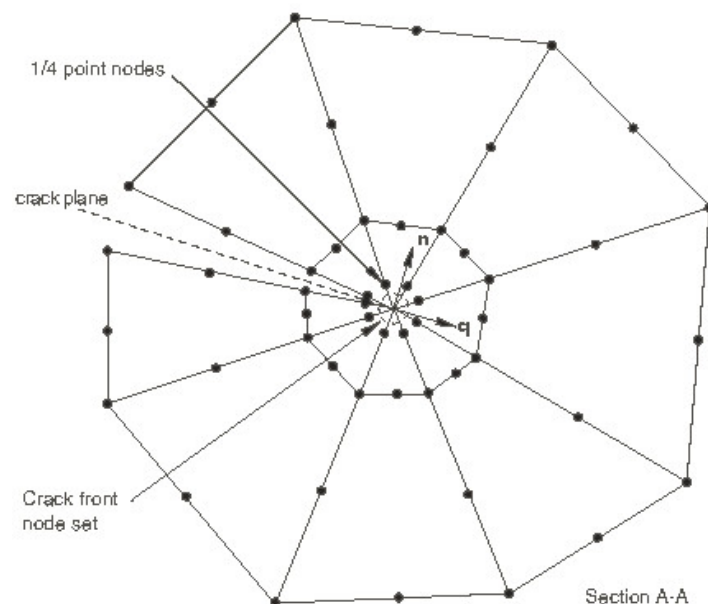


Figure 3.6 Typical focused mesh scheme for fracture mechanics evaluation (Dassault, 2014a).

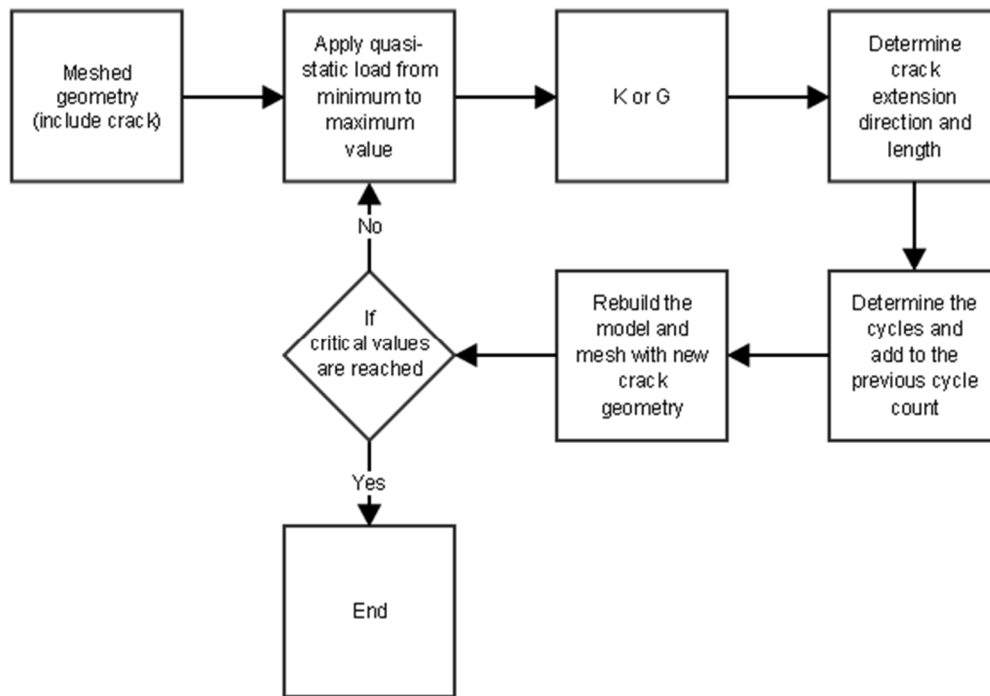


Figure 3.7 Flow chart of Finite Elements with Quarter Points method.

3.3.2 Mixed mode critical energy release rate

In the engineering practice, the fracture occurs under a combination of different modes, consequently an equivalent critical value is required to consider the contributions from each mode. Wu and Reuter (1965) proposed the power law model, which is given by the following formula:

$$\frac{G_{equiv}}{G_{equivC}} = \left(\frac{G_I}{G_{IC}}\right)^{a_m} + \left(\frac{G_{II}}{G_{IIC}}\right)^{a_n} + \left(\frac{G_{III}}{G_{IIIC}}\right)^{a_0} \quad (3.22)$$

where G_I , G_{II} and G_{III} are energy release rates, G_{IC} , G_{IIC} and G_{IIIC} are the critical energy release rates for modes I, II and III respectively. The factors a_m , a_n and a_0 are empirical constants. Because there is no a universally accepted method for determining the equivalent critical value, thus the power law is selected in this study.

3.3.3 Virtual Crack Closure Technique (VCCT)

Rybicki and Kanninen (1977) stated that the energy needed to grow a crack is equal to the work required to close a crack of the same length. Rybicki and Kanninen extent this work and developed the modified virtual crack closure integral method. According to this method the energy release rates can be expressed as the limitation between displacement and force. For Mode I and Mode II, the expression, Equation 3.23, is used to calculate the energy release rates, \mathcal{G} . Referring to Figure 3.8, F is the force required to keep nodes 2 and 5 separation; v are the displacement between nodes 1 and 6, d is the crack increment, and ℓ is the element length in front of the crack tip.

$$\begin{aligned} G_I &= \lim_{d \rightarrow 0} \frac{1}{2d} F_{y,2,5} v_{1,6} \\ G_{II} &= \lim_{d \rightarrow 0} \frac{1}{2d} F_{x,2,5} u_{1,6} \end{aligned} \quad (3.23)$$

$$G_{III} = \lim_{d \rightarrow 0} \frac{1}{2d} F_{z,2,5} w_{1,6}$$

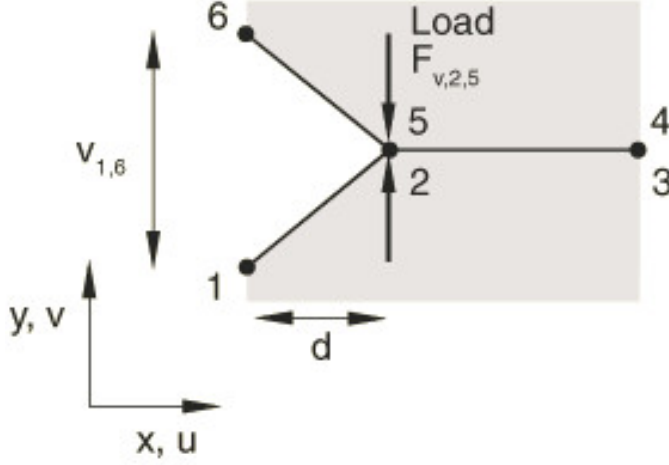


Figure 3.8 The explanation of modified Virtual Crack Closure Technique in pure Mode I (Dassault, 2014a).

For a pure Mode I problem, the first equation in Equation 3.23 can be deduced as below:

$$G_I = \frac{1}{2} \frac{v_{1,6} F_{v,2,5}}{bd} \quad (3.24)$$

where G_I is greater than the critical value G_{IC} , node 2 and 5 will deboned and the fracture starts. When it comes to a mix-mode problem, the criterion can be determined as:

$$f = \frac{G_{equiv}}{G_{equivC}} \geq 1.0 \quad (3.25)$$

where G_{equiv} is the equivalent strain energy release rate, which is calculated at a node while the G_{equivC} is the critical equivalent strain energy release rate calculated based on the mode-mix criterion mentioned. The power law model, which is explained in Section 3.3.2, is selected in this study.

3.3.4 Extended finite element method (XFEM)

The methods mentioned so far belong to conventional finite element methods. Significant modeling and re-meshing works as crack extension are required to obtain accurate results, in response to the deficiency of FEQP modeling technology. Belytschko and Black (1999) introduced a numerical technique based on the partition of unity method of Babuska and Melenk (1996), also known as Extended Finite Element Method (XFEM). The XFEM extends the piecewise polynomial function space of conventional finite element methods with extra enrichment functions. The XFEM approach can be used where conventional FEM fails or the computation is prohibitively expensive. For instance, in XFEM, the discontinuity may not align with mesh. In other word, the discontinuity is independent of mesh. That means that the frequent re-meshing is not required, and cracks could be modeled arbitrarily without considering the mesh. Therefore, this technique is widely used in many fields, such as composites and fracture mechanics.

For a linear elastic fracture problem, a crack can be represented as a combination of two sets of functions: Heaviside function - a discontinuous function - for representing displacement jump across crack face, and a set of asymptotic functions to model the crack tip singularity. Denoting the interior of the crack surface as Γ , crack tip as Λ , and nodes set as N . Let nodes belonging to elements cut by crack surface name as N_Γ and those nodes belonging to elements containing crack tip denote as N_Λ . Then the XFEM enriched displacement approximation can be expressed as Equation 3.26:

$$U^h(x) = \sum_{I \in N} N_I(x) [u_I + H(x)a_J + \sum_{\alpha=1}^4 \Phi_\alpha(x)b_K^\alpha] \begin{pmatrix} \{J \in \mathcal{N}_\Gamma\} \\ \{K \in \mathcal{N}_\Lambda\} \end{pmatrix} \quad (3.26)$$

where $N_I(x)$ represents the conventional shape function at node i that belongs to continuous part and the corresponding nodal displacement is denoted as u_I . The term a_J is nodal enriched degree of freedom of the nodes that belong to crack surface; and the asymptotic crack tip nodes are given the enriched degree of freedom as b_K^α . The rest terms of $H(x)$ represents the Heaviside distribution, in Equation 3.27, which is used to represent the discontinuous displacement field at the elements that across the crack line. In addition, $\Phi_\alpha(x)$ is the crack tip asymptotic function.

$$H(x) = \begin{cases} +1, & \text{if } (x - x^*) \cdot n \geq 0 \\ -1, & \text{otherwise} \end{cases} \quad (3.27)$$

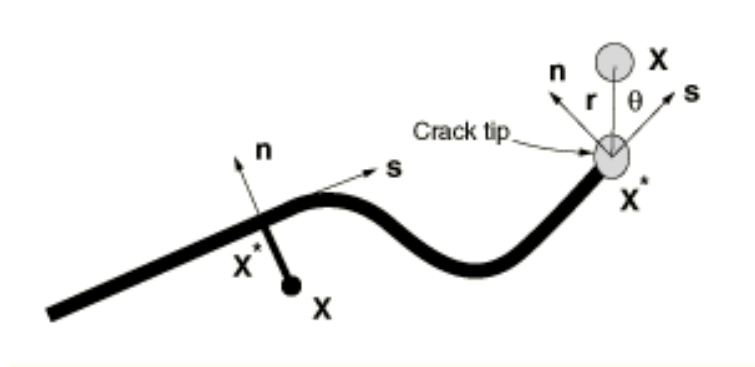


Figure 3.10 The crack path and tip described by Heaviside and asymptotic terms (Dassault, 2014a).

As depicted in Figure 3.10, the term x in Equation 3.27 is an integration point, x^* is the colsest point to x on the crack surface and n is the unit normal at x^* .

The Equation 3.28 demonstrates the displacement field basis functions for sharp crack in an isotropic linear elastic material. R and θ is a polar coordinate system originating at the crack tip and $\theta = 0$ is parallel to the crack path, as described by Sukumar *et al.* (1999).

$$\{F_i(r, \theta)\}_{i=1}^4 \equiv \left\{ \sqrt{r} \cos \frac{\theta}{2}, \sqrt{r} \sin \frac{\theta}{2}, \sqrt{r} \sin \frac{\theta}{2} \sin \theta, \sqrt{r} \cos \frac{\theta}{2} \sin \theta \right\} \quad (3.28)$$

Nodes to be enriched by Equation 3.27 and 3.28 are depicted in Figure 3.11, where the filled circles represent Heaviside nodes and crack tip enriched nodes are denoted by open circles.

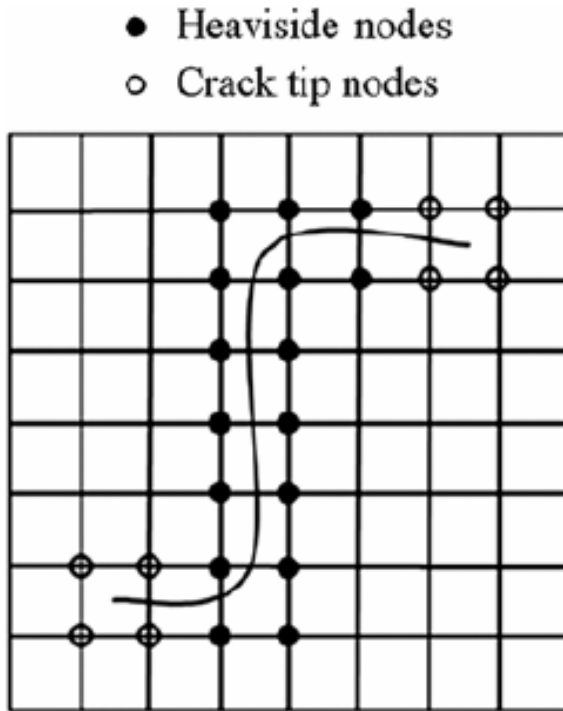


Figure 3.11 The enriched terms to describe the crack (Krishna et al., 2014).

3.3.5 Phantom node approach

Belytschko and coworkers introduced phantom node approach based on the superposed element formulation reported by Hansbo, Belytschko and Black. According to this approach, the discontinuous displacement field can be superposed with elements that containing phantom nodes. The superposed elements originally combined together as a single element, when the crack grows across the elements, phantom nodes and real nodes move away each other, illustrated in Figure 3.12. This behavior is used as implementation of crack propagation in ABAQUS. Because the asymptotic crack tip enrichment functions is not included in the approach, in other word, the stress singularity at the crack tip will be ignored.

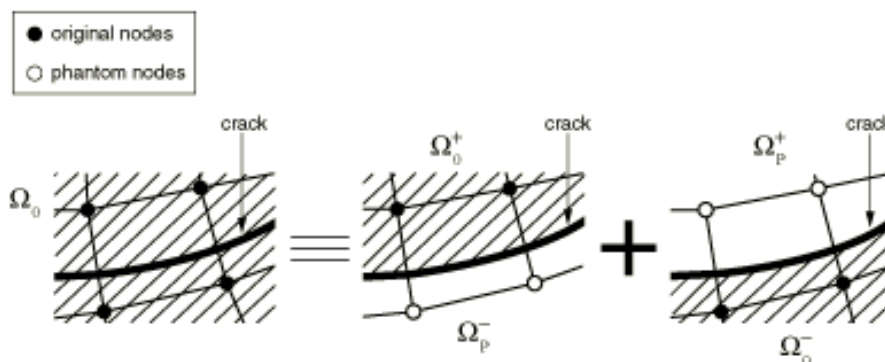


Figure 3.12 The superposing of phantom nodes (Dassault, 2014a).

3.3.6 Level set method

Because the model within the XFEM framework is independent of the finite element mesh. This gives rise to the problem that how to keep tracking the evolution of the crack

as they are not explicitly defined. In order to solve this problem, Osher and Sethian (1988) introduced a method to track the boundaries of crack evolution, also known as the Level Set Method. In the level set method, two orthogonal level set functions ϕ and ψ are used to completely describe the crack. The ψ level set is used to track the crack body, while the ϕ level set is used to track the crack tip. The ϕ and ψ level set functions are defined such in the Equation 3.29.

$$\begin{aligned}
 \psi(x) < 0 & \text{ below crack path} & \phi(x) < 0 & \text{ behind crack tip} \\
 \psi(x) > 0 & \text{ above crack path} & \phi(x) > 0 & \text{ in front of crack tip} \\
 \psi(x) = 0 & \text{ along crack path} & \phi(x) = 0 & \text{ at crack tip}
 \end{aligned}
 \tag{3.29}$$

The nodal value of the function ϕ is the signed distance of the node from the crack face; while the value of function ψ represents the distance of the node from an almost-orthogonal surface passing through the crack front. Figure 3.13 gives an example of how the level set method works.

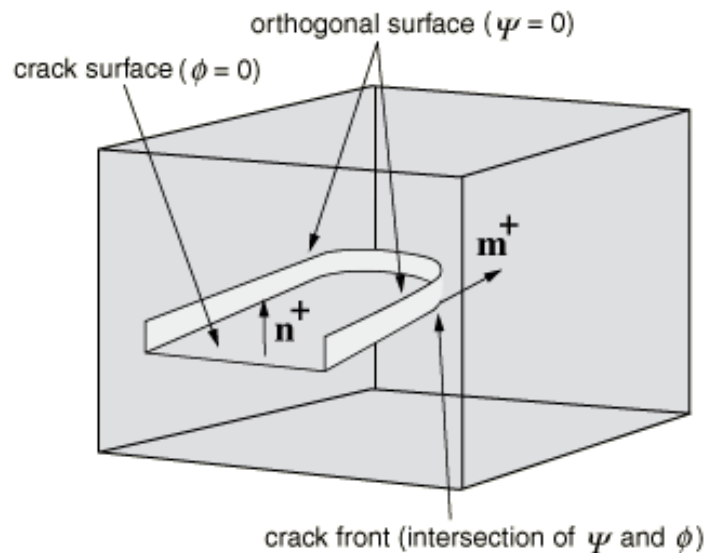


Figure 3.13 An example to explain the ϕ and ψ level set (Dassault, 2014a).

Shi *et al.* (2010) incorporated XFEM into ABAQUS to analyze cyclic crack growth using a modified VCCT method for calculating the energy release rates at the crack tip. A standard VCCT procedure can be followed as below:

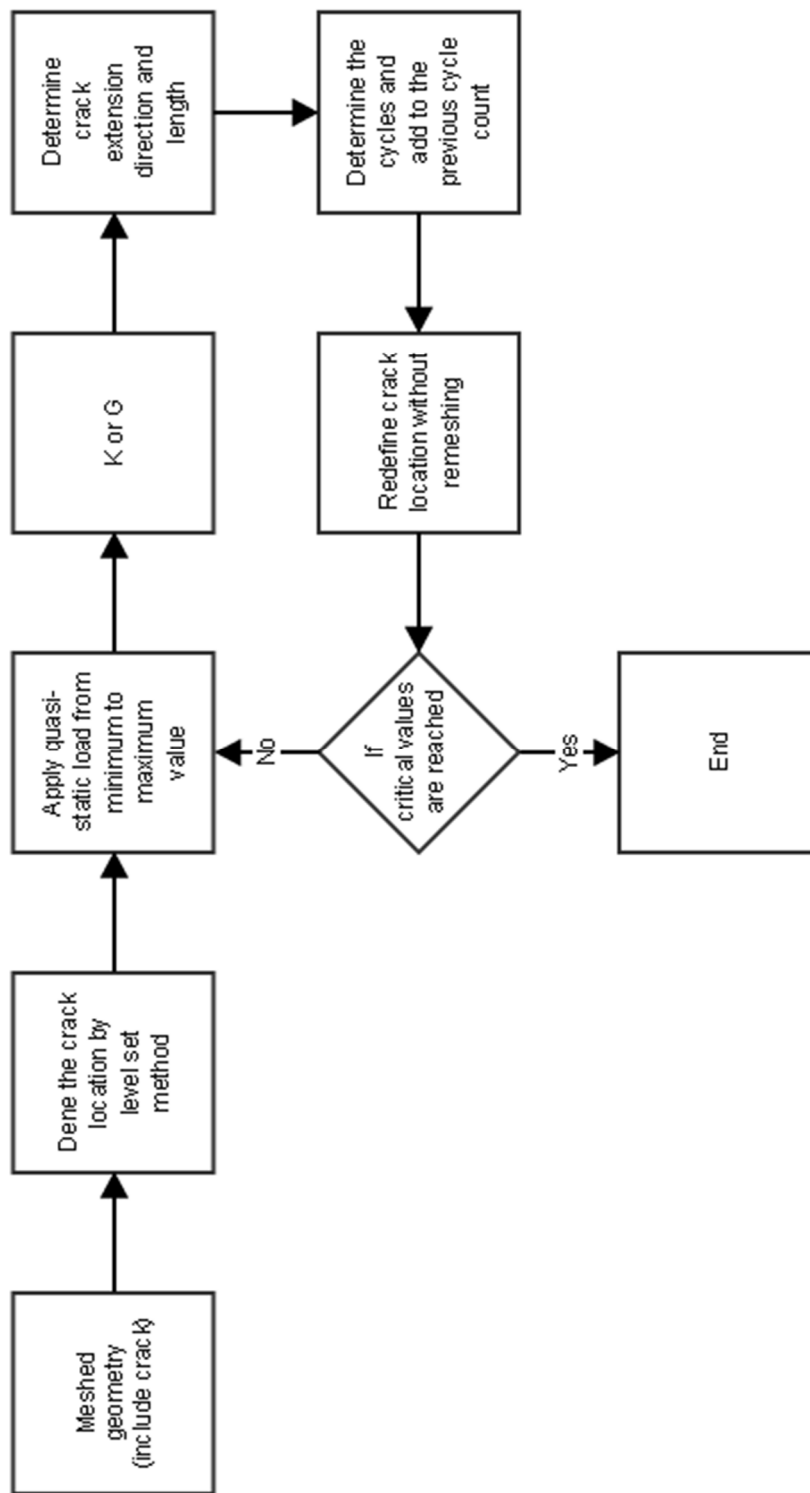


Figure 3.13 The flow chart to analyze crack growth based on modified VCCT.

4 Ultimate strength and buckling analysis

In ultimate strength analysis, the relationship between bending moment and curvature, as well as the relationship between neutral axis position and curvature is illustrated. In buckling analysis, the load-end shortening curve is proved.

4.1 Ultimate strength analysis

The Figure 4.1 shows the mid-ship section study vessel, which is a 308,000DWT double hull VLCC. The cross-section of this VLCC is divide into 113 stiffened elements and 12 corner elements. There is no unstiffened plate element in this study case, because all the plates of the cross-section were attached by T-profile stiffener.

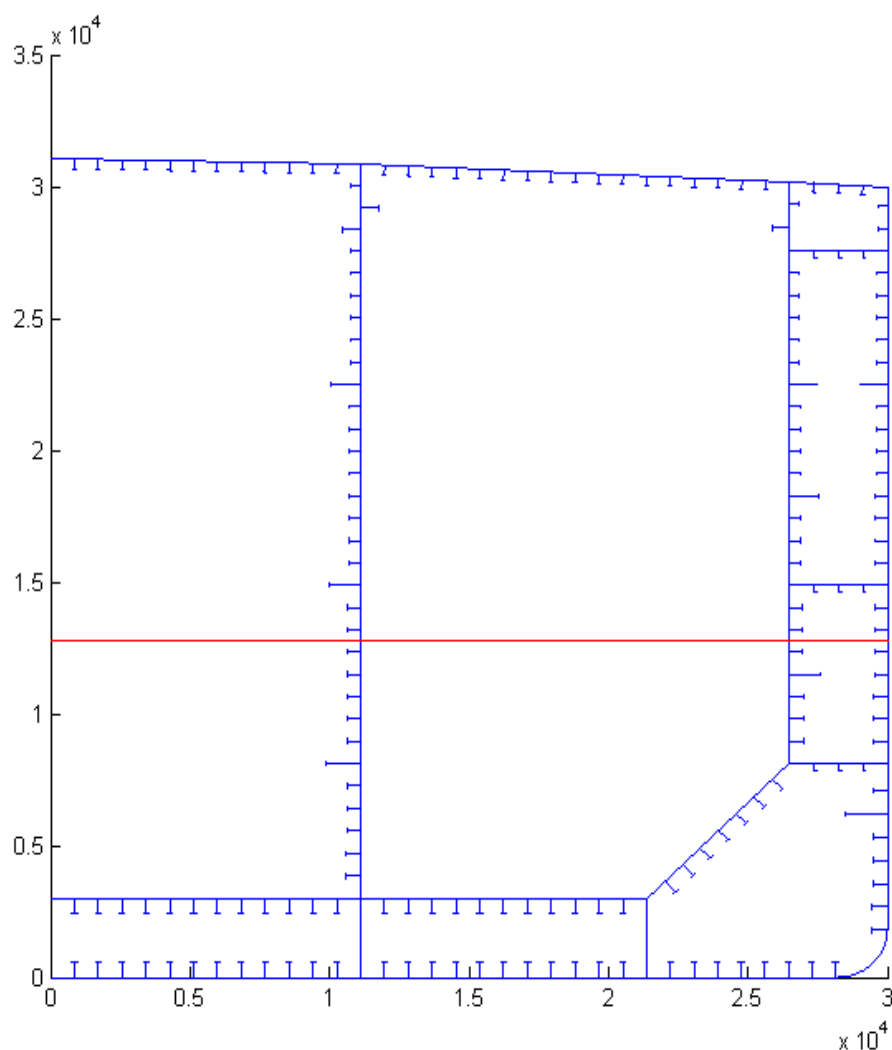


Figure 4.1 Mid-ship cross section with neutral axis position.

In the mid-ship section graph, the red line represents the initial neutral axis position which is approximately 12.9 m from base line. During the calculation process of iterative incremental approach, the adjustment of this position would be significant to the final results. In hogging and sagging condition, it will move to opposite direction.

4.1.1 Types of Elements

Because all the structure components in this ship are with stiffeners. There are only two structure elements in the definition. In Figure 4.2, there are only stiffened elements and corner elements without plate elements. So the calculation procedure can be simplified.

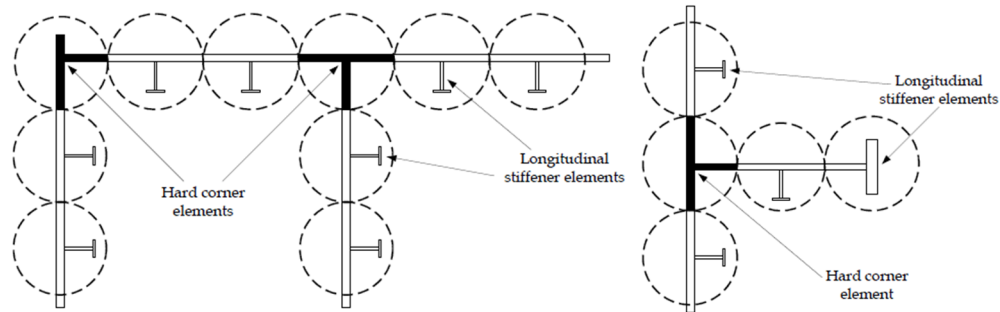


Figure 4.2 Two types of structure elements in this study case (ABS, 2012).

4.1.2 Load-end shortening curve

The nonlinear behavior of hull material is different in different hull structure elements. As the material was regarded as elasto-plastic material, most of the elements would have a stress-strain curve shows in the Figure 4.3, Figure 4.8, Figure 4.9. The structure element is fully plastic beyond yield in tension. However, in compression, the nonlinear elasto-plastic behavior takes place in some structure elements. This kind of material behavior which shows different in tension and compression is called 'load-end shortening'. Different type of elements have different load-end shortening curves. But in tensional condition, all elements are elastic-perfectly plastic material.

4.1.2.1 Plate element

There are two failure modes of plate element, yielding in tension and buckling in compression.

When the unstiffened plate element is under tension, it was regarded as elastic-perfectly plastic material.

$$\frac{\sigma}{\sigma_0} = \begin{cases} \bar{\varepsilon}, & 0 \leq \bar{\varepsilon} \leq 1 \\ 1, & \bar{\varepsilon} \geq 1 \end{cases} \quad (4.1)$$

When plate is under compression, σ_{UP}^E is the stress of unstiffened plate which should be not less than σ_{CP}^E , the critical buckling stress, and should be limited by σ_{Ux} , the ultimate strength, shown in Equation 4.2.

$$\sigma_{CP}^E \leq \sigma_{UP}^E \leq \sigma_{Ux} \quad (4.2)$$

When $\bar{\varepsilon} \leq \sigma_{Ux}/\sigma_0$

$$\sigma_{UP}^E = \sigma_0 \bar{\varepsilon} \quad (4.3)$$

When $\bar{\varepsilon} > \sigma_{Ux}/\sigma_0$

$$\frac{\sigma_{UP}^E}{\sigma_0} = \begin{cases} C, & \alpha > 1 \\ C \cdot \frac{s}{l} + 0.1(1 - \frac{s}{l})(1 + 1/\beta_E^2)^2, & \alpha < 1 \end{cases} \quad (4.4)$$

Where

$$\sigma_{Ux} = C_x \sigma_0 \quad (4.5)$$

$$C_x = \begin{cases} 1, & \beta \leq 1 \\ 2/\beta - 1/\beta^2, & \beta > 1 \end{cases} \quad (4.6)$$

where β is plating slenderness ratio.

$$C_E = \begin{cases} 1, & \beta_E \leq 1 \\ 2/\beta_E - 1/\beta_E^2, & \beta_E > 1 \end{cases} \quad (4.7)$$

where β_E is plating slenderness ratio corresponding to $\bar{\epsilon}$

$$\beta_E = s/t \sqrt{\bar{\epsilon}^n \sigma_{0p}/E} \quad (4.8)$$

Finally, the critical buckling strength of an unstiffened plate corresponding to $\bar{\epsilon}$ can be determined by the following equation

$$\sigma_{CP}^E = \begin{cases} \frac{\sigma_{Ex}}{\bar{\epsilon}^n}, & \sigma_{Ex} \leq P_r \sigma_0 \bar{\epsilon}^n \\ \sigma_0 [1 - P_r (1 - P_r) \frac{\sigma_0 \bar{\epsilon}^n}{\sigma_{Ex}}], & \sigma_{Ex} > P_r \sigma_0 \bar{\epsilon}^n \end{cases} \quad (4.9)$$

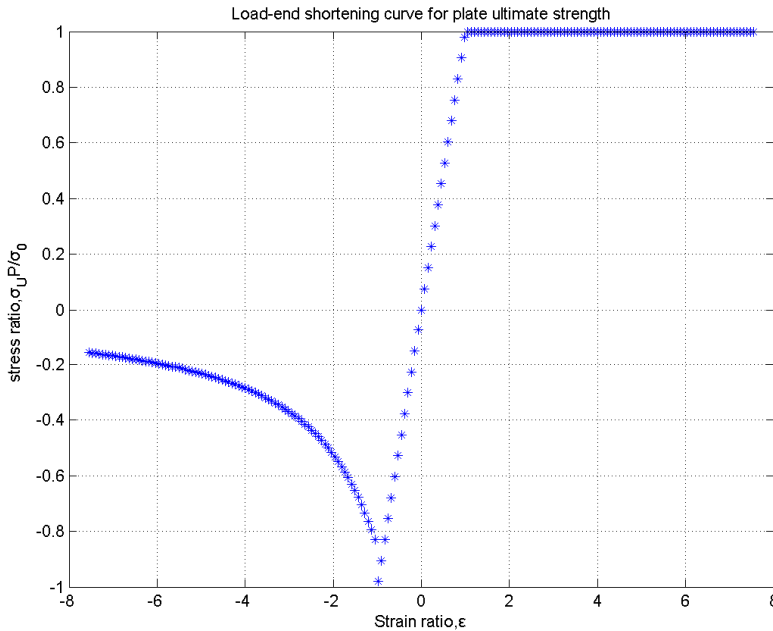


Figure 4.3 Load-end shortening curve for plate element.

4.1.2.2 Stiffener element

There four failure modes of stiffened element. In tension condition, the material is fully-plastic, so it is yielding in tension as other structure elements. In compression condition, there are three types of buckling models, beam-column buckling, torsional-flexural buckling and local buckling.

Yielding in tension

The load-end shortening curve same as that of unstiffened plate in tension.

Beam-column buckling

The beam-column buckling value can be calculated by the following equations.

Firstly, to determine the stress for beam-column buckling of longitudinal corresponding to $\bar{\epsilon}$, some other parameters need to be calculated.

$$\sigma_{C1} = \begin{cases} \sigma_0 \bar{\epsilon}, & \bar{\epsilon} \leq \sigma_{CA}/\sigma_0 \\ \sigma_{CA}^E \frac{A_s + s_e^E t}{A_s + st} \leq \sigma_{CA} \frac{A_s + s_e t}{A_s + st}, & \bar{\epsilon} > \sigma_{CA}/\sigma_0 \end{cases} \quad (4.10)$$

where σ_{CA} is critical buckling stress of longitudinal in axial compression computed by Equation 4.11. In the calculation of critical buckling stress of longitudinal in axial compression, the Euler's buckling stress of longitudinal $\sigma_{E(C)}$ need to determined by Equation 4.12.

$$\sigma_{CA} = \begin{cases} \sigma_{E(C)}, & \sigma_{E(C)} \leq P_r \sigma_0 \\ \sigma_0 [1 - P_r (1 - P_r) \frac{\sigma_0}{\sigma_{E(C)}}], & \sigma_{E(C)} > P_r \sigma_0 \end{cases} \quad (4.11)$$

$$\sigma_{E(C)} = \frac{\pi^2 E r_e^2}{l^2} \quad (4.12)$$

$$r_e = \sqrt{\frac{I_e}{A_e}} \quad (4.13)$$

where r_e is radius is the gyration of area, A_e .

The critical buckling stress of longitudinal corresponding to $\bar{\epsilon}$ can be calculated by Equation 4.14.

$$\sigma_{CA}^E = \begin{cases} \frac{\sigma_{E(C)}}{\bar{\epsilon}^n}, & \sigma_{E(C)} \leq P_r \sigma_0 \bar{\epsilon}^n \\ \sigma_0 [1 - P_r (1 - P_r) \frac{\sigma_0 \bar{\epsilon}^n}{\sigma_{E(C)}}], & \sigma_{E(C)} > P_r \sigma_0 \bar{\epsilon}^n \end{cases} \quad (4.14)$$

$$s_e^E = C_E s \quad (4.15)$$

$$C_E = \begin{cases} 1, & \beta_E \leq 1 \\ 2/\beta_E - 1/\beta_E^2, & \beta_E > 1 \end{cases} \quad (4.16)$$

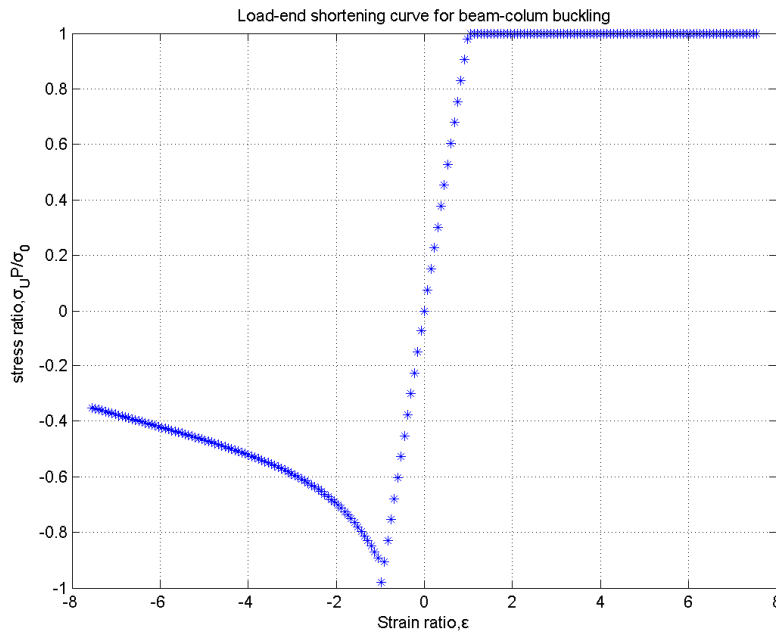


Figure 4.4 Load-end shortening curve for beam-column buckling.

Torsional-flexural buckling

The torsional-flexural buckling can be calculated by the following equations. To determine the stress for torsional-flexural buckling of longitudinal corresponding to $\bar{\varepsilon}$, the critical torsional-flexural buckling stress, critical buckling stress for associated plating corresponding to n-half waves and elastic torsional-flexural buckling stress are needed to be calculated firstly.

$$\sigma_{C2} = \begin{cases} \sigma_0 \bar{\varepsilon}, & \bar{\varepsilon} \leq \sigma_{CT} / \sigma_0 \\ \frac{\sigma_{CT}^E A_s + \sigma_{UPst}^E}{A_s + st}, & \bar{\varepsilon} > \sigma_{CT} / \sigma_0 \end{cases} \quad (4.17)$$

$$\sigma_{CT} = \begin{cases} \sigma_{ET}, & \sigma_{ET} \leq P_r \sigma_0 \\ \sigma_0 [1 - P_r (1 - P_r) \frac{\sigma_0}{\sigma_{ET}}], & \sigma_{ET} > P_r \sigma_0 \end{cases} \quad (4.18)$$

$$\sigma_{ET} = \frac{\frac{K}{2.6} + (\frac{q\pi}{l})^2 \Gamma + \frac{C_0}{E} (\frac{l}{q\pi})^2}{I_0 + \frac{C_0}{\sigma_{CL}} (\frac{l}{q\pi})^2} E \quad (4.19)$$

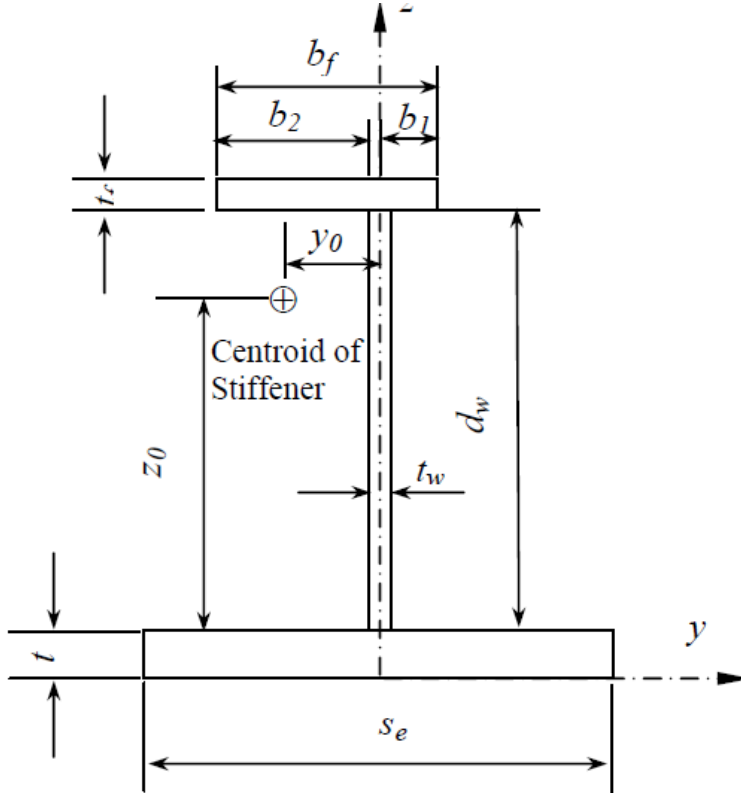


Figure 4.5 Sectional dimensions of a stiffened plate (Sun and Wang, 2005).

During the calculation for elastic torsional-flexural buckling stress and critical buckling stress for associated plating corresponding to n-half waves, the following parameters need to be determined. The parameters are influenced by the sectional dimensions of the stiffened plate which is illustrate in Figure 4.5. In this case b_1 equals to b_2 .

$$K = \frac{b_f t_f^3 + d_w t_w^3}{3} \quad (4.20)$$

$$I_0 = I_y + m I_z + A_s (y_0 + z_0) \quad (4.21)$$

$$m = 1.0 - u (0.7 - \frac{d_w}{b_f}) \quad (4.22)$$

$$u = 1 - 2 \frac{b_1}{b_f} \quad (4.23)$$

$$C_0 = \frac{Et^3}{3s} \quad (4.24)$$

$$\Gamma \cong mL_{zf}d_w^2 + \frac{d_w^3 t_w^3}{36} \quad (4.25)$$

$$I_{zf} = \frac{t_f b_f^3}{12} \left(1.0 + 3.0 \frac{u^2 d_w t_w}{A_s} \right) \quad (4.26)$$

$$\sigma_{cL} = \frac{\pi^2 E \left(\frac{p}{\alpha} + \frac{\alpha}{p} \right)^2 \left(\frac{t}{s} \right)^2}{12(1-\nu^2)} \quad (4.27)$$

The critical torsional-flexural buckling stress of a stiffener corresponding to $\bar{\epsilon}$ can be estimated by Equation 4.28.

$$\sigma_{CT}^E = \begin{cases} \frac{\sigma_{ET}}{\bar{\epsilon}^n}, & \sigma_{ET} \leq P_r \sigma_0 \bar{\epsilon}^n \\ \sigma_0 \left[1 - P_r (1 - P_r) \frac{\sigma_0 \bar{\epsilon}^n}{\sigma_{ET}} \right], & \sigma_{ET} > P_r \sigma_0 \bar{\epsilon}^n \end{cases} \quad (4.28)$$

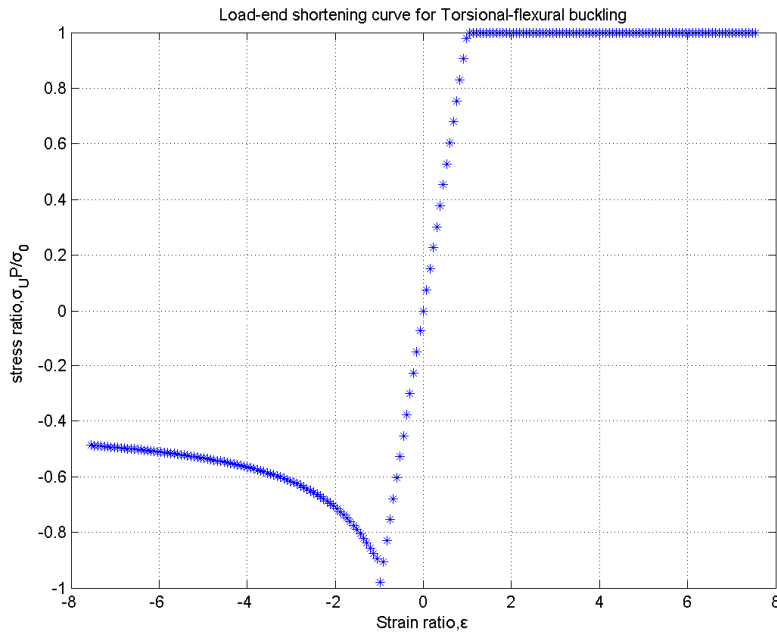


Figure 4.6 Load-end shortening curve for torsional buckling.

Local buckling of stiffeners

Same as the previous two types of buckling, to calculate stress for local buckling of longitudinal corresponding to $\bar{\epsilon}$, some other parameters should be determined at the first step.

$$\sigma_{C3} = \begin{cases} \sigma_0 \bar{\epsilon}, & \bar{\epsilon} \leq \sigma_{cL} / \sigma_0 \\ \frac{\sigma_{cL}^E A_s + \sigma_{UP}^E st}{A_s + st}, & \bar{\epsilon} > \sigma_{cL} / \sigma_0 \end{cases} \quad (4.29)$$

$$\sigma_{cL}^E = \begin{cases} \frac{\sigma_{EL}}{\bar{\epsilon}^n}, & \sigma_{EL} \leq P_r \sigma_0 \bar{\epsilon}^n \\ \sigma_0 \left[1 - P_r (1 - P_r) \frac{\sigma_0 \bar{\epsilon}^n}{\sigma_{EL}} \right], & \sigma_{EL} > P_r \sigma_0 \bar{\epsilon}^n \end{cases} \quad (4.30)$$

Where:

$$\sigma_{EL} = \min(\sigma_{EW}, \sigma_{EF}) \quad (4.31)$$

$$\sigma_{EW} = k_s \frac{\pi^2 E}{12(1-\nu^2)} \left(\frac{t_w}{d_w}\right)^2 \quad (4.32)$$

$$k_s = 4C_s \quad (4.33)$$

$$C_s = \begin{cases} 1.0, & \text{for angle or tee bar} \\ 0.33, & \text{for bulb plates} \\ 0.11, & \text{for flat bar} \end{cases} \quad (4.34)$$

$$\sigma_{EF} = 0.44 \frac{\pi^2 E}{12(1-\nu^2)} \left(\frac{t_f}{b_2}\right)^2 \quad (4.35)$$

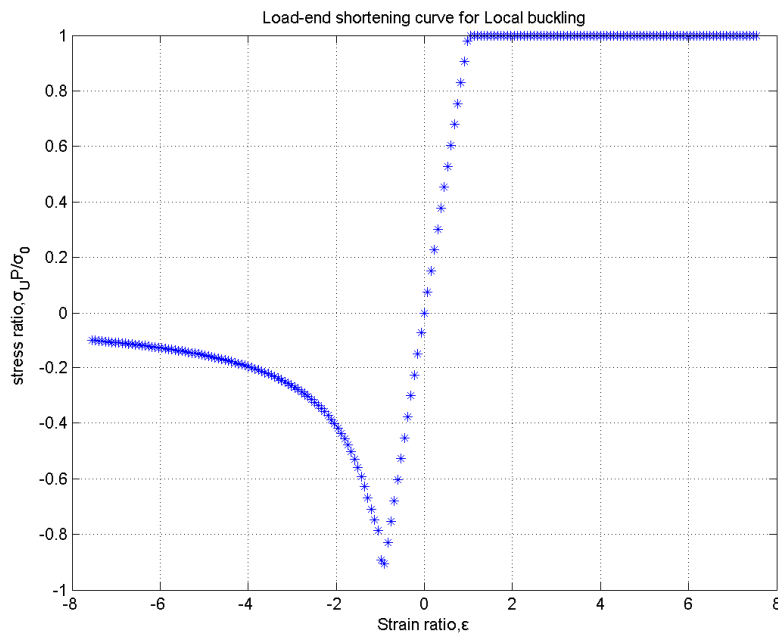


Figure 4.7 Load-end shortening curve for local buckling.

As the three failure mode has different stress value during buckling, the lowest value of them should be selected as the critical value. In Figure 4.8, the blue curve is for Beam-column buckling, red is for torsional-flexural buckling and green is for local buckling.

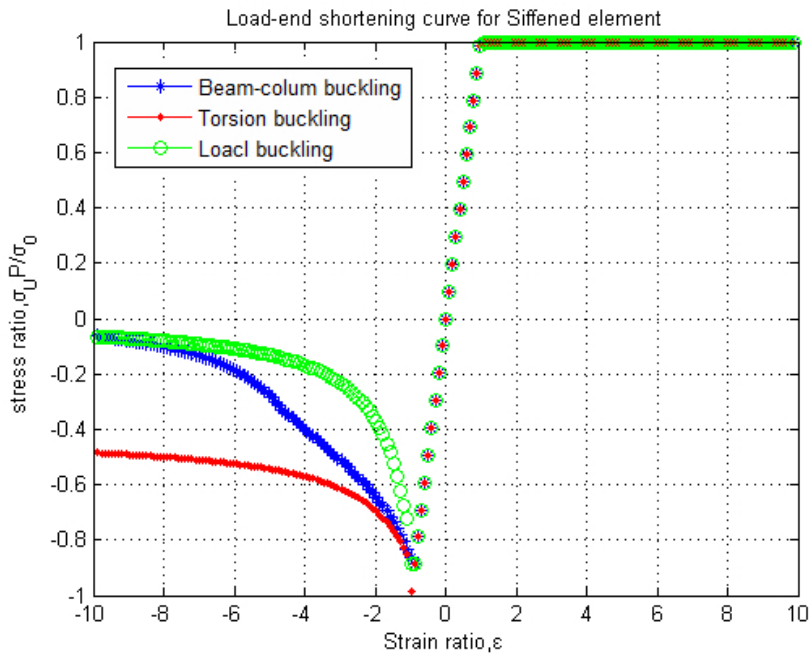


Figure 4.8 The comparison for the three kind of buckling in stiffened element

4.1.2.3 Corner element

Corner elements were regarded as stocky elements, which can be idealized as elastic-perfectly plastic material.

$$\frac{\sigma}{\sigma_0} = \begin{cases} -1, & \bar{\epsilon} < -1 \\ \bar{\epsilon}, & -1 \leq \bar{\epsilon} \leq 1 \\ 1, & \bar{\epsilon} > 1 \end{cases} \quad (4.36)$$

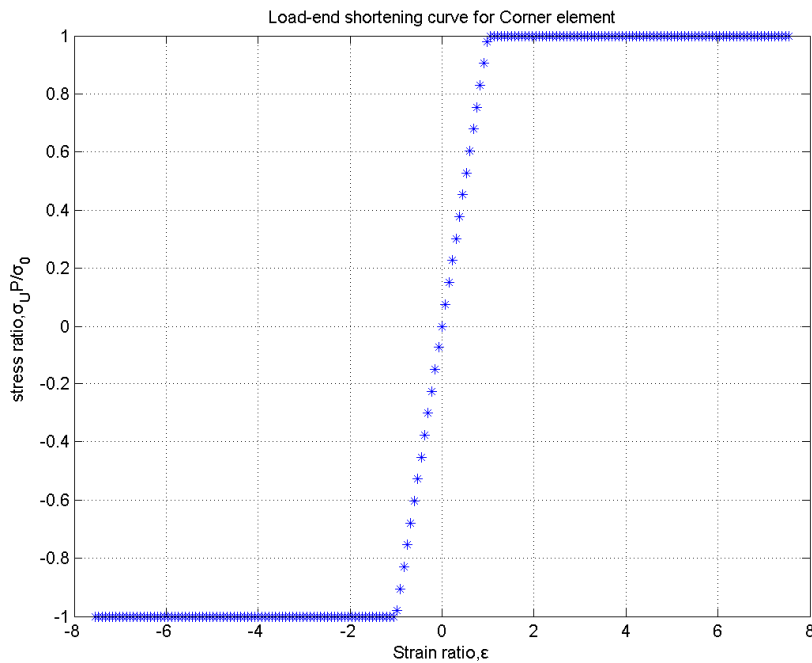


Figure 4.9 Load-end shortening curve for corner element.

4.1.3 Result of ultimate strength

It can be seen in Figure 4.10 when the curvature is in a small range around 0, the material behavior is linear elastic. But starting from 1 and -1 in hogging and sagging, moment-curvature relationship starts to be nonlinear. At this time, a little number of components start to yield, while other components close to neutral axis still follow linear elastic behavior. When the moment-curvature curve reaches a peak value, most of the components at compression side has already reached their critical buckling stress and the occurrence of strength reduction happens in some components. So the moment-curvature begins to drop which follows the elasto-plastic behavior.

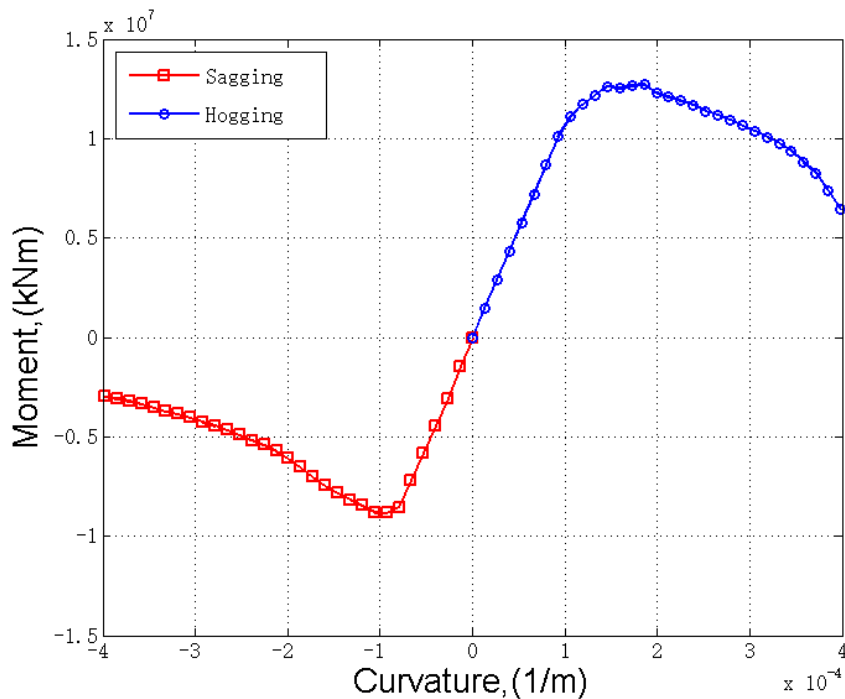


Figure 4.10 Relationship between bending moment and curvature

From the moment-curvature curve, the ultimate strength is around 12,500,000 kNm and -9,000,000 kNm in hogging and sagging condition respectively. Compared with the designed moment 9,900,000 kNm and -7,200,000 kNm for hogging and sagging in harbor, this results calculated by incremental iterative approach is sufficient to cover the maximum designed moment. It means that the designed value is relatively conservative compared with the calculation result from incremental iterative approach.

On the other side, because of the incremental iterative approach only consider one cross section, this value is not accurate enough to represent the entire hull structure in complicated load condition. However, it still can be a reference to evaluate the ship ultimate strength.

In general, the collapse is always firstly occur at the components which are most far away from neutral axis. Due to the stress at neutral axis is 0, a gradient stress distribution will act on the cross-section. Local collapse starts from deck or bottom to the components which are close to neutral axis. Because of the elasto-plastic material behavior, strength of yielded components would remain constant at yielding stress. However, strength of buckled components would reduce due to buckling. So the total

force of the entire cross section would not remain 0. To keep the total force remain 0, neutral axis should move to maintain the force equilibrium. From the Figure 4.11, after the ultimate strength was attained, neutral axis moves to yielding side.

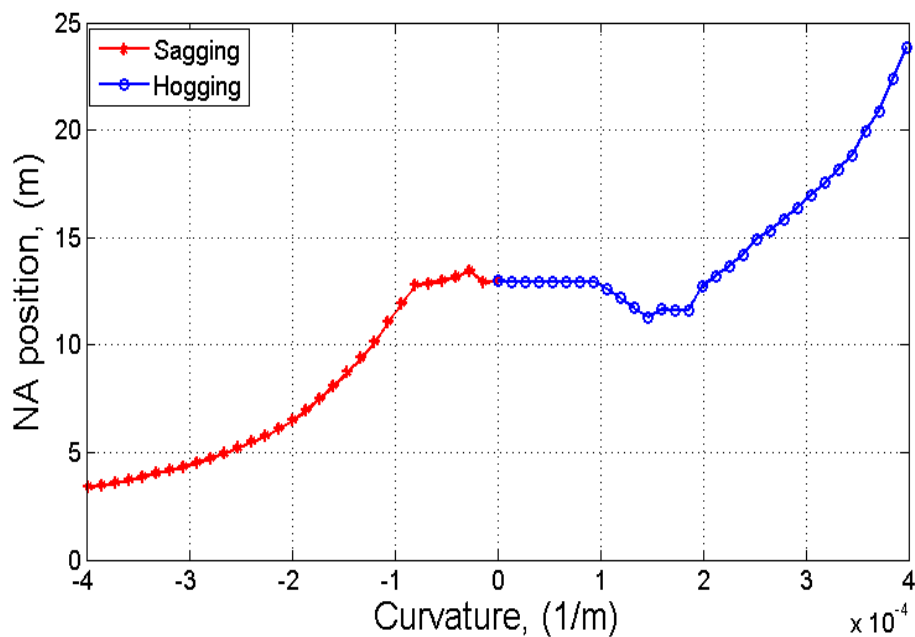


Figure 4.11 Relationship between neutral axis position and curvature

In hogging condition, the cross-section above neutral axis is in tension and beneath neutral axis is in compression. So yielding takes place at deck, while buckling takes place at bottom. When the curvature started to grow from beginning, due to elastic material behavior, the movement of neutral axis position is not obvious. Then after further increase of curvature, deck plate starts to yield and outer bottom plate starts to buckle. The position of neutral axis drops a little. At this time, result from the yielding in deck, the effectiveness of deck plate cannot remain as before. When the neutral axis position value reaches valley, the ultimate strength attained, and entire bottom structure has already buckled. Due to the strength reduction caused by buckling, the neutral axis position move upward quickly after the valley point.

Vice versa in sagging condition, the cross-section above neutral axis is in compression and beneath neutral axis is in tension. So yielding takes place at bottom, while buckling takes place at deck. The direction of neutral axis movement in sagging condition is opposite to that in hogging condition. At the beginning, the position of neutral axis does not change significantly. However, after the ultimate strength has reached, the height of neutral axis decreases in a rapid speed to compensate the strength reduction from buckling.

Finally, the ultimate strength value in sagging condition is smaller than that in hogging condition. This is because bottom and deck is under compression in hogging and sagging condition respectively. The bottom is much stronger in compression load. Compared with bottom plates, deck plates have less stiffeners and less components. Therefore, buckling is much easier to take place at deck than at bottom.

4.2 Buckling analysis

To simplify the analysis, an unstiffened plate in the deck was applied. The material of this plate is elasto-plastic A36 high tensile strength steel. The yielding stress of A36 high strength steel is 355MPa and the tangent modulus is 1000MPa. The plate thickness is 19 mm, which has already minus 3 mm corrosion margin of plate. The length and width of the plate is 5250 mm and 855 mm, which is the space of transvers floor and longitudinal stiffeners respectively, shown in Figure 4.12. In this analysis, one-bay plate model was adopted to simplify the analysis.

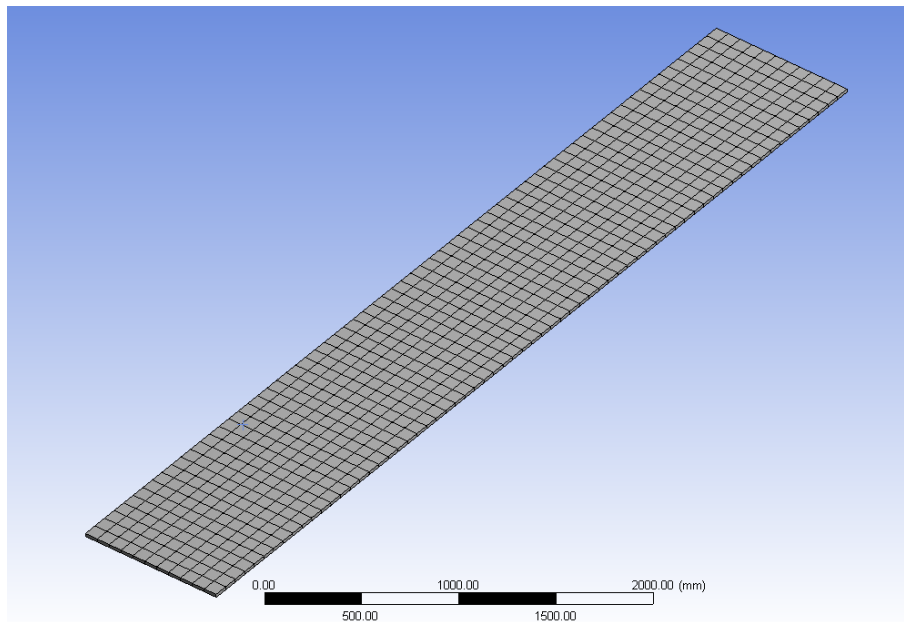


Figure 4.12 An one-bay plate model.

4.2.1 Boundary conditions and Load

In this model, the boundary condition at four edges are all simply support without displacement in Z direction. To simulate the bi-axial compression, the boundary condition at D edge should be no displacement in any direction. And the rest of three edges can be move freely in plane.

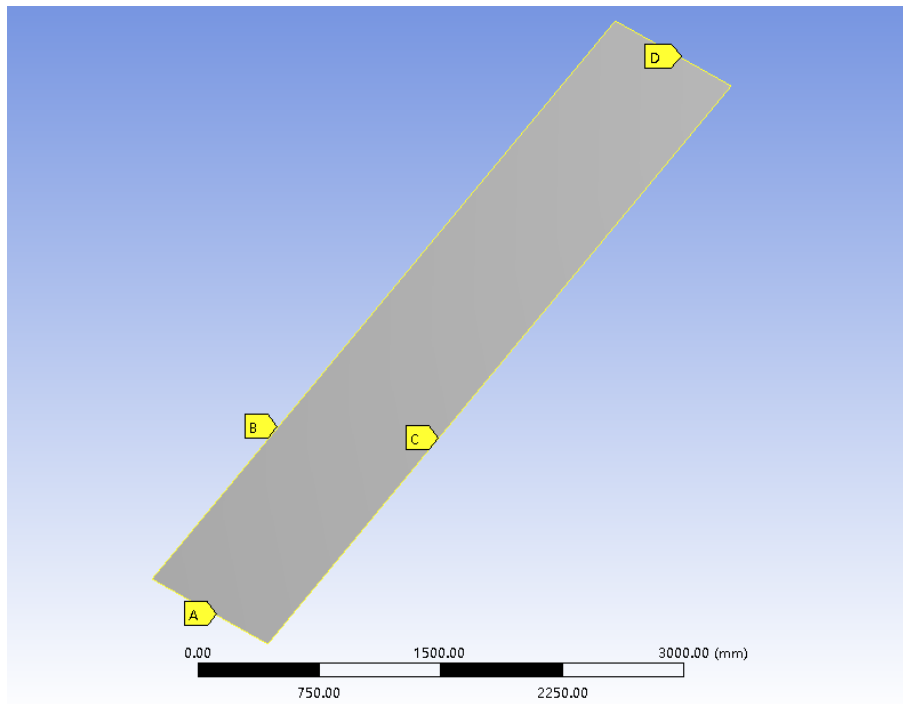


Figure 4.13 Boundary conditions at four edges.

There are three types of acting load in this model. It can be seen in Figure 4.14. A is a compression load acting on one edge. B and C are lateral pressure and a small force acting on the plate surface respectively. As in the buckling analysis, an imperfection of shape is required. The effect of load C is to make a tiny imperfection or initial deflection of the plate surface.

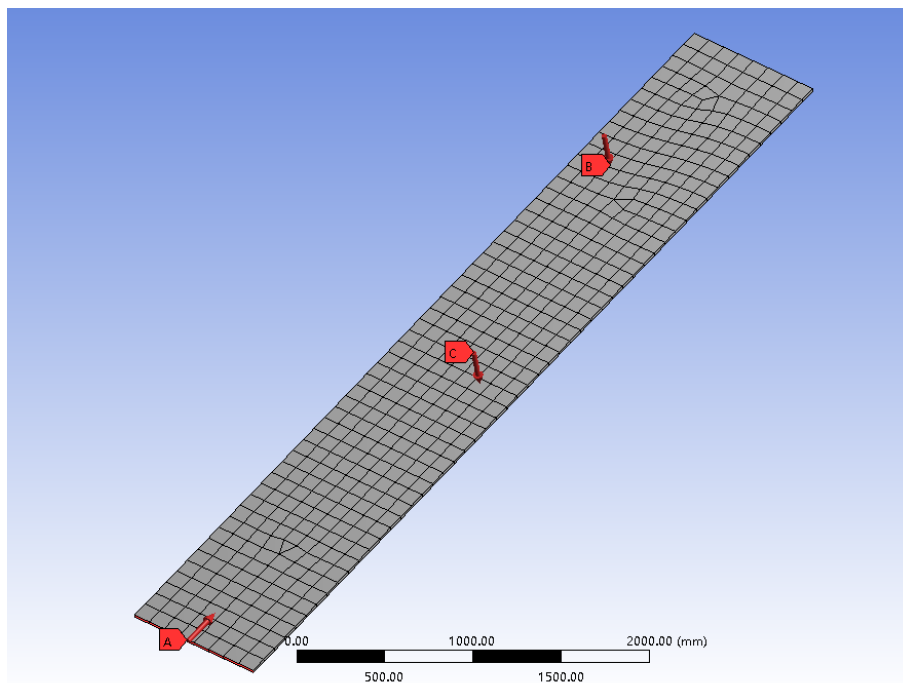


Figure 4.14 Acting load on the plate.

The C load lead to a small deflection which is less than the maximum value and in an allowable range. This initial deflection can be regard as the imperfection of shape geometry.

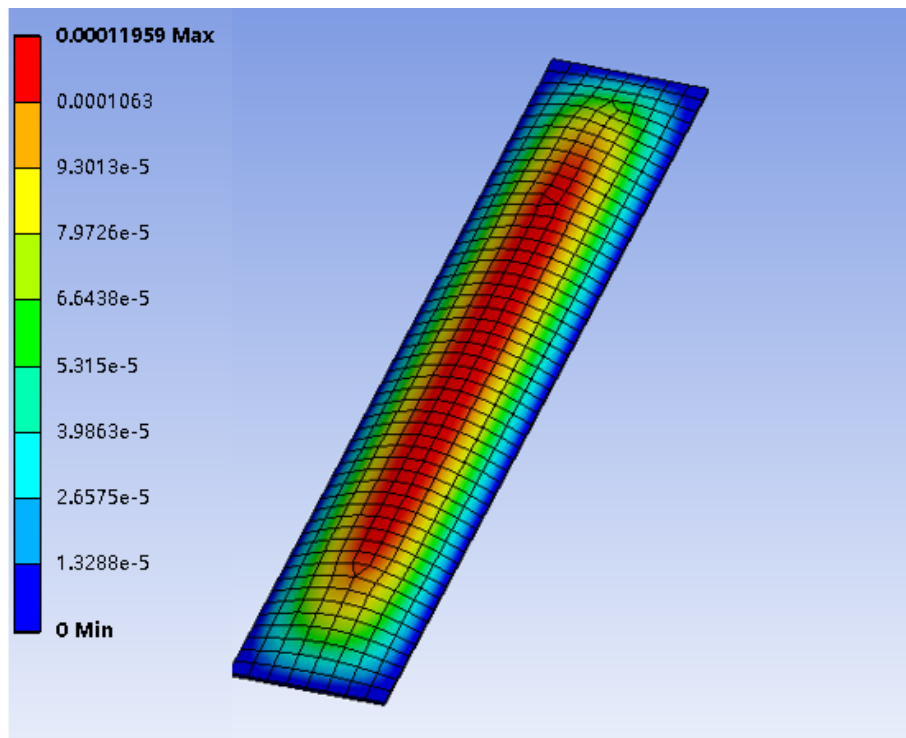


Figure 4.15 Initial deflection of the plate.

The most critical buckling condition can be found after the loads acting on the plate model. In this plate model, the most critical buckling condition can be four half-wave condition in this analysis, in Figure 4.16. As a matter of fact, the half-wave number is determined by the eigenvalue analysis. It can be explained by the combination of different factors, such as geometrical shape, material behavior, boundary conditions and combination of acting loads. If one or several of them are changed, the most critical condition may become other buckling eigen-modes.

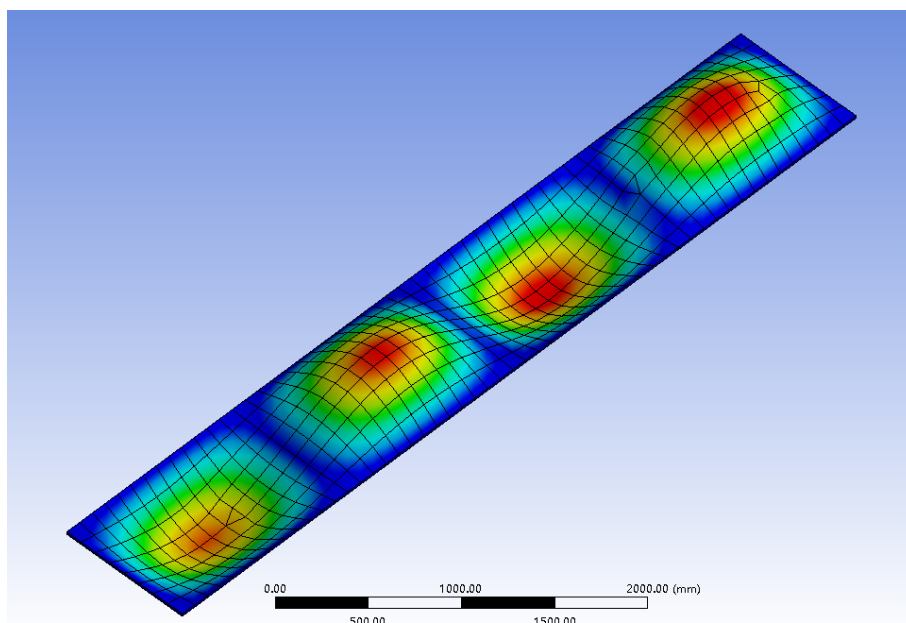


Figure 4.16 Deformation shape for the most critical buckling mode with four half-waves.

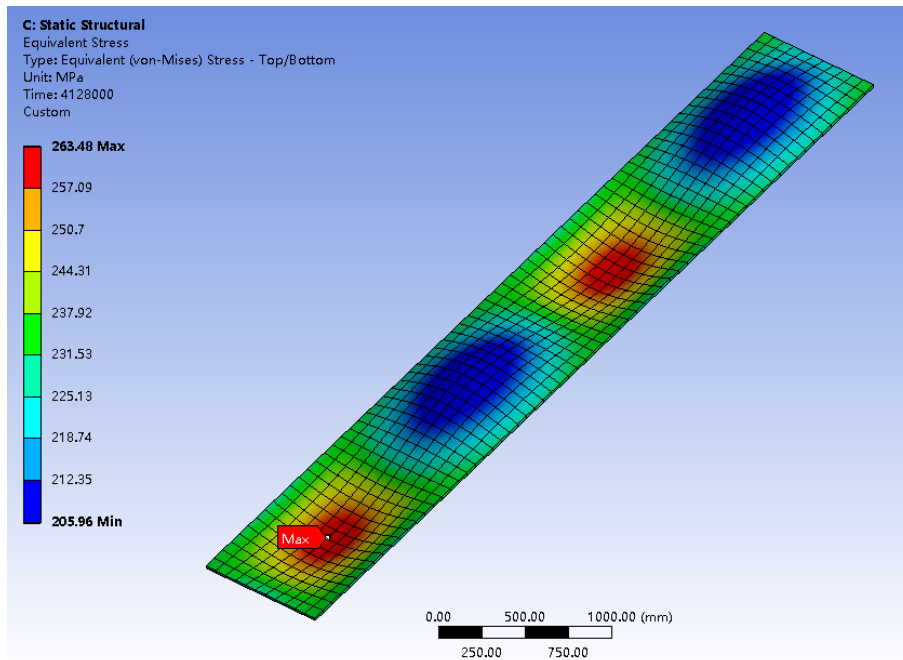


Figure 4.17 Von-Mises stress distribution when the plate starts to buckle.

4.2.2 Result of buckling analysis

As the load is a linear function of time in ANSYS, the load will increase by the time step. Finally, the entire plate was buckled due to the compression load, Figure 4.18. The behavior of plate material becomes plastic. Then some parts of the plate start to yield.

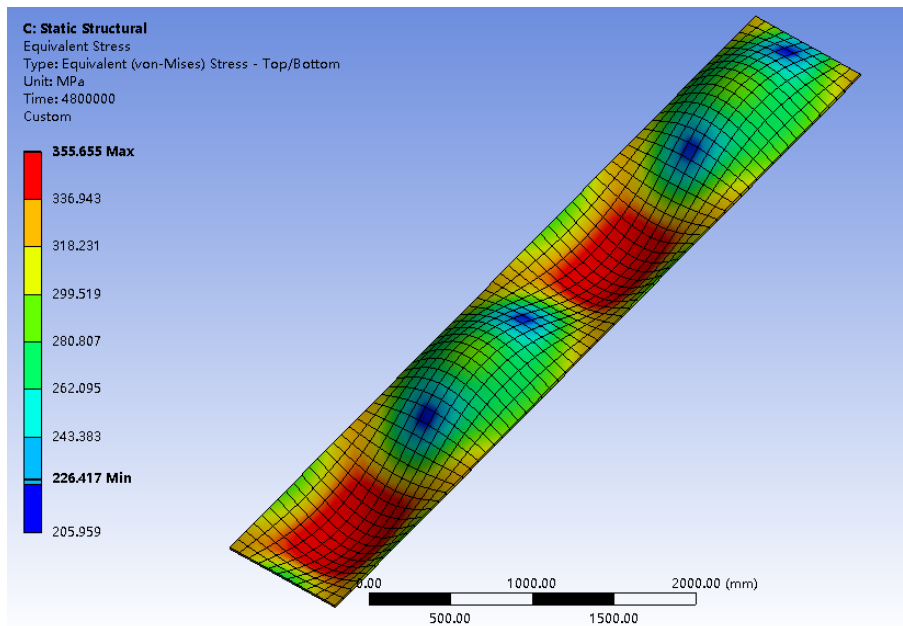


Figure 4.18 Deformed shape and the Von-Mises stress distribution of the plate.

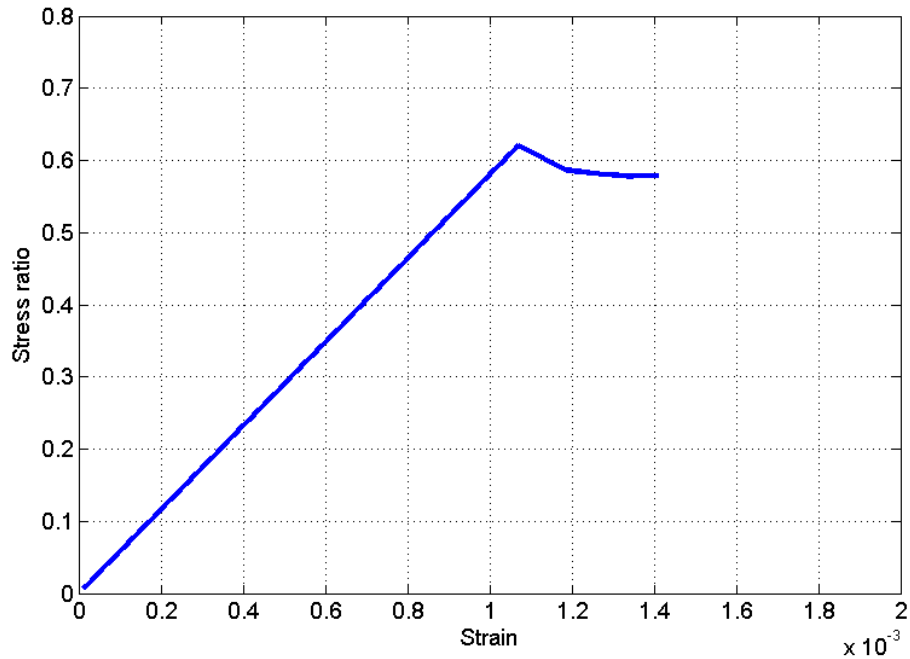


Figure 4.19 Stress ratio versus strain curve

The stress ratio is the ratio between applied stress and yielding stress. The applied stress is caused by the axial compression load. In Figure 4.19, the plate material act as elastic firstly until it starts to buckle. The critical buckling stress of this plate is approximate 220 MPa which is the peak value for the applied stress. When the applied stress reach a peak, it starts to drop and converge around 210 MPa. Compared with the critical buckling stress for this plate in common structure rules, the value from FEM calculation is 4.5% smaller than the rule result, which means if FEM is applied in buckling analysis, the result can be accurate and more close to the real buckling condition.

5 Crack propagation estimation in Franc2D/3D

The crack growth speed and relevant structural behavior will be investigated in this chapter. The simulation will be implemented in three different commercial software. The comparison and benchmark study will be carried out to define the difference between aforementioned programs.

In this study, the crack starts with an initial crack, a_0 , then crack propagates until the crack length reaches to a given length (60mm in Franc2D and 3D, about 20 mm in ABAQUS). During the propagation, growth rates follow the crack growth model Paris law. Different methods mentioned in Section 3 are performed in the analysis; the procedures and results will be described in the following sections.

5.1 Introduction of FRANC2D and FRANC3D

As regards to determine the stress intensity factors, FRANC2D version 3.1 and FRANC3D version 6.0 were selected to find out SIF values. These two programs are developed by Cornell University and Cornell Fracture Group. FRANC2D, also known as two-dimensional Fracture Analysis Code incorporates the 2-D problems with arbitrary crack geometries based on the Finite Element Method.

While FRANC3D can analysis three-dimensional fracture problems based on boundary element method. The Displacement Correlation Method is used in this program to determine the stress intensity factors. Propagation direction is evaluated at discrete points along the crack front using 2-D plane strain equations that is applied in the plane normal to the crack front tangent. The crack growth magnitude is calculated using simple expressions such as Paris' model with a supplied maximum extension. In total, the procedure in FRANC3D can be summarized as:

- 1) Accurate extraction of stress intensity factors along an 3-D crack front,
- 2) Determination of the direction of extension and the crack growth increment based on the stress intensity factors,
- 3) The effect of neighboring features.

5.2 Estimation in FRANC2D

5.2.1 Analysis procedures and models

A two-dimensional longitudinal stiffener is considered herein to determine the crack path and simulate crack growth. The cross section profile of the stiffener is a 500 mm height and 10 mm thick. The length of the stiffener is 3000 mm and connected with an attached plate at the middle point along the longitudinal direction. Two types of width (200 mm and 300mm) of the attached plate are analyzed, as shown in Figure 5.1. A 50 MPa tension load is applied at left and right ends of the stiffener. The top free surface of the attached plate is fixed in three translation degrees of freedom, while the left and right free surface of the base plate is fixed in vertical and transverse translation degrees of freedom. ASMT A36 steel is commonly used in marine industry, and the material properties are given in Table 5.1.

Table 5.1 The material data of ASMT A36 steel.

C	m	E MPa	ν	σ_y MPa	K_{IC} mm/cycle $(MPa\sqrt{mm})^m$	J_{IC} N/mm
5.21e-13	3	210000	0.3	250	2977	42.2

The study cases is combined with three cases, 1) a analytical case (without attached plate), 2) the width of the attached plate equals to 200 mm and 3) the width grows to 300 mm. Table 5.2 illustrates the detail of the geometry information.

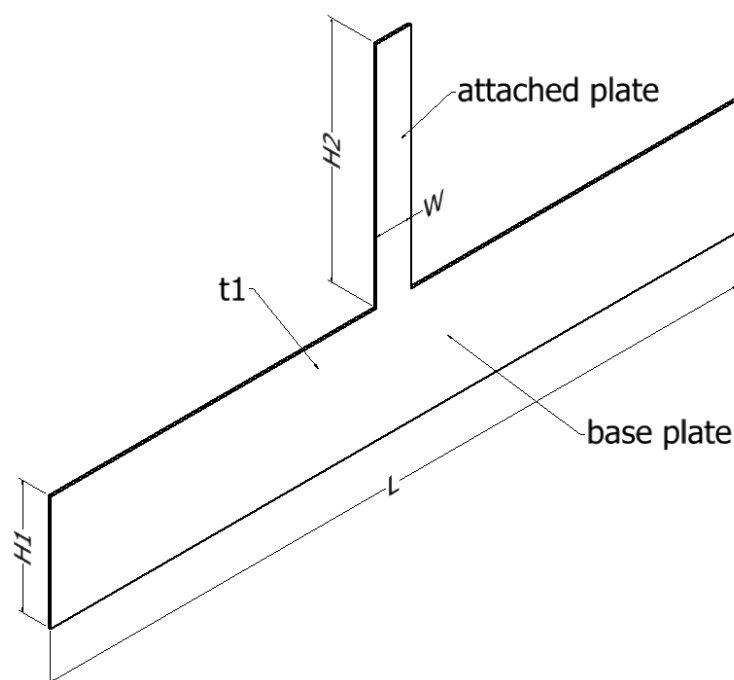


Figure 5.1 The geometry profile of 2-D case.

Table 5.2 Difference of cycle counting between different geometries.

Case No.	Case name	W mm	L mm	H1 mm	H2 mm	t1 mm
1	Analytical	--	3000	500	1000	10
2	W = 200	200	3000	500	1000	10
3	W = 300	300	3000	500	1000	10

The meshes of the analyzed model were implemented with the relevant preprocessor (Casca). The meshed model was created as shown in Figure 5.2. The finest mesh size of 1 mm around the crack tip region limits the lower bond of mesh densities, in contrast the coarsest size reaches to 5 mm. The Paris law equation was used to determine the crack growth rates with the constants in the equation listed in Table 5.1. All of the

material properties that did not apply to the crack analysis in this thesis were left at default values. FRANC2D processed crack growth by increasing the crack length with a user defined value, 5 mm, until the crack length reached to 60 mm. The stress intensity factors for a bitterly crack length was determined by an interpolation in MATLAB based on the data retrieved from FRANC2D, by using the cubic spline interpolation tool – *csapi()* and *fnval()*. Cycles were counted over each increment for the final estimate of fatigue fracture life in MATLAB codes following the Paris law, which is shown in Appendix B.

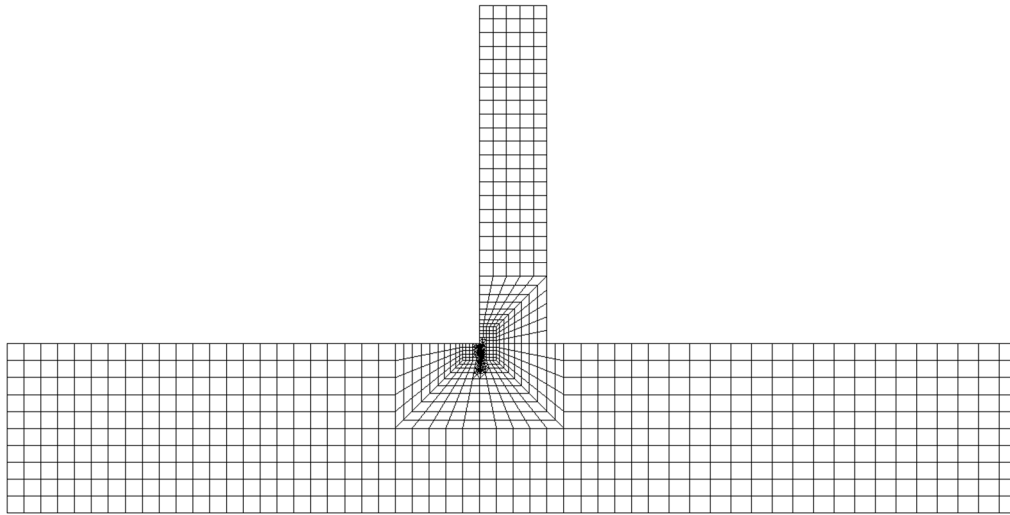


Figure 5.2 The two-dimensional meshing scheme.

The stress intensity factor is an important parameter of elaborating the crack status. The load independent factor, geometry factors, are then investigated. The geometry factor of analytical model was given by empirical formulations (Anderson, 1994):

$$F\left(\frac{a}{w}\right) = 1.22 - 0.231\left(\frac{a}{w}\right) + 10.550\left(\frac{a}{w}\right)^2 - 21.710\left(\frac{a}{w}\right)^3 + 30.382\left(\frac{a}{w}\right)^4 \dots \quad (5.1)$$

where a is the crack length and w means the height of the stiffener. The reverent stress intensity factor was then calculated by Equation 5.2 (Moreira *et al.*, 2009).

$$K_I = \sigma\sqrt{\pi a}F\left(\frac{a}{w}\right) \quad (5.2)$$

In order to demonstrate the difference between each geometry, the Root Mean Square Difference (RMSD) was calculated as Equation 5.3 and the maximum difference calculation is presented in Equation 5.4. The value n represents the total number of crack length used to calculate cycle numbers.

$$RMSD = \sqrt{\frac{1}{n} \sum_{k=1}^n \left(\frac{\text{Cycles in current geometry}}{\text{Cycles in analytical geometry}} - 1 \right)^2} \times 100\% \quad (5.3)$$

$$\% \text{ Diff} = \max \left(\frac{\text{Cycles in current geometry}}{\text{Cycles in analytical geometry}} - 1 \right) \times 100\% \quad (5.4)$$

5.2.2 Results in FRANC2D analysis

Comparison of geometry factors

From Figure 5.3 it can be seen that the analytical case shows a totally different trend compared with the other two geometries. For the analytical case, the geometry factor keep rising as the crack grows, the factors of No.2 and 3 cases are dropping instead. What is more, the geometry factor of geometry No.3 shifts up almost parallel with the No.2 geometry. That implies that the larger width of the attached plate gives rise to a bigger geometry factor at each crack length proportionally.

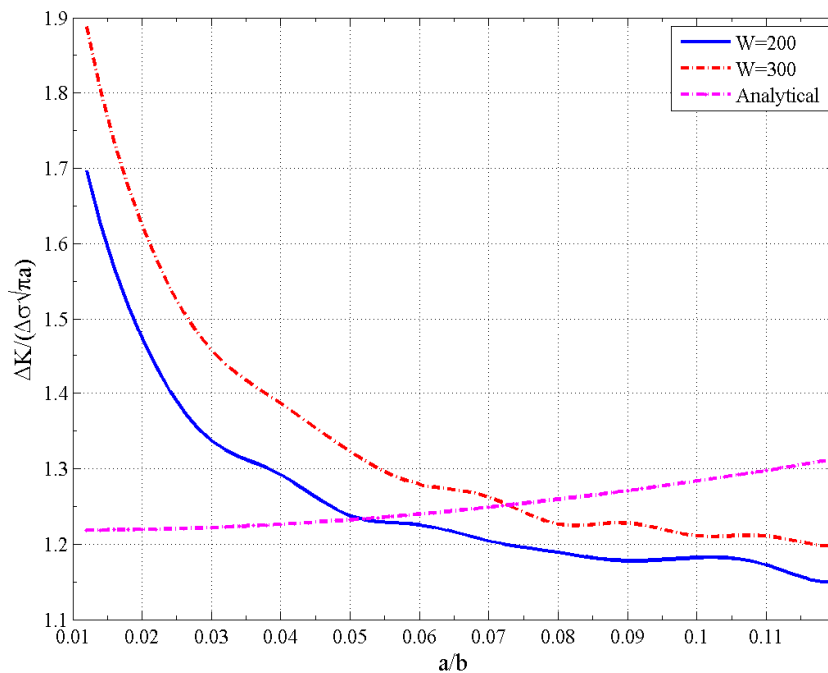


Figure 5.3 Comparison of geometry factors, $F\left(\frac{a}{w}\right)$, during the crack propagation.

Comparison of crack propagation speed

Figure 5.4 plots the cycle number counting versus crack length curves in three different geometry cases. In the figure, the crack grow from the initial crack length of 5 mm to 60 mm. It is obviously that the extra attached plate gives rise to a faster crack growth speed, in other word the wider attached plate the higher speed will be retrieved. On this account the attached plate will accelerates the crack propagation speed as the increase of width of the attached plate.

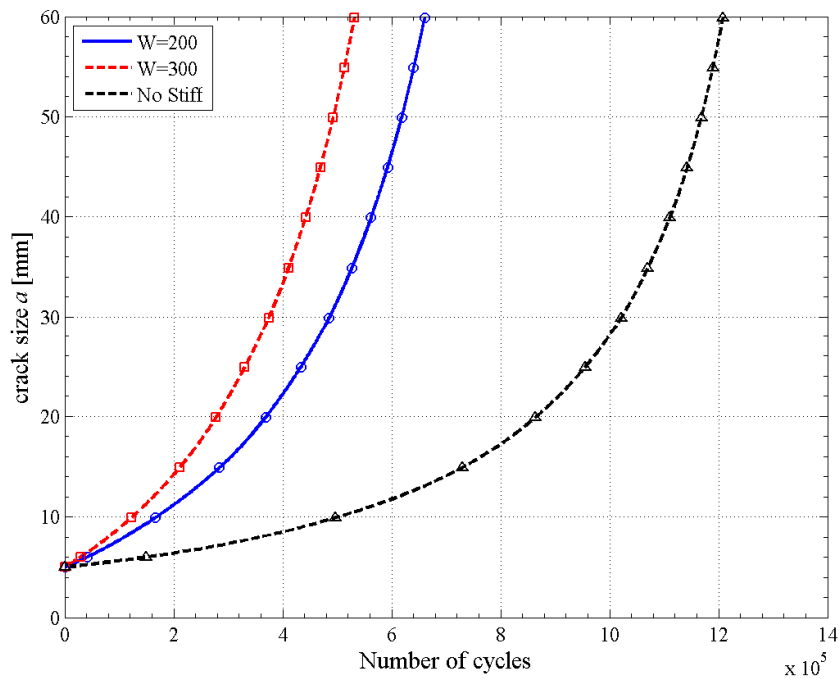


Figure 5.4 Comparison of cycle counting with crack propagation for different geometries.

Table 5.3 shows the difference between three geometries. For the geometry No. 2 case (W=200 mm), the crack grows about 54% faster than the analytical case, and the maximum difference approaches to 74.5%. On the other hand, the maximum difference in the geometry No. 3 case (W=300 mm) is about 82% with the RMSD value of 64.6%. Figure 5.5 plots the difference of cycle number counting.

Table 5.3 Difference of cycle counting between different geometries.

Case No.	Case name	Cycle % Difference	
		Max.	RMSD
1	Analytical	--	--
2	W = 200	-74.5	54.3
3	W = 300	-81.7	64.6

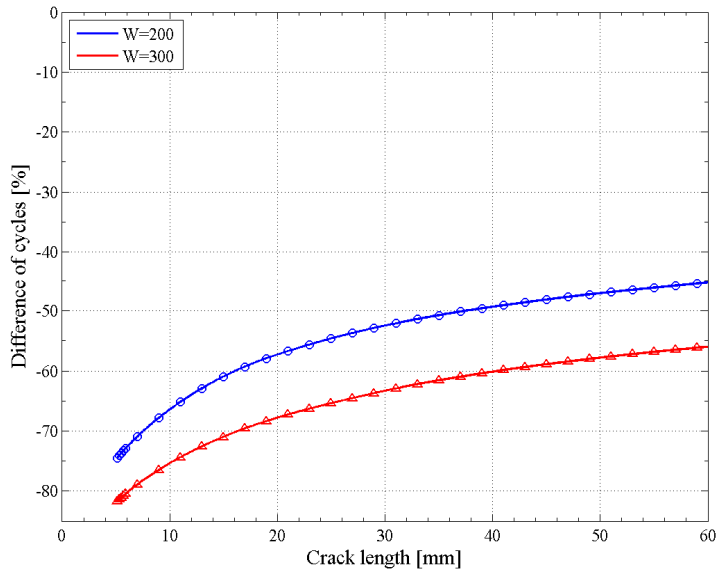


Figure 5.5 Difference in cycle counting during crack propagation for No.2 case and No.3 case compared with analytical case (No. 1 case).

5.3 Estimation in FRANC3D

5.3.1 Analysis procedures and models

Three-dimensional longitudinal stiffener is analyzed in FRANC3D to find out the crack propagation behaviors. The geometry is similar to the two-dimensional case, except for the inverse angle bar is used instead of flat bar. The geometry dimension is illustrated in Table 5.4 and Figure 5.6. Aforementioned (in Section 5.2) loads and boundary conditions were applied and the material properties used for analysis are given in Table 5.1.

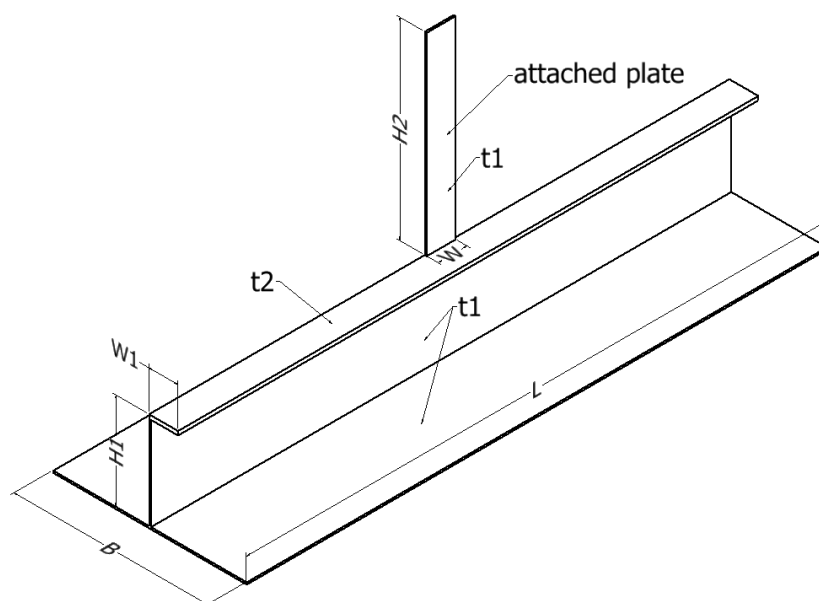


Figure 5.6 The crack tip meshing template in FRANC3D.

Table 5.4 Geometry parameters of study case in FRANC3D.

Case No.	Case name	W mm	W1 mm	L mm	B mm	H1 mm	H2 mm	t1 mm	t2 mm
1	W = 200	200	150	3000	1000	500	1000	10	20
2	W = 300	300	150	3000	1000	500	1000	10	20

The modeling and meshing of the structure were implemented in ABAQUS, and the quadratic tetrahedron elements were selected since the mid-side nodes in this type elements is needed. In order to reduce the computation time, the whole model was divided into two parts: the region where was in the vicinity of the crack was defined as local model; the rest of the mode was defined as the global model. The program FRANC3D meshed the model and defined an initial circle crack near the intersection corner of the attached plate and inverse angle bar, as illustrated in Figure 5.8. As mentioned in Section 5.2.1, the crack was manually grown from a_i to a_c . At each increase, the FRANC3D required a re-meshed model to match the new geometry. A circular partition strategy, which is defined in FRANC3D as a template as illustrated in Figure 5.7a, was used to evaluate the stress intensity factors and J-integral by using contour integrals method.

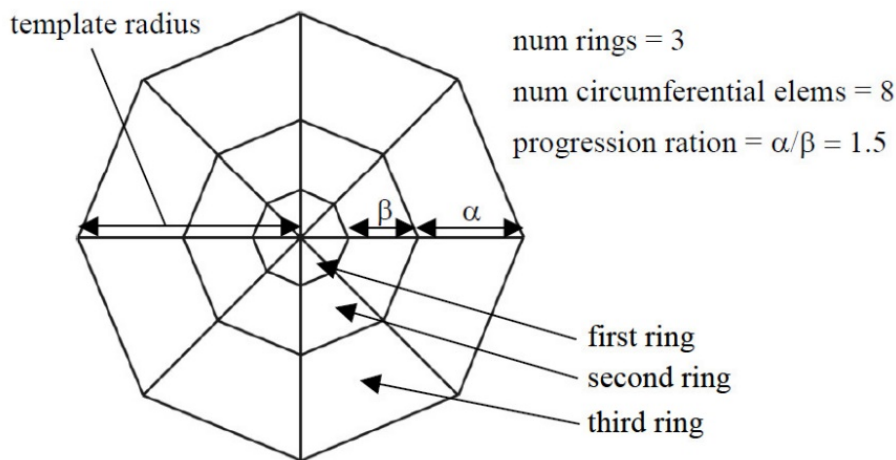


Figure 5.7a The example of crack tip meshing template in FRANC3D (Fracture Analysis Consultants Inc, 2011).

SIFs can be extracted from the J for a LEFM problem using Equation 5.5, while the direction of the propagation was determined by the "kink" angle, which was defined by the amount that the crack will deviate from the self-similar direction measured in a plane perpendicular to the crack front. Figure 5.7b demonstrates the definition of the kink angle, which is calculated by following the max tensile stress algorithm (MTS) mentioned in Section 3.2.1. The resulting of mesh is shown in Figure 5.8.

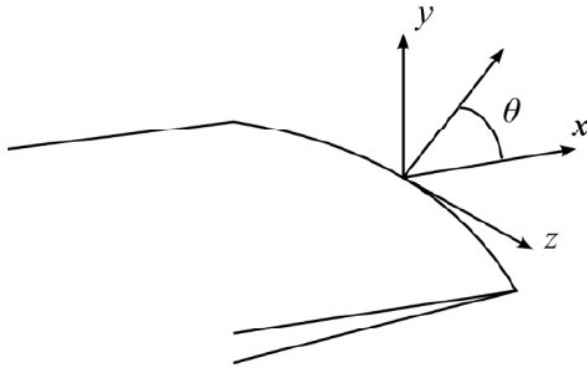


Figure 5.7b The definition of the "kink angle" θ (Fracture Analysis Consultants Inc, 2011).

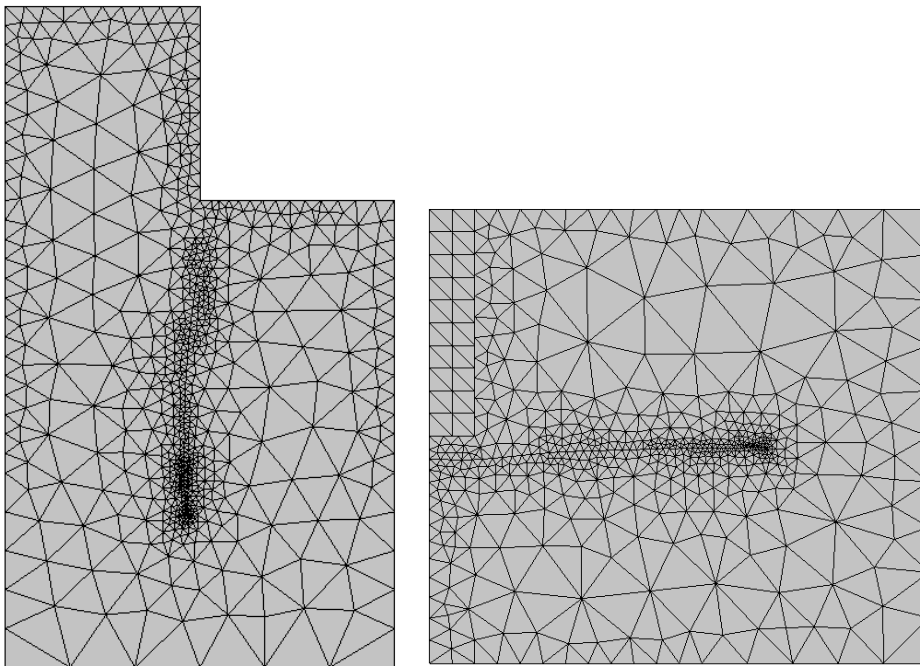


Figure 5.8 The meshed geometry No.2 in FRANC3D.

$$J = \mathcal{G} = \frac{1}{E} (K_I^2 + K_{II}^2) + \frac{1}{2G} K_{III}^2 \quad (5.5)$$

There was a distribution of K values along the crack front in a three-dimensional problem, and there might not be an obvious crack dimensions that uniquely characterized the crack length. In order to solve these issues, a user defined path was selected to describe the crack path and relevant stress intensity factors. Because the K values are numerical results, they tend to be "noisy" and frequently show spurious behavior near free surfaces where the assumptions and numerical techniques used to compute the K can break down. Due to this reason, the 10% inside of the free surface path is selected, which is shown in Figure 5.9.

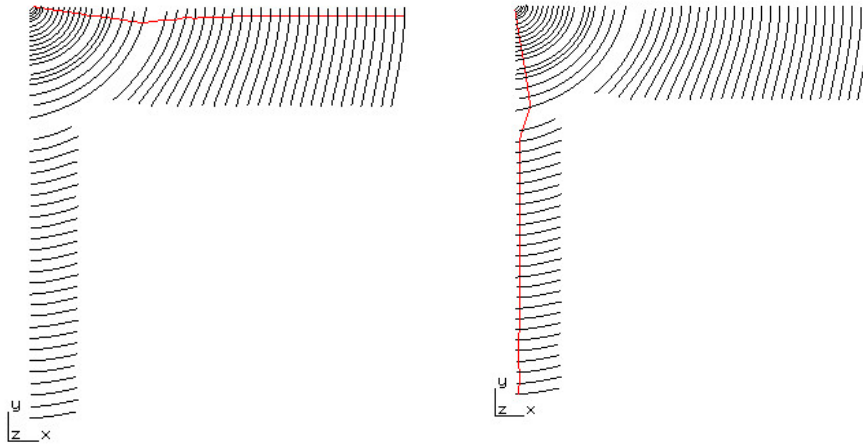


Figure 5.9 The user defined paths of the crack during crack propagation. The left figure shows the selected path on flange plate; the left figure illustrated the path on web plate.

Once the SIFs were extracted at each crack increase, a cycle by cycle counting method was implement based on the Paris Law, which is discussed in Section 3.2. A cubic spline interpolation technique was used to plot the SIFs versus crack length curve, where the stress intensity factors for a given arbitrary crack length can be extracted from. FRANC3D computes separate stress intensity factors for all three modes of fracture (K_I , K_{II} , and K_{III}), however only one stress intensity factor range is required for calculating the crack growth rates. In this analysis, the ΔK can be expressed as $K_{max} - K_{min}$ in each cycle. Because the $K_I \gg K_{II}$ and K_{III} , then mode one stress intensity factors is used to computing the maximum and minimum defective stress intensity factors. All of above mentioned relation of stress intensity factors are expressed in Equation 5.6. According to this algorithm, codes were programed in MATLAB to plot the crack length versus cycle number curve, which is shown in Appendix B.

$$\begin{aligned}
 K_{max}^{equivalent} &= K_{I,max} \\
 K_{min}^{equivalent} &= K_{I,min} \\
 \Delta K^{equivalent} &= K_{max}^{equivalent} - K_{min}^{equivalent}
 \end{aligned} \tag{5.6}$$

The complexity of three-dimensional problem is that the additional flange plate give extra elastic stiffness than two-dimensional case. In order to inventive the different crack propagation behaviors on these plate receptively, the difference analysis was carried out. The RMSD and maximum difference are determined in Equation 5.7 and 5.8.

$$RMSD = \sqrt{\frac{1}{n} \sum_{K=1}^n \left(\frac{\Delta K \text{ on web plate}}{\Delta K \text{ on flange plate}} - 1 \right)_k^2} \times 100\% \tag{5.7}$$

$$\% \text{ Diff} = \max \left(\frac{\Delta K \text{ on web plate}}{\Delta K \text{ on flange plate}} - 1 \right) \times 100\% \tag{5.8}$$

5.3.2 Results in FRANC3D analysis

Stress intensity factor history

Figure 5.10 shows the stress intensity factors history on the web plate of the No.2 case (The result on No.1 case are shown in Appendix A.). Each horizontal line in Figure 5.10 means the SIF values along the crack front at each step. It's obviously that the stress intensity factor increase as crack propagation. In addition, the SIF values varies slightly along the crack front, after the crack propagates beyond the attached plate influencing region, the SIF values start to keep even.

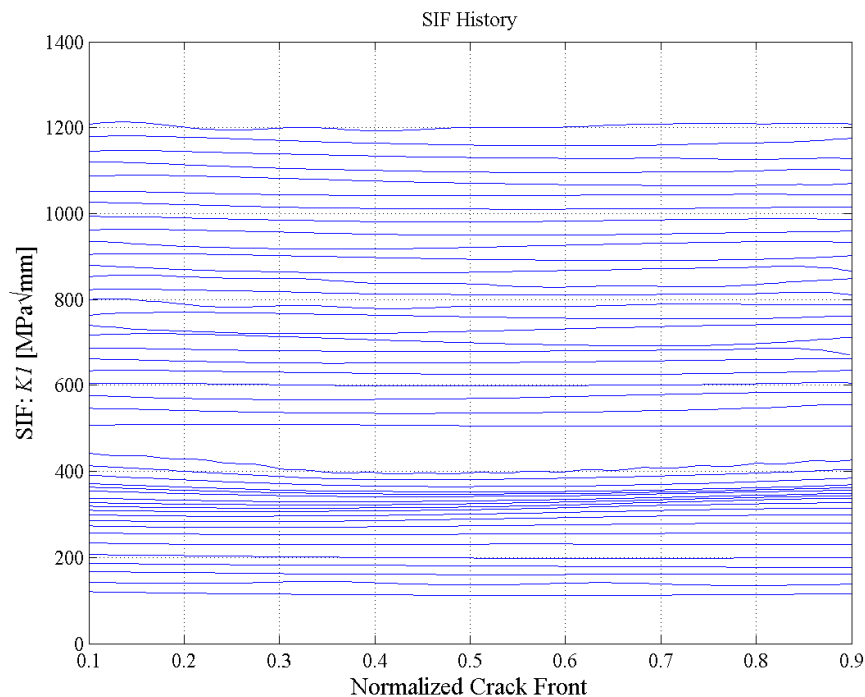


Figure 5.10 The stress intensity factor history on web plate at each step of propagation (No.2 case).

Comparison of geometry factors between flange and web plates (No.2 case)

The geometry factor curves on flange and web plates, in Figure 5.11, demonstrate that factors keep dropping down from the initial crack length to about 20 mm length, then on both flange and web plates, the geometry factors rise up as crack length increasing. The phenomenon on the dropping stage agrees with the observation in two-dimensional cases. After the cracks grow beyond 20 mm, the behavior of cracks propagate turns to be similar to the analytical case in two-dimensional analysis.

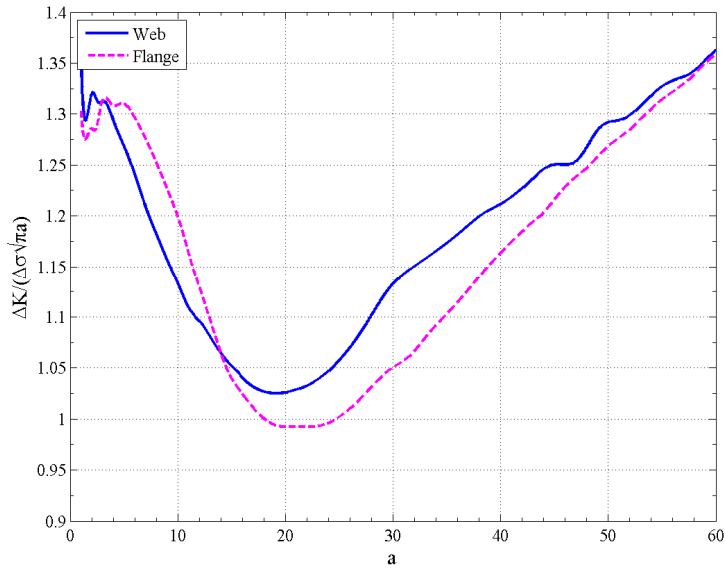


Figure 5.11 Comparison of geometry factors, $F(a)$, during the crack propagation (No.2 case).

Figure 5.12 plots the difference of stress intensity factor range between web and flange plates. The SIF range value on web is bigger than flange when the curve is above zero and vice versa. The maximum difference is about 8% and the RMSD is about 4%, which is smaller than 5%. It implies that the difference between them turns to zero as the increase of crack length. Consequently both of web and flange plate can determine the fracture toughness of the inverse angle bar. In other word, one can simplifies the problem and keep eyes only on web or flange plate only. The results in No.1 case are shown in Appendix A.

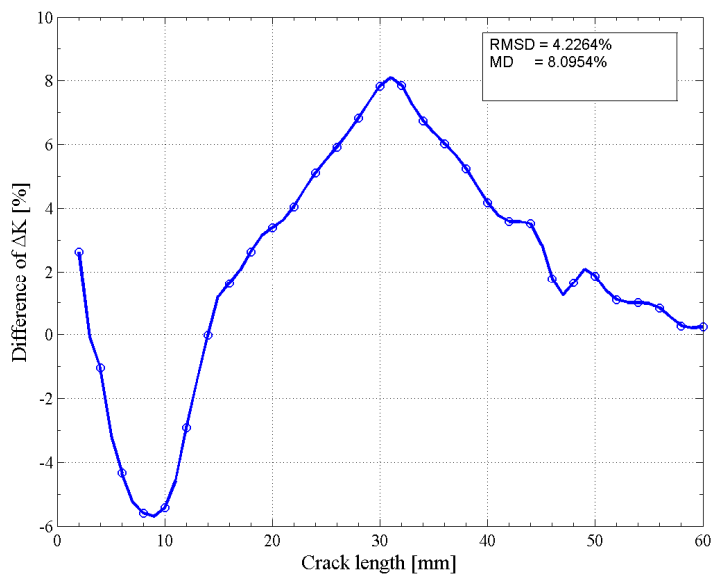


Figure 5.12 Difference of stress intensity factor ranges between flange and web plates (No.2 case).

Comparison of crack propagation speed between flange and web plates (No.2 case)

The Figure 5.13 and 5.14 verifies the aforementioned conclusion. The cycles counting number versus crack length curves on web and flange plate match each other very well. The difference of cycle numbers between them shows that the RMSD is only 2% when the crack grows to 60 mm.

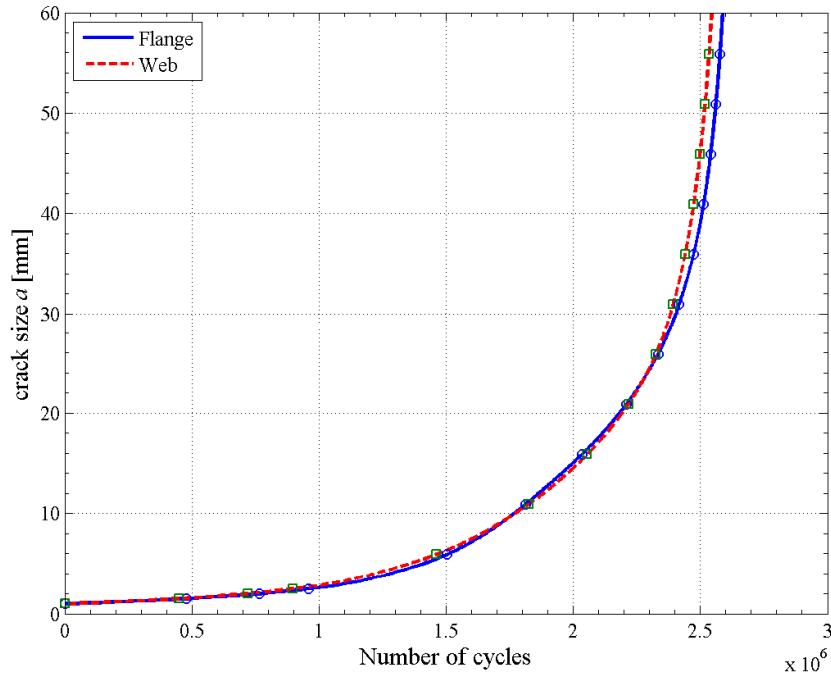


Figure 5.13 Comparison of cycle counting with crack propagation for flange and web plates (geometry No.2 case).

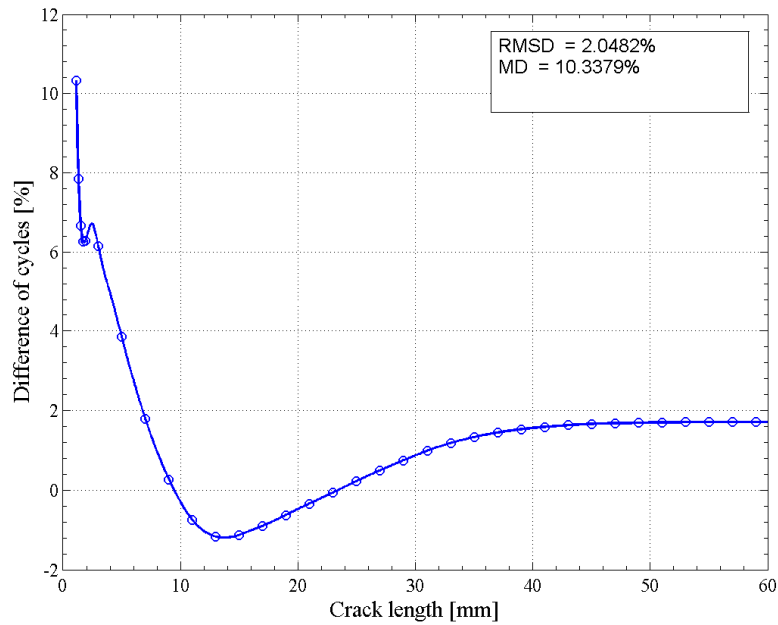


Figure 5.14 Difference of cycles counting number between flange and web plates (geometry No.2 case).

Comparison of crack propagation speed on web plate between No.1 and No.2 cases

Recalling the result from two-dimensional case, the wider attached plate will give rise to a higher crack growth speed. This result works well in three-dimensional case as well. Figure 5.15 proves this phenomenon, moreover the RMSD value in Figure 5.16 shows the 300 mm width attached plate accelerates the crack propagation speed about 27% than 200 mm case. However it's almost three times larger than the value obtained in two-dimensional case.

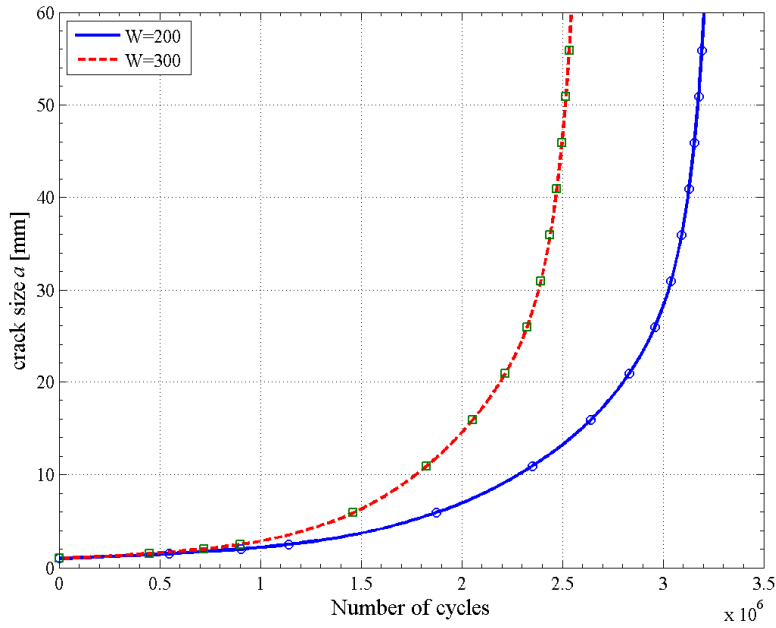


Figure 5.15 Comparison of cycle counting during crack propagation on web plate between No.1 and No.2 cases.

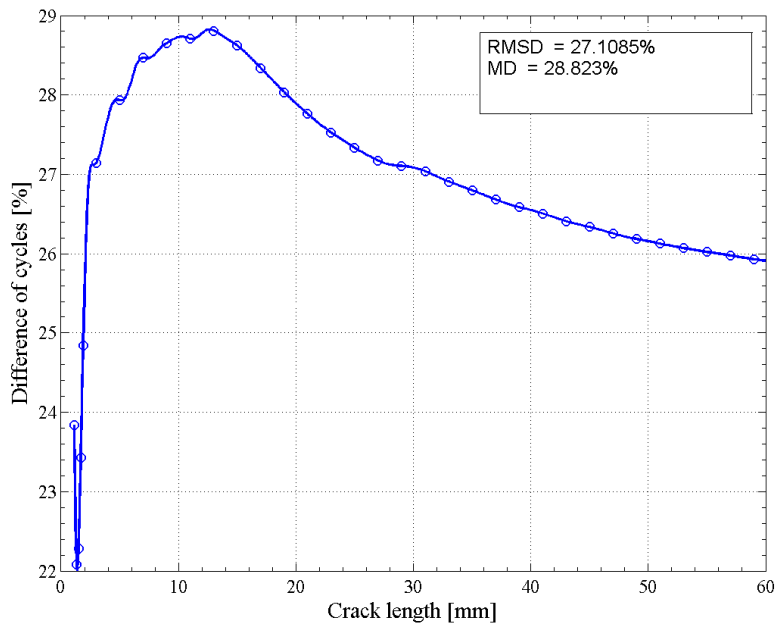


Figure 5.16 Difference of cycles counting during crack propagation on web plate between No.1 and No.2 cases.

Comparison of crack propagation path on web plates between No.1 and No.2 cases

In Figure 5.17, the cracks on web plate are presented. In both No.1 and No.2 cases, the cracks turn close to the direction where the attached plate locates, and then the cracks show the tendency of growing vertically. The wider attached plate pulls the crack further from the initial location.

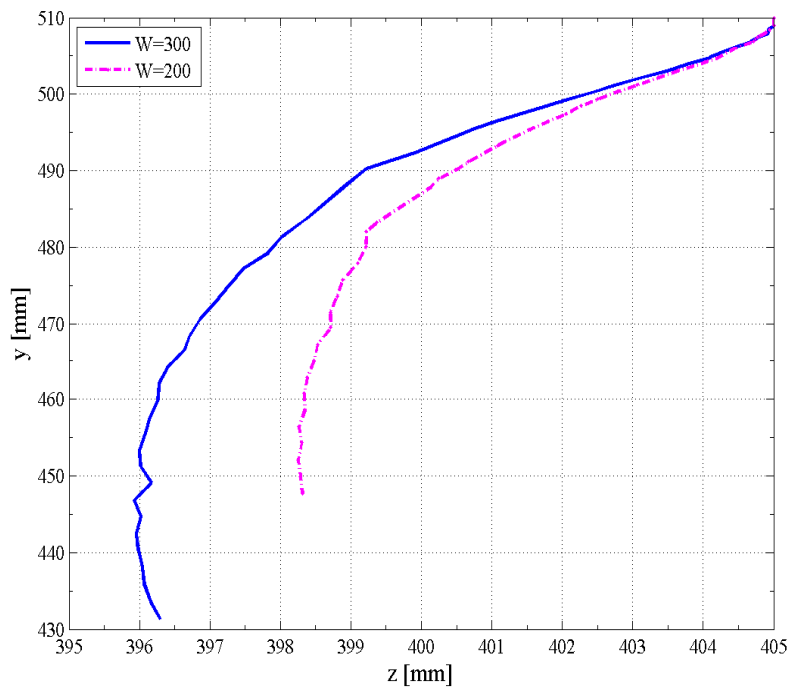


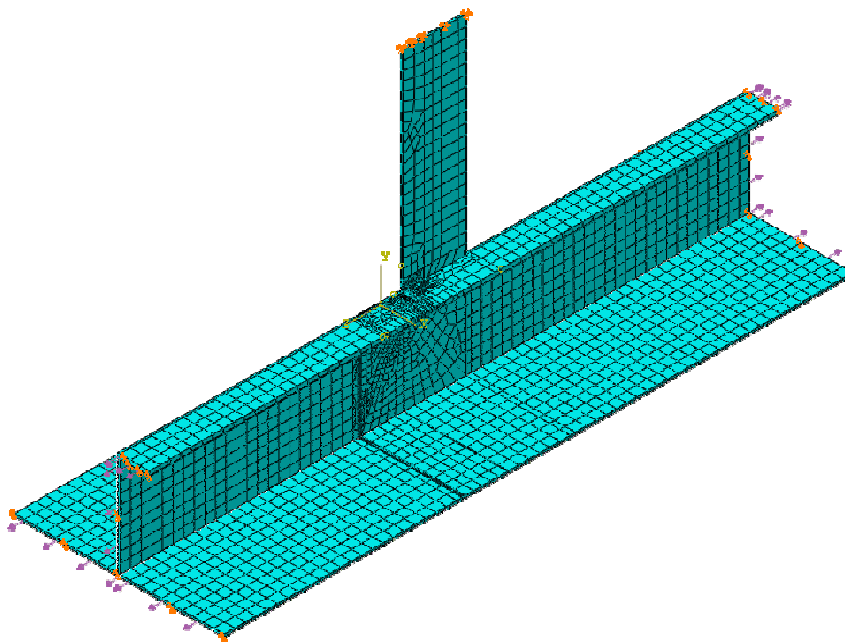
Figure 5.17 Comparison of crack growth path on web plate between No.1 and No.2 cases.

6 Crack propagation estimation in ABAQUS (XFEM)

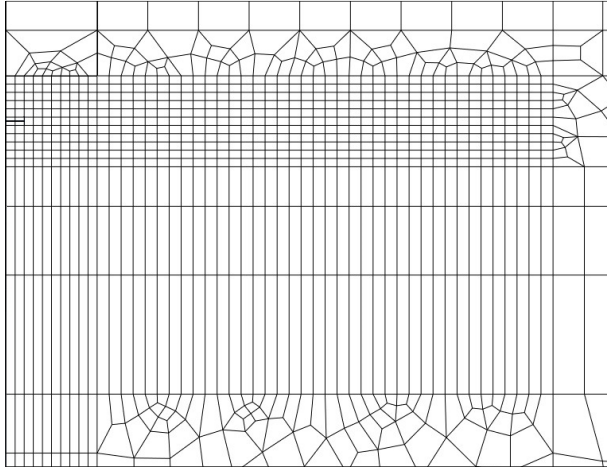
6.1 Analysis procedures and models

The XFEM based directly low-cycle fatigue analysis was carried out to evaluate the ability of crack propagation. Being different from the conventional FEM fracture analysis, the XFEM allows a crack to propagate along a solution dependent path without mesh dependence. Because the crack tip asymptotic functions is ignored when the crack is propagating in a XFEM analysis, the stress intensity factors and strain energy release rates cannot be calculated in this analysis. However the ABAQUS allows the output of energy release rate, and the Equation 3.13 gives the possibility to convert the energy release rate to stress intensity factor. Due to the time limitation and expensive computation power, the XFEM analysis was only carried out in No.2 case herein.

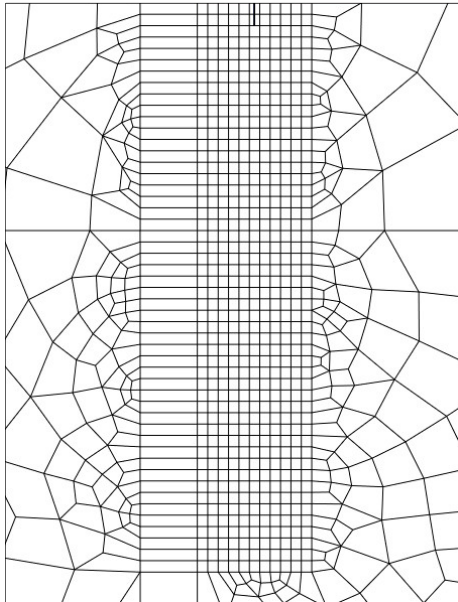
The whole mode consists with two parts: a three-dimensional solid part modeling the geometry of No.2 case mentioned in FRANC3D analysis (in Section 5.3); and a three-dimensional shell part representing the initial crack. The focused meshing strategy was applied to maximize the number of elements in the vicinity of crack propagation zone while reducing the mesh density elsewhere. This strategy will help to obtain a converged result and reduce the computation time. In Figure 6.1, which depicts the partitioning scheme, the minimum element size is 1 mm while the maximum size reaches to 50mm. In the enrichment elements region where the crack was placed, the C3D8 elements were selected for a better accuracy. The other geometry were meshed with C3D8R elements..



a) Boundary conditions and applied loads with the representation of global meshing



b) Focused meshing scheme in vicinity of enriched region on flange plate.



c) Focused meshing scheme in vicinity of enriched region on web plate.

Figure 6.1 Meshing scheme of model and boundary conditions setting in a XFEM analysis.

The analysis was carried out under two steps: a static general step and a direct cyclic step. The loads rise up to σ_{max} at the end of static step then the cyclic load will oscillate between σ_{max} and σ_{min} . The loading amplitude curve is shown in Figure 6.2. It can be seen that the cyclic load follows a sinusoidal curve, which can reduce the stabilization ratios compared to a triangular shaped curve. In addition, this setting help to reduce the computation times and assist stabilization in each cycle.

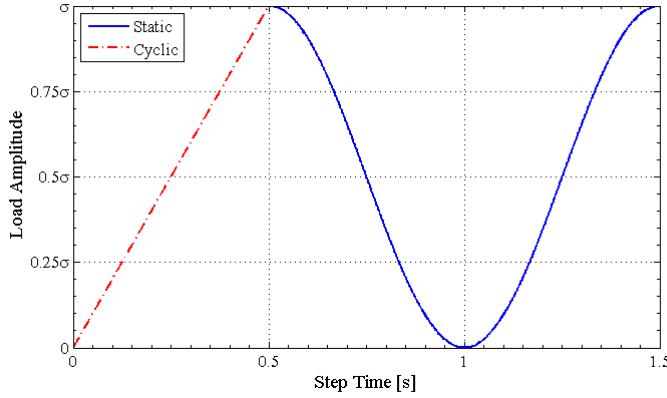


Figure 6.2 Load definition in XFEM analysis.

In order to calculate the stabilized cyclic response of the structure directly, the ABAQUS uses a truncated Fourier series to construct a displacement function that describes the response of the structure at all times t during a load cycle with period T . The residual, which is the differences between the applied load and the internal forces are calculated using a Fourier series of the same form as the displacement solution as well. The Fourier Series used for nodal displacement and residuals are presented in Equation 6.1 and 6.2 respectively.

$$\bar{u}(t) = u_0 + \sum_{k=1}^n (u_k^s \sin k\omega t + u_k^c \cos k\omega t) \quad (6.1)$$

$$\bar{R}(t) = R_0 + \sum_{k=1}^n (R_k^s \sin k\omega t + R_k^c \cos k\omega t) \quad (6.2)$$

Where:

\bar{u} : nodal displacement

u_0 : unknown constant displacement coefficient

u_k^s, u_k^c : unknown periodic displacement coefficients

\bar{R} : nodal residual vector

R_0 : an unknown constant residual coefficient

R_k^s, R_k^c : unknown periodic residual coefficients

ω : the angular frequency

t : time

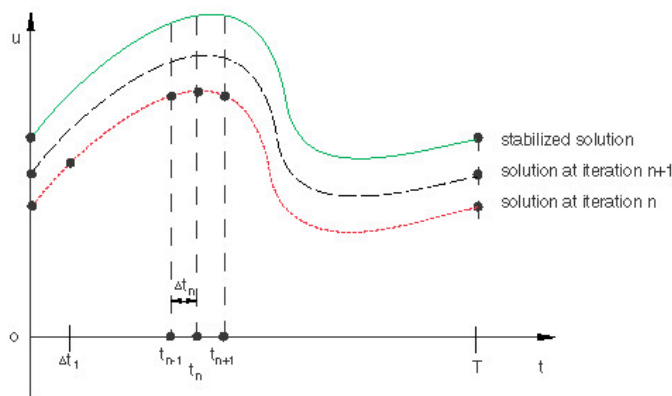


Figure 6.3 A displacement function at all times t during a load cycle with period T at different iterations (Dassault, 2014).

The ABAQUS requires that the ratio of the maximum residual coefficient to the time averaged force, CR_n^α , and the ratio of the maximum correction to the displacement coefficients to the largest displacement coefficient, CU_n^α , are less than the tolerances. The user-specified tolerances CR_0^α and CU_0^α are used to detect the plastic ratchetting. All of aforementioned ratios were left as default value, 0.005. The number of Fourier terms was set as 25 to reduce the expensive of calculation and assists the convergence. A fixed time increment was set to 0.05 without temperature effects engaged. The critical energy release rate, G_{IC} , G_{IIC} and G_{IIIC} , was set to 42.2 N/mm and the power coefficients were assumed to a value of unity. These parameters shown in Section 5.2.1 are used herein.

The onset of fracture is controlled in ABAQUS with Equation 3.2.1 in Section 3.2, while the crack growth rates are determined by the Paris law, which is in terms of $\Delta\mathcal{G}$, in Equation 6.4 where c_1 , c_2 , c_3 and c_4 are empirical constants determined based on material. Constants c_1 and c_2 were both set to zero, which means that the growth starts immediately when a stable $\Delta\mathcal{G}$ is obtained. Equation 6.5 and 6.6 are deducted to determine the constants c_3 and c_4 . The value of C and m is selected according to the recommendation value form BS 7910, which is used as a guidance for marine structure designs.

$$N = c_1(\Delta\mathcal{G})^{c_2} \quad (6.3)$$

$$\frac{da}{dN} = c_3(\Delta\mathcal{G})^{c_4} \quad (6.4)$$

$$c_3 = C(E)^{m/2} \quad (6.5)$$

$$c_4 = \frac{m}{2} \quad (6.6)$$

As mentioned in Section 3.2, the Paris law is only valid in the region 2 of crack growth. The energy release rate threshold, \mathcal{G}_{th} , defines the lower bound of crack growth; the \mathcal{G}_{pl} , defines the upper bound where the crack growth rate turns to unstable. As recommended by Dowling (2007), the critical stress intensity factor can be selected as the upper bound, in other word, that means that $\mathcal{G}_{pl}/\mathcal{G}_c$ should be set to 0.999. Because the K_{th} , $63 \text{ N/mm}^{3/2}$ as recommended in BS 7910, is much smaller than the fracture toughness of the selected material, the ratio of $\mathcal{G}_{pl}/\mathcal{G}_c$ was set to 0.001. Consequently, the crack growth tends to occur at all applied loads. Figure 6.4 explains the meaning of above notations.

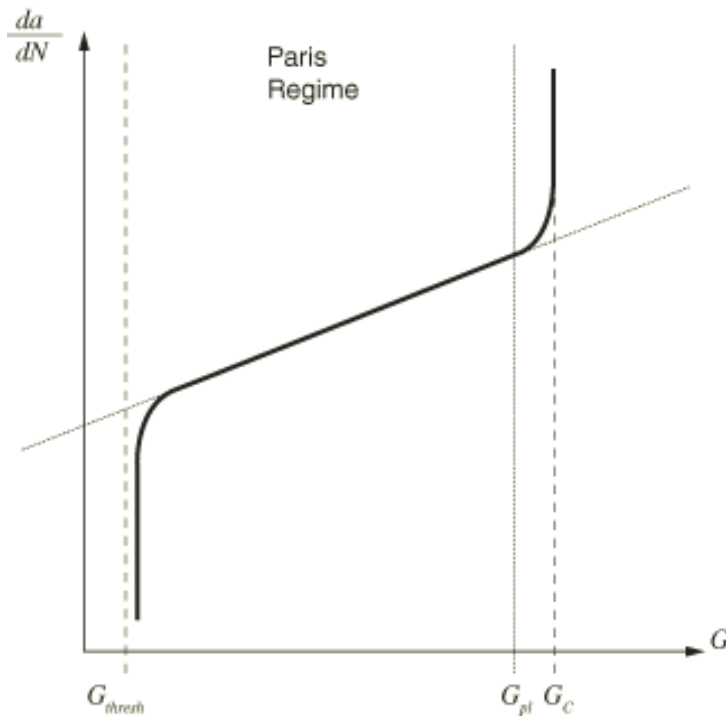


Figure 6.4 An explanation of notation of parameters to define the Paris regime (Dassault, 2014).

Once the fracture criterion, described in Equation 3.3.4 in Section 3.3.3 reached, the elements is completely fractured; while the real nodes is separated apart from its coincident phantom node. The number of cycles to fracture this element, which is calculated according to Equation 6.3, will be added to the total cycle count and then the analysis repeats until to a user defined maximum limitation or the analysis will stop when the fracture ratio G_{pl}/G_c is reached. However, it is undesirable because the computational cost is prohibitively expensive when G_{pl}/G_c criterion satisfies. Thus in this study, a reasonable limitation of total cycle number was defined to terminate the computation.

For discontinuous analysis the default time integration scheme in ABAQUS may result in premature cutbacks and termination. ABAQUS abandons iterations and cutbacks the time increment if the residuals are found increasing in two consecutive iterations after I_0 equilibrium iterations. On the other hand, the starting point for the logarithmic rate of convergence checks, I_R , is another routine. The discontinuous analysis option allows the user increase the value of I_0 from 4 to 8 and I_R from 8 to 10. Moreover, the I_A parameter controls the maximum number of cutbacks in one increment. In this study, this value was increased from 5 to 20 in both static and direct cyclic step.

An *INP* file was manually compiled since the ABAQUS CAE does not support the directly low-cycle fatigue analysis currently.

In the program FRANC3D, the new crack front is determined based on an extrapolation technique. The kink angle and extension curve-fits domain the direction and shape of the incoming crack front in the next step. In addition, the crack increment is in proportion with the SIF value. As mentioned in Figure 5.10, the difference of SIF values along the crack front is small, thus the crack growth along the front in each step keeps same speed more or less. Figure 6.5 shows the cracks on the outwards surface of flange and web plate have a similar increment in each step. This will give rise to the different

of crack propagation behaviors between FRANC3D analysis and XFEM analysis, which can be seen in the coming section.

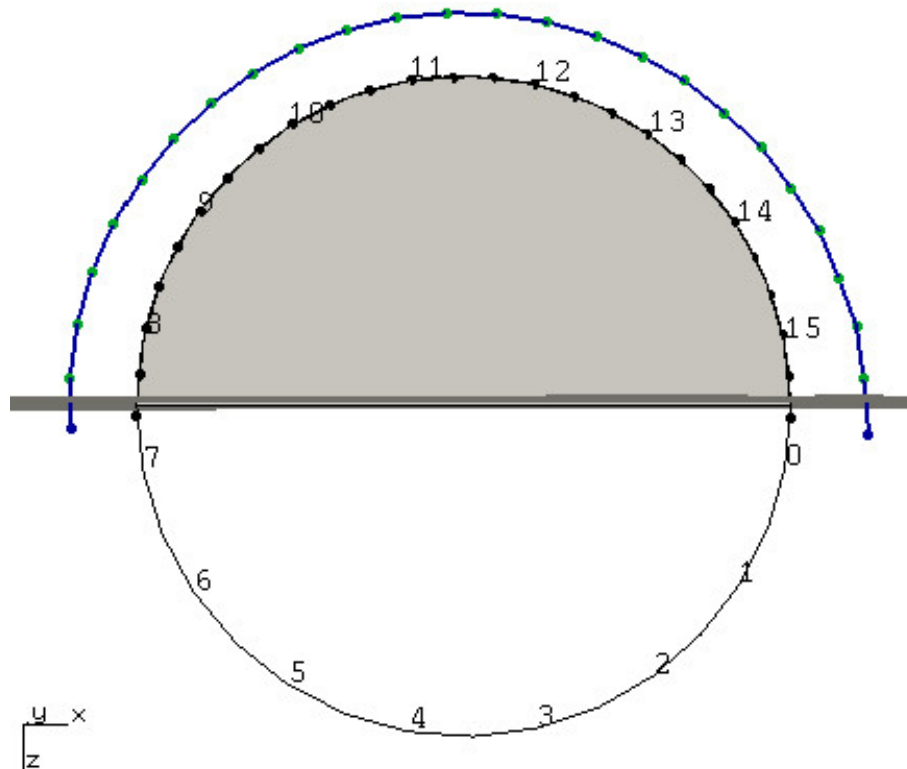


Figure 6.5 New front fit based on kink angle and extension curve-fits in FRANC3D. The shaded grey area is initial crack boundary edge. The black dots on the original crack front correspond to the fitted front points, where the extension and kink angle are applied to produce the new fitted points. The new front points as green dots, and the curve fit shown as a blue line (Fracture Analysis Consultants Inc, 2011).

Since there is no output request of crack tip locations and the crack length in current version of ABAQUS, a user designed algorithm was compiled in Python to extract and calculate crack tip coordinates as well as the propagation length from ODB output database file. The code is shown in Appendix B. The scheme of the code is tracking the status of the first element close to the most outwards surface of the flange and web plates. Due to the complexity of three-dimensional problems, the crack front along the thickness direction is ignored in this study; on the other hand, this decision matches the path of crack selected in Section 5.3 when FRANC3D analysis was carried out.

The RMSD analysis, defined in Equation 6.7 and 6.8 were used to find out the difference of crack propagation speed between XFEM and FRANC3D.

$$RMSD = \sqrt{\frac{1}{n} \sum_{K=1}^n \left(\frac{\text{number of cycles in xfem}}{\text{number of cycles in franc 3d}} - 1 \right)_k^2} \times 100\% \quad (6.7)$$

$$\% \text{ Diff} = \max \left(\frac{\text{number of cycles in xfem}}{\text{number of cycles in franc 3d}} - 1 \right) \times 100\% \quad (6.8)$$

6.2 Results in ABAQUS analysis

Crack growth history in No.2 case

The crack growth histories are shown in Figure 6.6, it is easy to realize that the telltale sign of the crack propagation behaviors are different from what has been seen from FRANC3D analysis. In ABAQUS analysis, the crack along the flange face will grow first and then the web outward free face will fracture; after both cracks on the top surface of flange and web plate complete, the crack tries to propagate inside along the thickness direction.

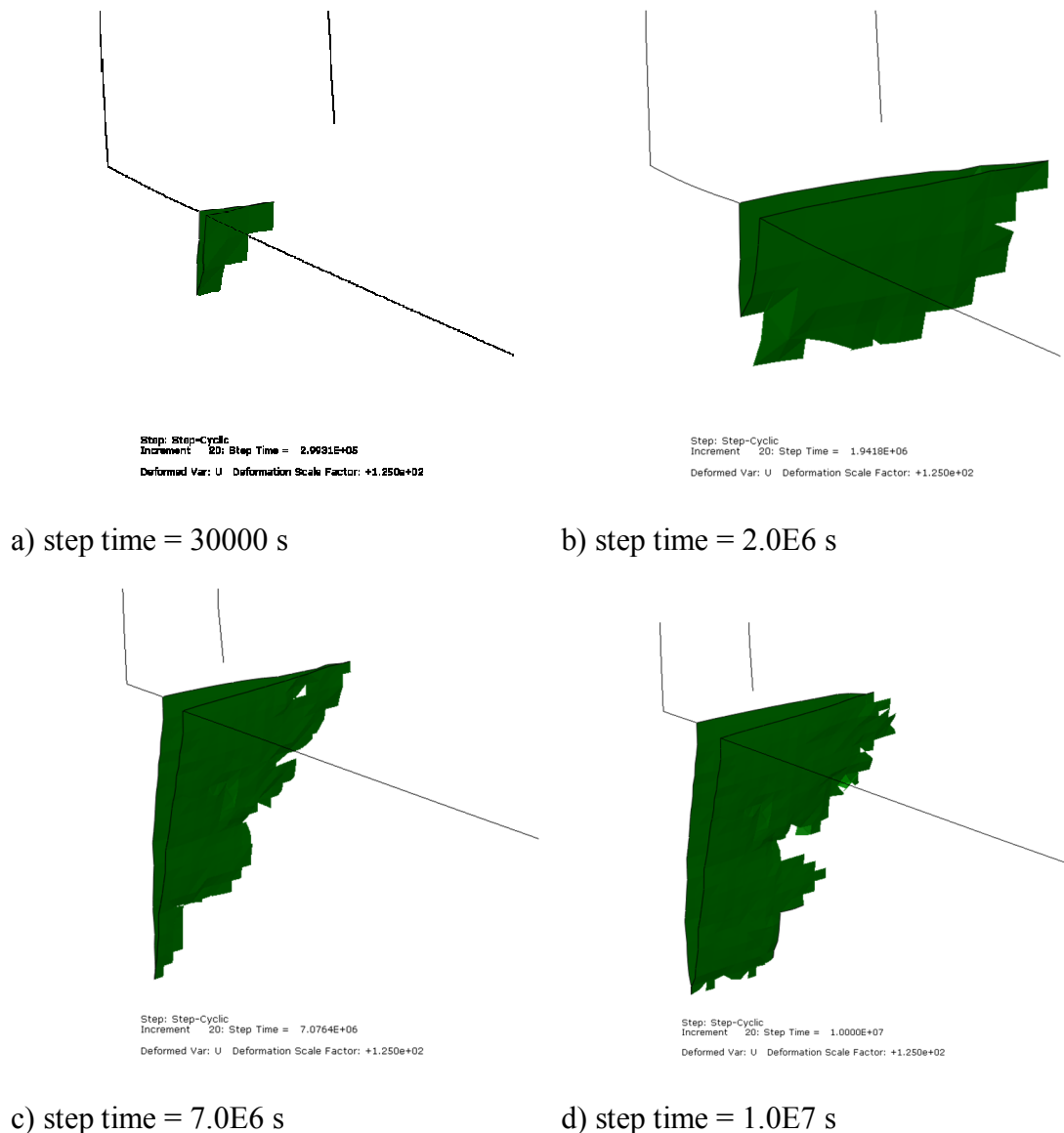


Figure 6.6 Crack propagation history in ABAQUS XFEM analysis. a) step time at 30000 seconds, b) step time at 2.0e6 seconds, c) step time at 7.0e6 seconds, and d) step time at 1.0e7 seconds.

Comparison of crack propagation speed between flange and web plates (No.2 case)

Figure 6.7 plots the crack propagation speed on flange (red line) and web (blue line) plates. As a result, the speed on the flange plate is faster than web plate. The crack on flange plate keeps an almost constant growth speed until it reaches to about 14mm, then

it propagates with a slower speed. Nevertheless, the crack on the web plate has two periods of blunt stage. A lot of cycle numbers are spent during the crack growing from 3 mm to 4mm and 12mm to 13.5mm. Figure 6.6 approves this phenomenon, the crack on the web plate “stops” twice, one is between 0.2e6 to 2e6 cycles and the other one is from 3.2e6 to 5e6 cycles. The result in No.1 case will be shown in Appendix A.

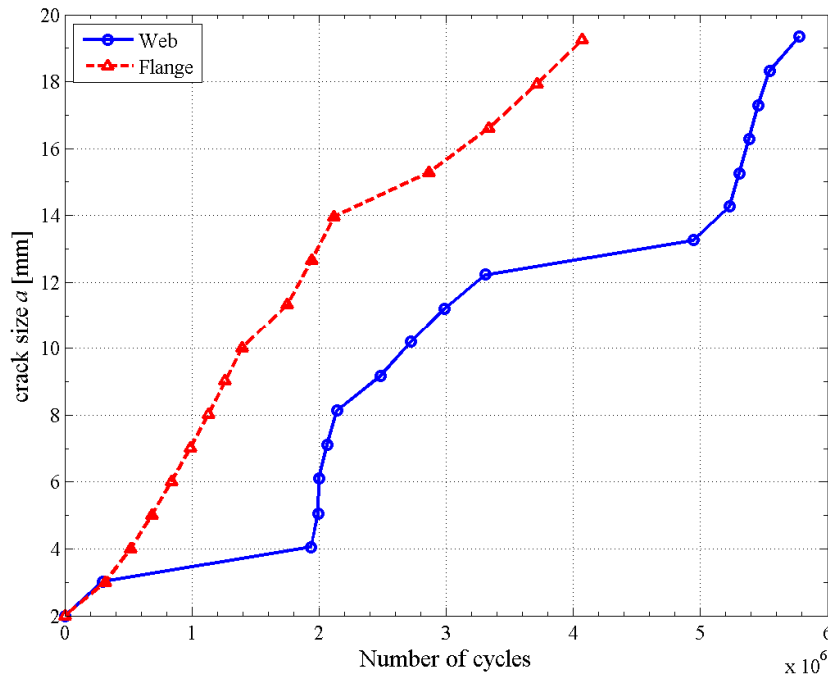


Figure 6.7 Comparison of cycle counting during crack propagation on flange and web plates (No.2 case).

In order to specify the difference of the propagation speed on flange and web plates, the difference study was carried out. Figure 6.8 illustrates that the crack on the web plates always need more cycle number than on flange plate. Then difference trends to reduce during the growth of cracks. At beginning, the difference peaks to 260%, the value drop to 50% at end instead. An oscillation zone appears during the crack propagates from 12 mm to 14mm. It shows significant different from the result in FRANC3D analysis (Section 5.3.2), which gives the result that flange and web plates keep a similar propagation speed.

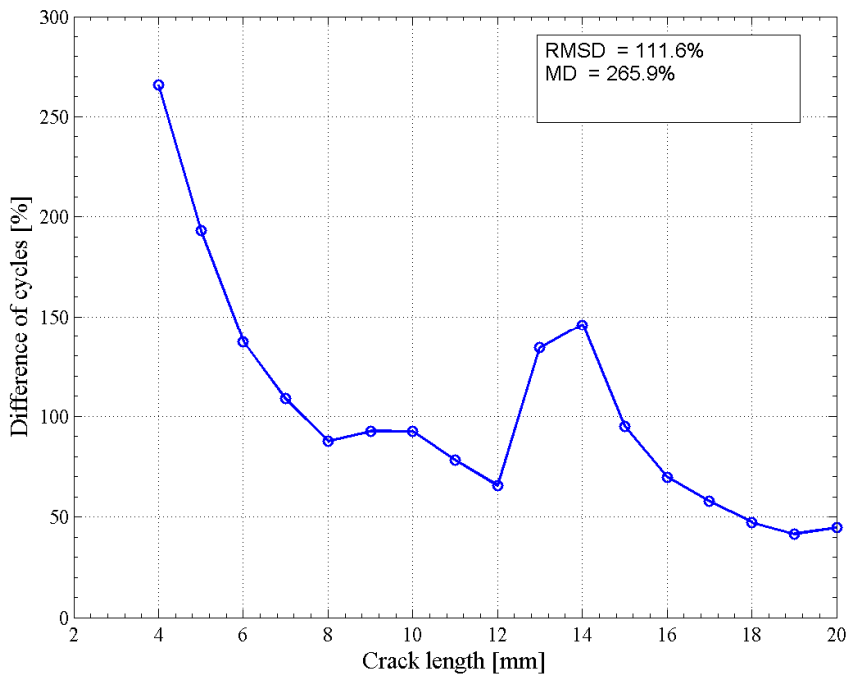


Figure 6.8 Difference of cycles counting during crack propagation between web and flange plates (No.2 case). The curve above zero means that the cycle number for a given crack length on web plate is larger than flange plate.

Comparison of geometry factors on web plate between XFEM and FRANC3D analyses (No.2 case)

Figure 6.9 depicts the geometry factors from the crack length 2 mm to 20mm. The blue curve represents the result from XFEM analysis while the red one is from FRANC3D. The difference between these two curves shows the deviation between through thickness crack (FRANC3D analysis) and the shallow surface crack (XFEM analysis). When the crack length grows further than 7 mm, the geometry factor of the shallow surface crack becomes smaller than the thorough thickness crack for a given crack length. This implies that more cycles are spent on fracturing the inside materials, consequently dragging down the crack propagation speed. This phenomenon is invisible in the FRANC3D, while revealed by ABAQUS XFEM analysis. The result in No.1 case will be given in Appendix A.

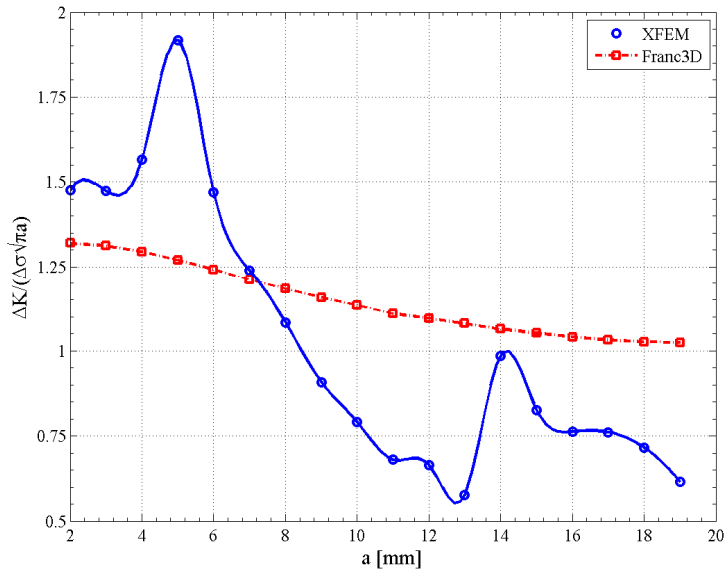


Figure 6.9 Comparison of geometry factors, $F(a)$, during the crack propagation on web plate (No.2 case).

Comparison of crack propagation speed on web plate between XFEM and FRANC3D analyses (No.2 case)

Figure 6.10 plots the number of cycles versus the crack length curve on the web plate in No.2 case. The blue line represents the result from XFEM analysis and the other line comes from analysis using FRANC3D. A tremendous difference between these two curves reveals that the XFEM analysis gave a much slower simulation of the crack propagation speed than FRANC3D. On that account, a large number of cycles are spent on fracturing the elements along the thickness direction in XFEM analysis; in other word, the analysis in FRANC3D overestimated the crack propagation speed.

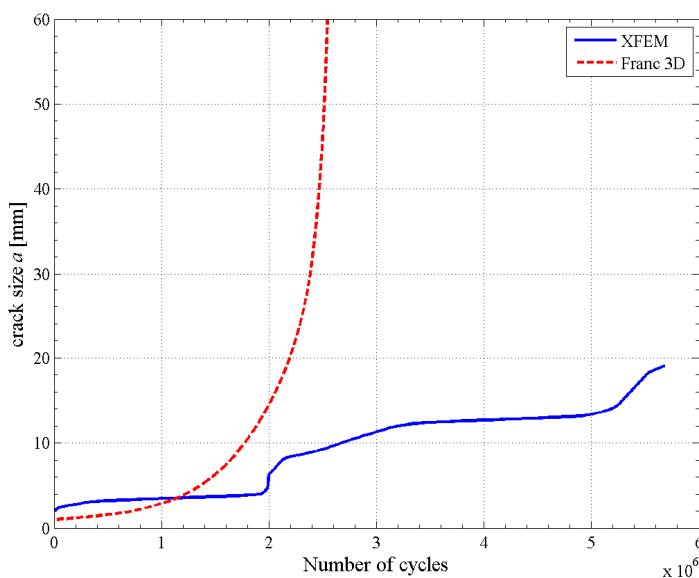


Figure 6.10 Comparison of cycle counting during crack propagation on web plate between XFEM and FRANC3D analysis (No.2 case)

Figure 6.11 shows the difference of crack propagation speed on web plate between XFEM and FRANC3D analysis. At the beginning of the propagation, the crack growth speed in XFEM is slower than in FRANC3D, when the crack length became greater than 4 mm, a local peak difference, 275%, reached. Then the difference oscillated around 150% and following with a surge to 310% when the crack grew to 14 mm. The maximum difference is about 312% and the RMSD gives the value of 224%.

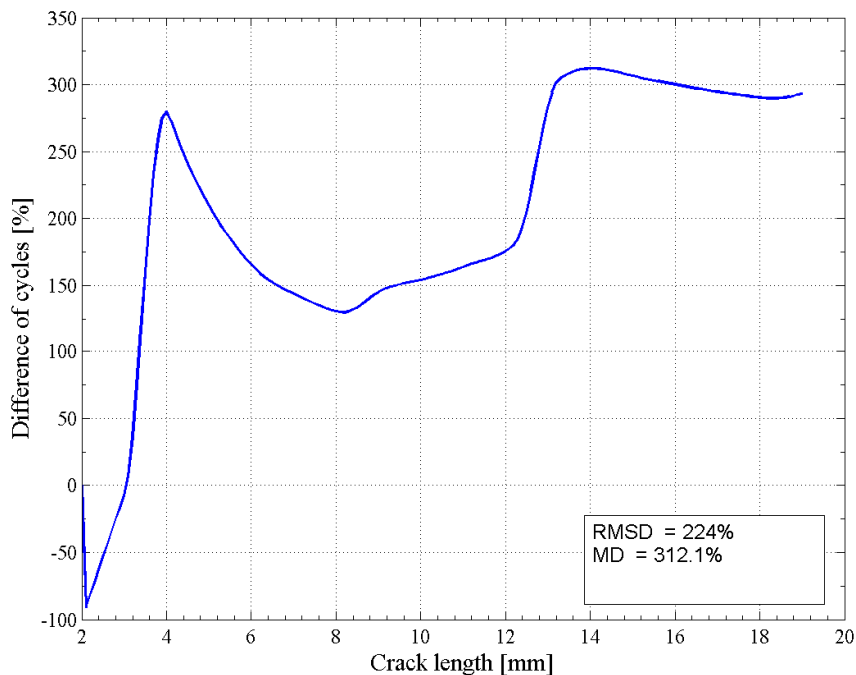


Figure 6.11 Difference of cycles counting number on web plate between XFEM and FRANC3D analysis (No.2 case). The curve above zero means the cycle numbers for a given crack length on web plate is larger than flange plate and vice versa when the curve below zero.

Comparison of crack propagation path on web plate between XFEM and FRANC3D analyses (No.2 case)

As described in Section 3.2.1, the direction of the crack path is determined by the stress intensity factors. Figure 6.12 plots the crack propagation path on the web plate in No.1 and 2 cases. Both the results from FRANC3D and XFEM show the same trends of the propagation direction, however, the paths deviate away as cracks grow downwards.

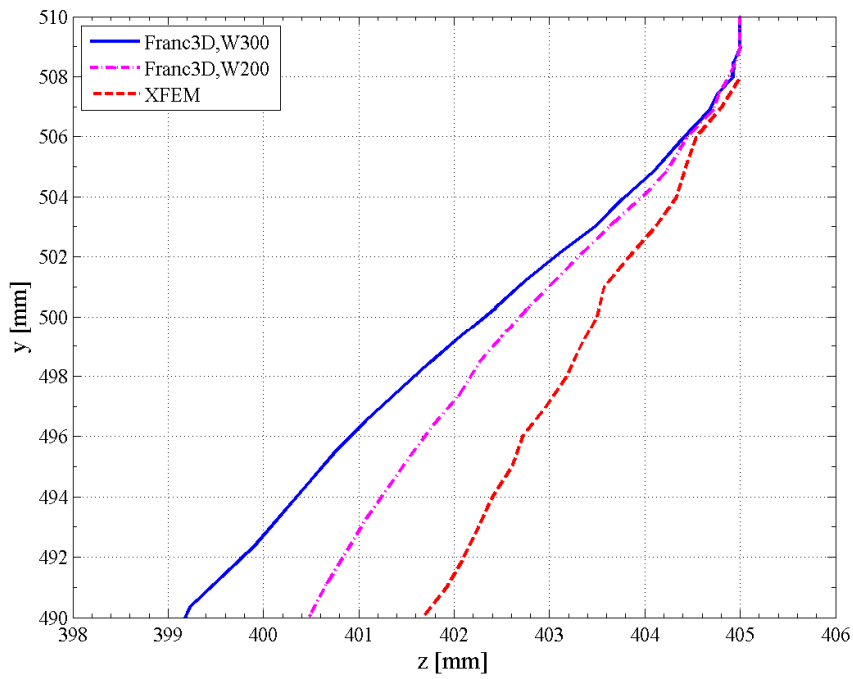


Figure 6.12 Comparison of crack path on web plate between FRANC3D and XFEM analysis.

7 Conclusion

The thesis has implemented the incremental iterative approach to perform the ultimate strength analysis of ship structures. The FE method is also applied to estimate the local buckling behavior of a simple plate structure to provide input for the ultimate strength assessment in the mid-section of the ship structure.

The incremental iterative approach is a sufficient method that is based on Smith's method. During the calculation, there are several parameters need to be emphasized here. Firstly, when calculating the total force on the aimed cross section, the force value should be zero, if the position of neutral axis is correct. But it is not easy to satisfy that criterion in real conditions. In terms of the current theories, there is still no exact limitation of this error. However, if the threshold for the error is too small, the calculation time will be very long and it is hard to converge to a satisfied force value. In contrast, if the threshold for the error is too large, the neutral axis will be not at the correct position, despite the force value is satisfied. As a result, the accuracy will be decreased. In this analysis, the threshold for error was set at 10 N, which makes the calculation in a relatively fast speed and can get an accurate result.

It also should pay attention to the adjustment of neutral axis, which is related accuracy of results and calculation speed. Large adjustment makes it hard to find out the correct neutral axis position. And it is very easy to fall and drop into an infinite loop. However, small adjustment is accurate enough in the correct position movement, but it takes too much time to iterate. In this analysis, it was set at 0.0001m as rule required.

The combination of the adjustment for neutral axis and the force error dominate the moment iterative computation time. But there is one more parameter can affect calculation time, the incremental step of curvature. Compared with the previous both parameters, the incremental step affects the time directly. Small incremental step value would give more point on the moment-curvature curve. It would not influent the accuracy a lot, but makes the curve smooth. In this analysis, there are 60 points in the curve. Combined with the other two parameters, the average calculation time is 21 min on a Core i5 2.6 GHz CPU with 4 GB of memory PC. So compared with FE software, this is a very fast calculation speed.

In fracture analysis, the primary aim of the study is to investigate the difference when various commercial software used to model the crack propagation and estimate fatigue fracture life on a ship structural component.

Although a great number of researches have been done on the single edge-crack flat plate specimens, the influence of the attached additional plate, which forms an inverse T shape together with the base flat plate, is still unknown. Unlike the single edge-crack flat plate, the high stress concentration around the connection region in this type of structure gives rise to a different behavior of the crack propagation. On a flat plate, the geometry factor will climb up as the growth of the crack. However, the introduction of the attached plate will dramatically increase the geometry factor as well as the stress intensity factors. As long as the crack propagates, the geometry factors will sharply drop and then turn to even. A hypothesis of this phenomenon is that at the early stage of the crack growth, the stress concentration domains the value of the high geometry factor. When the crack propagates enough far away the initial crack zone, the additional attached plate will provide higher stiffness than the flat plate, and gives a relevant small geometry factor.

The drawback of the high stress intensity factor during the early stage of the crack propagation is that the crack growth speed in the inverse T shape structure is much higher than the single edge-crack flat plate. This leads to this shape structure will state in a lower fatigue strength capacity than the flat plate structure. On the other hand, the width of the attached plate plays an important role too. Wider plate will lead to a higher growth speed. It is clear that the wider plate will not only increase the stiffness of the whole structure but the stress concentration also. When the width of the attached plate increases 50%, the RMSD of the cycle counting will surge about 20%. In some case, the wider attached plate means a stronger connection, but in the meanwhile, this design reduce the fatigue strength.

As a key component in the ship structure, the inverse angle bar is wildly used in ship design. The flange plate of the inverse angle bar makes the problem much more complex, as the problem is extended from 2-D to 3-D space. Right now, the FE methods to simulate the crack propagation in a 3-D structure are either conventional FEM or extended FEM. Both of them request the usage of solid elements and dramatic expensive computation power.

In the analysis of using FRANC3D, the normal crack growth magnitude is determined by user and the relevant growth magnitude along the crack front is determined based on interpolation. This setting implies that the simulation accuracy is based on the density of the user defined crack increment at each step. However, if the density is too high, that will give rise to the difficulty of re-meshing; on the other hand, the low density will sacrifice the accuracy of results. Another significant problem is that this method cannot correctly simulate the crack propagation along the thickness direction, because the crack growth along the crack front is determined by interpolation. The observation from results demonstrates that cracks on flange plate and web plate will propagate simultaneously, which deviates from the XFEM results. Due to above reasons, the simulation in FRANC3D simplified the realistic condition and accelerate the crack propagation speed.

Only considering the results in FRANC3D analysis, for an initial circle crack, the crack on the flange and web plates almost grow in a same speed, within 10% difference. Moreover, it is similar to the result in 2-D analysis, wider attached plate leads to a higher propagation speed.

Due to the above mentioned limitations, the XFEM based low-cycle fatigue analysis was used as a reference. The XFEM results tell that the crack will form on the flange plate at the early stage firstly, then the crack will start to propagate on the web plate. The FRANC3D ignores the difference of sequence of the crack growth on flange and web plates. Furthermore, the crack propagation speed simulated in XFEM is much slower than that in FRANC3D. The deviation between them is right the time spent on the thickness direction crack growth. Although the XFEM gives more realistic results, the prohibitively expensive computation time cannot be ignored. For a $10e7$ cycles simulation in this study, it took more than 12 hours on a Core i7 3.0 GHz CPU with 8 GB of memory PC. If the output recorded at each frequency, the *ODB* file can reach to 100 GB per simulation. However, once the model has been set, human power can be free from the tedious operations and performances.

These results show that the 2-D problem is easy to be manipulated in current commercial software. The program FRANC3D satisfies the requirement to simulate the crack propagation on a 3-D ship structural component, but the accuracy need to be verified carefully. At last the XFEM based low-cycle fatigue analysis in ABAQUS is

the most directly way to observe the crack propagation, however the computation power request limits its application.

8 Future works

In the ultimate strength analysis, several extra methods should be applied to calculate the ultimate strength. More structure models should be built in FEA to investigate the ultimate strength, since there is only one unstiffened plate applied in this thesis. The whole ship FEA is preferred to introduce to improve the accuracy of the results. In the FEA, it is easy to find out the weak and buckled position. Consequently, it can be a guide for the reinforcement of local structures.

The current studies carried out in this thesis covered both 2-D and 3-D problems, but due to the special geometries, the results herein cannot be supported by any experiment data. In order to verify and improve the confidence of the results, several extra steps should be implemented in the future.

To begin with, the analytical case (which is describe in Section 5.2), should be carried out in ABAQUS using XFEM. Therefore the accuracy of the XFEM result can be judged. Secondly, the convergence shall be analyzed to prove the accuracy of results. In addition, in the FRANC3D analysis, a smaller increment of the crack in each step can be tried to investigate the sensitivity of such factors. Moreover, when the XFEM analysis is implemented, the “W=200” case will be completed as well. Then the crack propagation speed in No.1 and No.2 cases can be compared each other. Likewise, the crack growth will be ended until the crack length reaches to 60mm if the computation power is allowed. Despite the XFEM is mesh independent, a convergence study still need to be carried out to find out the best meshing scheme.

Finally the cracked structure component shall be involved in the hull girder ultimate strength study. The influence and effects of the crack on the ULS can be studied. As a consequence the reduction of the ultimate strength due to the presence of fatigue cracks can be investigated. What is more, an estimation of the time window of keeping ship safe can be evaluated as a suggestion of the shipping management and maintenance.

References

- ABS (2012): Common Structural Rules for Oil Tanker.
- Anderson, T. L. (1994): *Fracture Mechanics: fundamentals and applications*, 2nd ed. CRC Press, ISBN 0-8493-4260-0, U.S.A.
- Anderson, T. L. (1995): *Fracture Mechanics: Fundamentals and Applications*, 2nd ed. CRC Press, Inc., Boca Rotaon, NY, U.S.A.
- Belytschko, T., Black, T. (1999): Elastic Crack Growth in Finite Elements with Minimal Remeshing. *International Journal for Numerical Methods in Engineering*, 45, 1999, pp. 601-620.
- British Standards Institution (BSI) (2000): *Guidance on Methods for Assessing the Acceptability of Flaws in Fusion Welded Structures*. British Standards Institution (BSI), London, British.
- Byskov, E. (1970): The Calculation of Stress Intensity Factors Using the Finite Element Method with Cracked Elements. *International Journal of Fracture Mechanics*, 6(2), 1970, pp. 159-167.
- Cotterell, B., Rice, J. (1980): *Slightly Curved or Kinked Cracks*. pp. 155-169.
- Dassault Systemes Simulia Corp. (2014a): *ABAQUS 6.14: ABAQUS Analysis User's Guide*. Providence, RI.
- Dassault Systemes Simulia Corp. (2014b): *ABAQUS 6.14: ABAQUS Theory Guide*. Providence, RI.
- Do, H. C., Jiang, W., Jin, J., & Chen, X. Ultimate Limit State Assessment Of Stiffened Panel Structures For Very Large Ore Carrier Via Nonlinear Finite Element Method.
- Dowling, N. E. (2007): *Mechanical Behavior of Materials: Engineering Methods for Deformation, Fracture, and Fatigue*, 3rd ed. Pearson Education, Inc., Upper Saddle River, NJ.
- Erdogan, F., Sih, G. (1963): On the Crack Extension in Plates Under Plane Loading and Transverse Shear. *Journal of Basic Engineering*, 85(4), 1963, pp. 519-525.
- Forman, R., Kearney, V., Engle, R. (1967): Numerical Analysis of Crack Propagation in Cyclic-Loaded Structures. *Journal of Basic Engineering*, 89(3), September 1967, pp. 459-463.
- Fracture Analysis Consultants Inc (2011): *FRANC3D Reference Manual*. NY, U.S.A.
- Gordo, J. M., & Guedes Soares, C. (2000, April). Residual strength of damaged ship hulls. In *Proceedings of the 9th international congress of international maritime association of the mediterranean, Ischia, Italy*.
- Gordo, J. M., Guedes Soares, C., & Faulkner, D. (1996). Approximate assessment of the ultimate longitudinal strength of the hull girder. *Journal of Ship Research*, 40(1), 60-69.
- Griffith, A.A. (1920): *Philosophical Transactions*. Series A, Vol. 221, No. 2, pp. 163-198.
- Grondin, G. Y., Elwi, A. E., & Cheng, J. J. R. (1999). Buckling of stiffened steel plates—a parametric study. *Journal of Constructional Steel Research*, 50(2), 151-175.

- Hardy, R. H. (1974): *A High-Order Finite Element for Two-Dimensional Crack Problems*. PhD Thesis. Georgia Institute of Technology, Atlanta, GA.
- Henshell, R., Shaw, K. (1975): Crack Tip Finite Elements are Unnecessary. *International Journal for Numerical Methods*, 9(3), 1975, pp. 495-507.
- Hussain, M., Pu, S., Underwood, J. (1974): *Strain Energy Release Rate for a Crack under Combined Mode I and Mode II*. Fracture Analysis, ASTM STP 560, American Society for Testing and Materials, pp. 2-28.
- Irwin, G.R. (1948): *Fracture Dynamics. Fracturing of Metals*, American Society for Metals, Cleveland, U.S.A.
- ITOPF (2015): *Oil tanker Spill Statistics 2014*, International Tanker Owners Pollution Federation, London, United Kingdom, 1-12
- Jordan, C. R., Cochran, C. S. (1978): *In-service Performance of Structural Details*, Report SSC-272, Ship Structure Committee, U.S. Coast Guard, Washington, DC.
- Krishna, L. S., Kamal, K., Mallikarjun, V. (2014): Crack growth simulation of stiffened fuselage panels using XFEM techniques. *Indian Journal of Engineering & Materials Sciences*, Vol. 21, August 2014, pp. 418-428.
- Kumar, M. S., Alagusundaramoorthy, P., & Sundaravadivelu, R. (2007). Ultimate strength of square plate with rectangular opening under axial compression. *Journal of Naval Architecture and Marine Engineering*, 4(1), 15-26.
- Melenk, J. M., Babuska, I. (1996): The partition of unity finite element method: Basic theory and applications. *Comput. Methods Appl. Mech. Eng.*, 139, 1996, pp.289–314.
- Moreira, P., Pastrama, S., De, C. (2009): *Eng Fract Mech*, 76, 2009, pp.2298-2308.
- Nicolas, M., John, D., Ted, B. (1999): *Int J Numer Methods Eng*, 46, 1999, pp.131-150.
- Orowan, E. (1949): *Fracture and Strength of Solids*. Report of Progress in Physics, Vol. 12.
- Osher, S., Sethian, J. A. (1988): Fronts Propagating with Curvature-Dependent Speed: Algorithms Based on Hamilton-Jacobi Formulations. *Journal of Computational Physics*, 79(1), 1988, pp. 12-49.
- Özgüç, Ö. & Barltrop, N. D. (2008). Analysis on the hull girder ultimate strength of a Bulk Carrier using simplified method based on an incremental-iterative approach. *Journal of Offshore Mechanics and Arctic Engineering*, 130(2), 021013.
- Paik, J. K., Kim, B. J., & Seo, J. K. (2008). Methods for ultimate limit state assessment of ships and ship-shaped offshore structures: Part I—Unstiffened plates. *Ocean Engineering*, 35(2), 261-270.
- Paik, J. K., Kim, B. J., & Seo, J. K. (2008). Methods for ultimate limit state assessment of ships and ship-shaped offshore structures: Part II stiffened panels. *Ocean Engineering*, 35(2), 271-280.
- Paik, J. K., Kim, B. J., & Seo, J. K. (2008). Methods for ultimate limit state assessment of ships and ship-shaped offshore structures: Part III hull girders. *Ocean Engineering*, 35(2), 281-286.
- Paik, J. K., Wang, G., Kim, B. J., & Thayamballi, A. K. (2002). Ultimate limit state design of ship hulls. *SNAME Transactions*, 110, 285-308.

- Paris, P., Erdogan, F. (1963): A Critical Analysis of Crack Propagation Laws. *Journal of Basic Engineering*, 85(4), December 1963, pp. 528-533.
- Paris, P., Gomez, M., Anderson, W. (1961): A Rational Analytic Theory of Fatigue. *The Trend in Engineering*, 13, 1961, pp. 9-14.
- Rhee, H., Salama, M. (1987): Mixed-mode stress intensity factors solutions for a warped surface flaw by three-dimensional finite element analysis. *Engineering Fracture Mechanics*, 28(2), 1987, pp.203-209.
- Rice, J. (1968): A Path Independent Integral and the Approximate Analysis of Strain Concentration by Notches and Cracks. *Journal of Applied Mechanics*, 35(2), 1968, pp. 379-386.
- Roylance, D. (2001): *Introduction to Fracture Mechanics*. Massachusetts Institute of Technology, Cambridge, U.S.A.
- Rybicki, E. and Kanninen, M. (1977): A Finite Element Calculation of Stress Intensity Factors by a Modified Crack Closure Integral. *Engineering Fracture Mechanics*, 9(4), 1977, pp. 931-938.
- Shi, J., Chopp, D., Lua, J., Sukumar, N., Belytschko, T. (2010): ABAQUS Implementation of eXtended Finite Element Method Using a Level Set Representation for Three-Dimensional Fatigue Crack Growth and Life Predictions. *Engineering Fracture Mechanics*, 77(14), 2010, pp. 2840-2863.
- Shih, C., Asaro, R. (1988): Elastic-Plastic Analysis of Cracks on Bimaterial Interfaces: Part I-Small Scale Yielding. *Journal of Applied Mechanics*, 1988, pp. 299-316.
- Smith, M. J., & Pegg, N. G. (2003). Automated assessment of ultimate hull girder strength. *Journal of Offshore Mechanics and Arctic Engineering*, 125(3), 211-218.
- Sukumar, N., Moës, N., Moran, B., Belytschko, T. (1999): Extended finite element method for three-dimensional crack modelling. *International Journal for Numerical Methods in Engineering*, Vol. 48, No. 11, 2000, pp. 1549-1570.
- Sun, H., Wang, X., Paik, J. K., & Hutchison, B. L. (2005). Buckling and ultimate strength assessment of FPSO structures. Discussion. *Transactions-Society of Naval Architects and Marine Engineers*, 113, 634-660.
- Tanaka, K (1974): Fatigue crack propagation from a crack inclined to the cyclic tension axis. *Engineering Fracture Mechanics*, 6, 1974, pp. 493-507.
- Walker, K. (1970): *The Effects of Stress Ratio during Crack Propagation and Fatigue for 2024-T3 and 7075-T6 Aluminum*. Effects of Environment and Complex Load History on Fatigue Life, ASTM STP 462, American Society for Testing and Materials, U.S.A., pp. 1-14
- Wang, X., Sun, H., Yao, T., Fujikubo, M., & Basu, R. (2011). Methodologies on hull girder ultimate strength assessment of FPSOs. *Journal of Offshore Mechanics and Arctic Engineering*, 133(3), 031603.
- Wilson, W. (1973): *Finite Element Methods for Elastic Bodies Containing Cracks*. Mechanics of Fracture, G. Sih, ed, Noordhoff International Publishing, Leyden.
- Wu, E. M. and R. C. Reuter Jr. (1965): *Crack Extension in Fiberglass Reinforced Plastics*. T and M Report, University of Illinois, vol. 275, 1965.
- Yao, T. (2003). Hull girder strength. *Marine Structures*, 16(1), 1-13.

Appendix A

The following figures show the additional result discussed in Section 5 and 6. Figure A.1 to A.3 list the results of SIF history in 2-D and 3-D cases. Figure A.4 to A.7 represent the SIF values along the crack front at each step in the FRANC3D analysis. Next, Figure A.8 to A.11 show the comparison of geometry factors and stress intensity factor ranges in FRANC3D analysis, following with the comparison of cycle numbers between flange and web plates (Figure A.12 to A.15). Finally the comparisons between FRANC3D and XFEM analysis are illustrated from Figure A.16 to A.21.

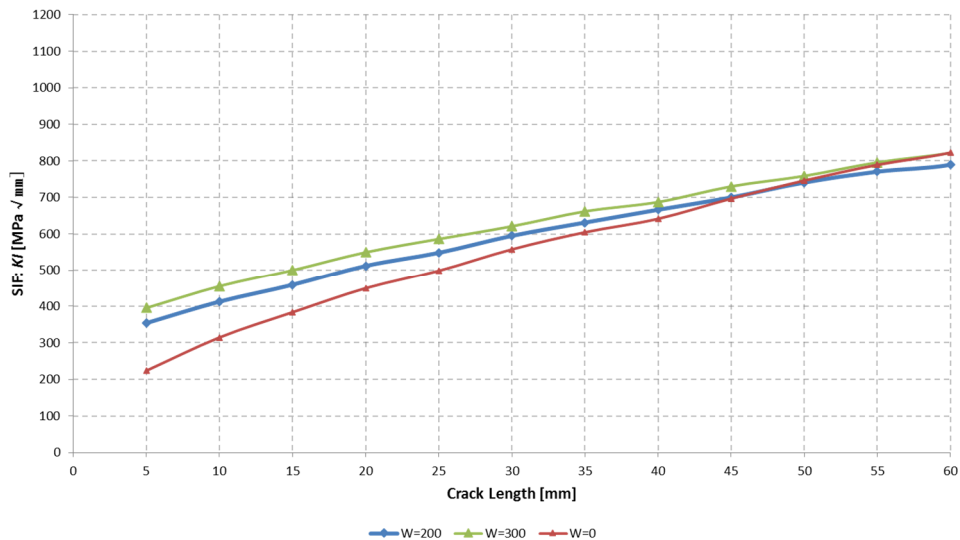


Figure A.1 Stress intensity factor history in FRANC2D analysis.

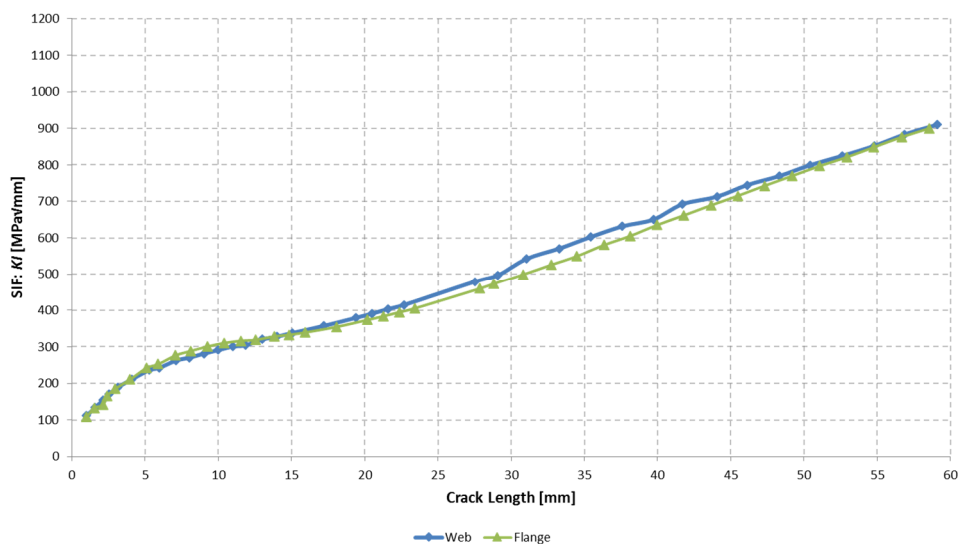


Figure A.2 Stress intensity factor history in FRANC3D analysis (No. 1 case).

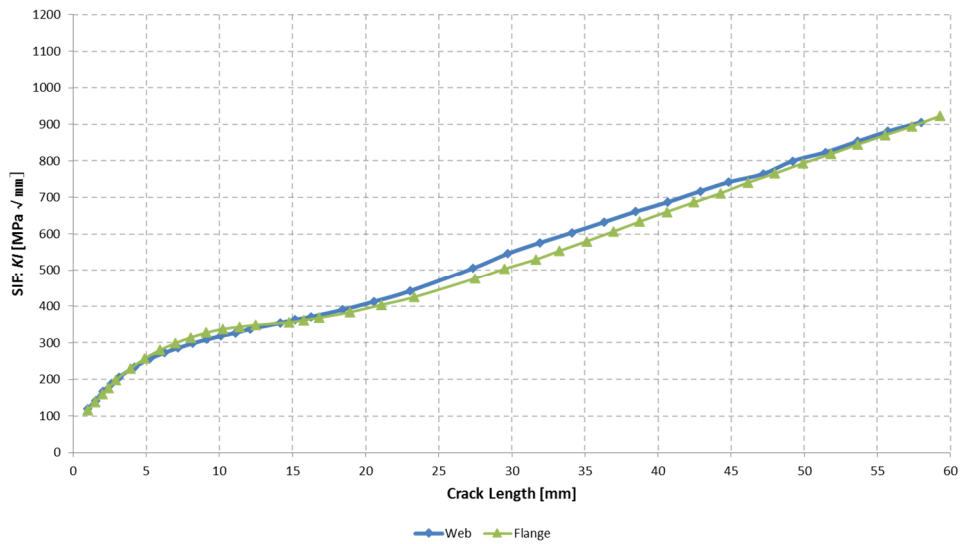


Figure A.3 Stress intensity factor history in FRANC3D analysis (No. 2 case).

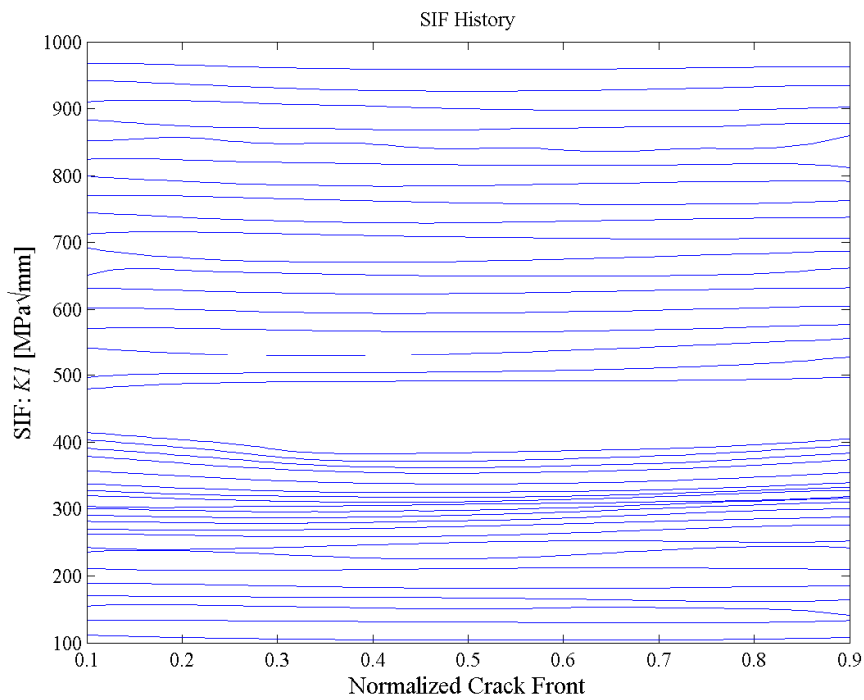


Figure A.4 The stress intensity factors history on web plate at each step of propagation (No.1 case).

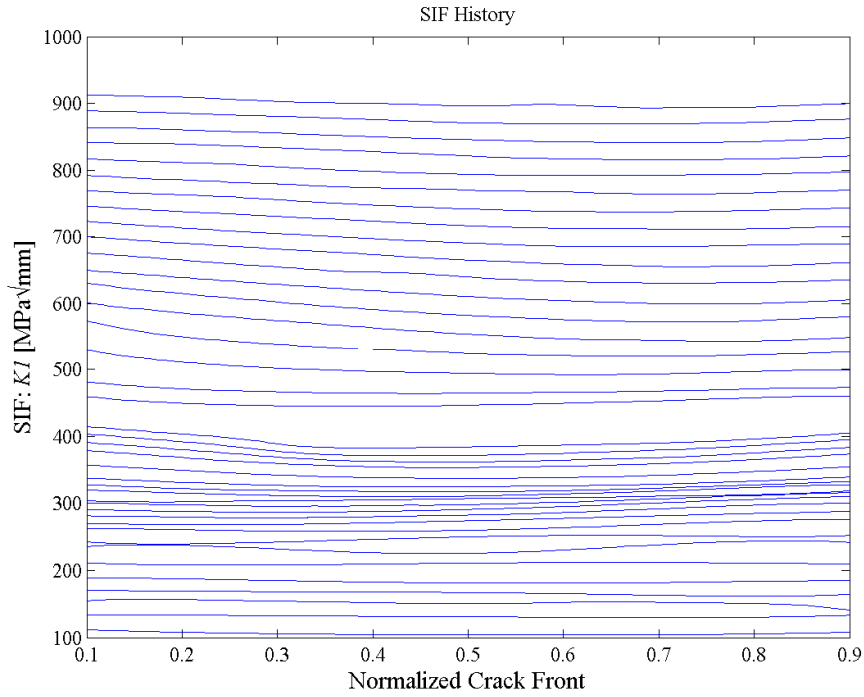


Figure A.5 The stress intensity factors history on flange plate at each step of propagation (No.1 case).

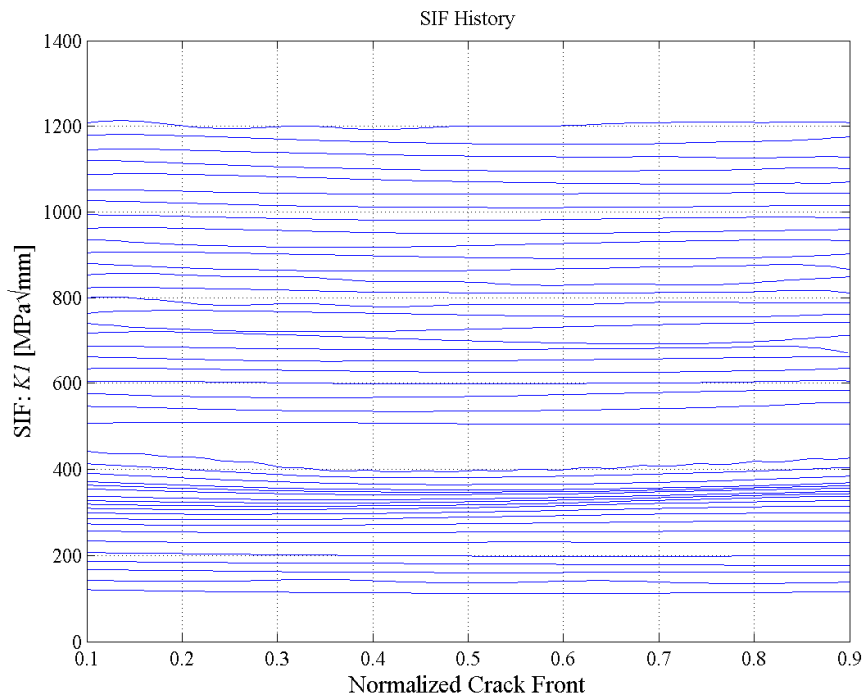


Figure A.6 The stress intensity factor history on web plate at each step of propagation (No.2 case).

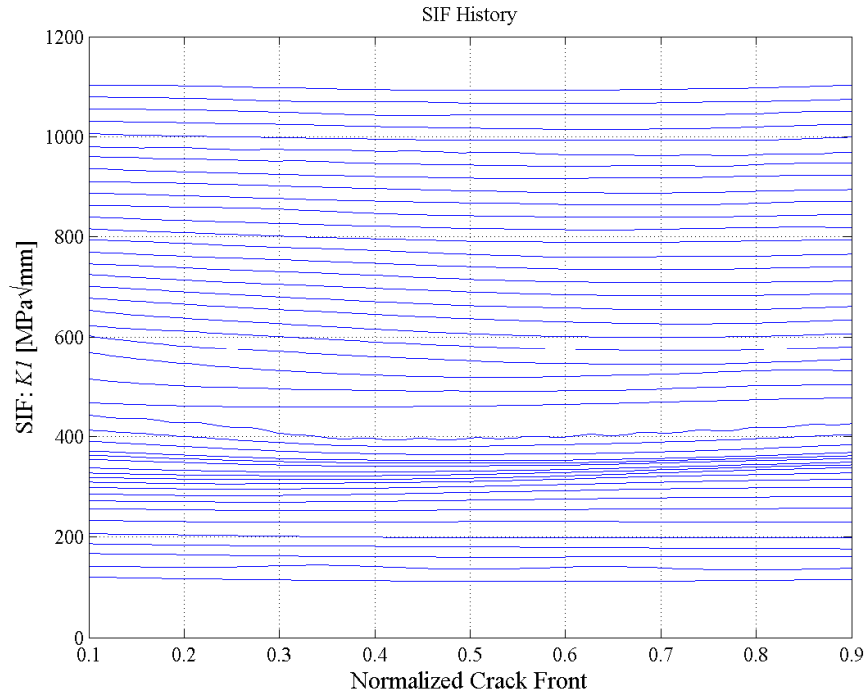


Figure A.7 The stress intensity factors history on flange plate at each step of propagation (No.2 case).

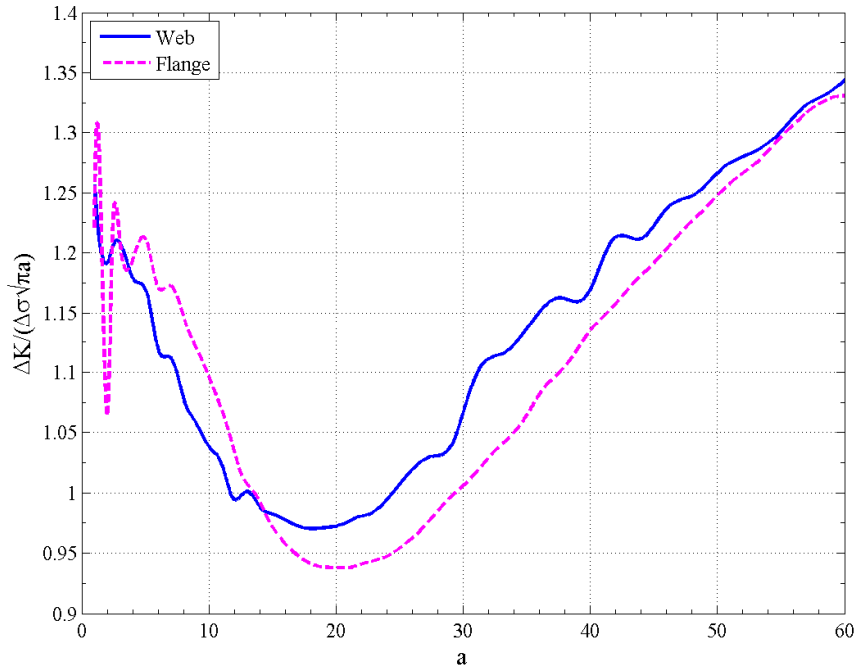


Figure A.8 comparison of geometry factors, $F(a)$, during the crack propagation (No.1 case).

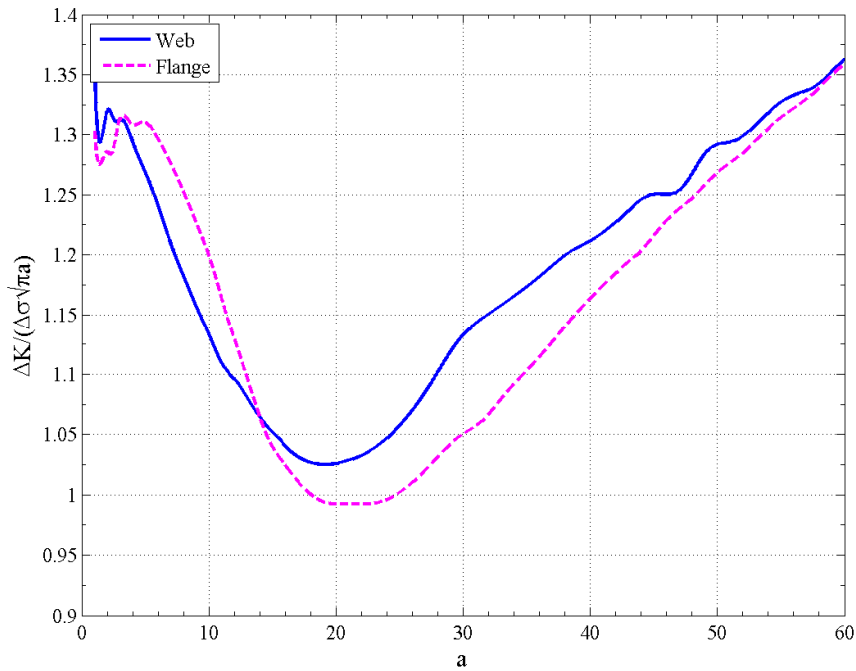


Figure A.9 Comparison of geometry factors, $F(a)$, during the crack propagation (No.2 case).

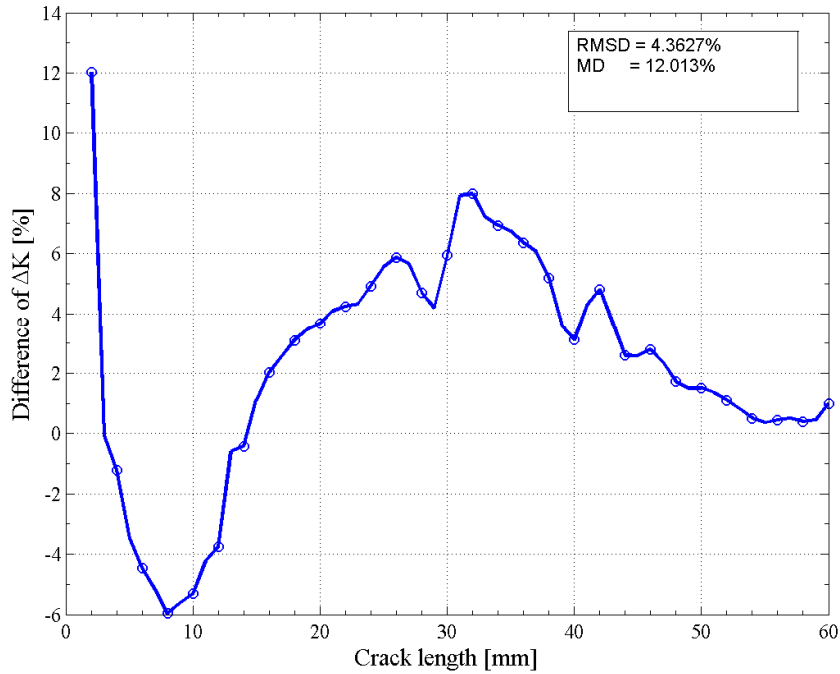


Figure A.10 Difference of stress intensity factor range between flange and web plates (No.1 case).

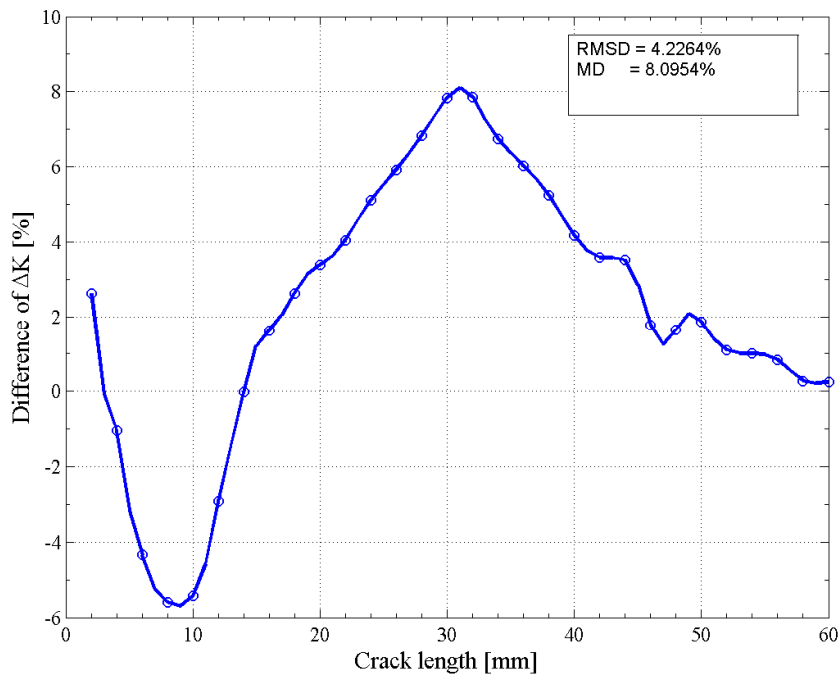


Figure A.11 Difference of stress intensity factor range between flange and web plates (No.2 case).

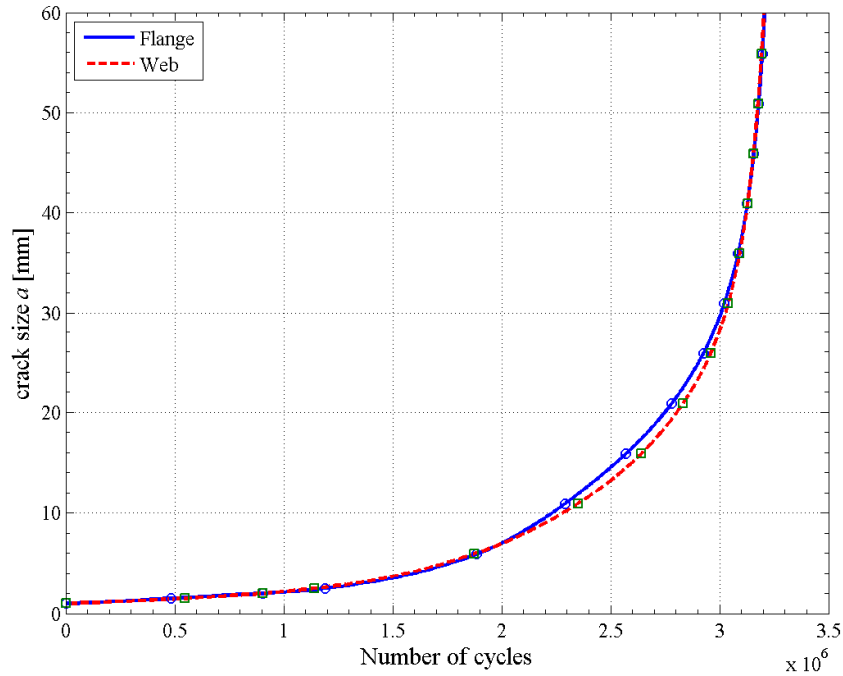


Figure A.12 Comparison of cycle counting during crack propagation on flange and web plates (No.1 case).

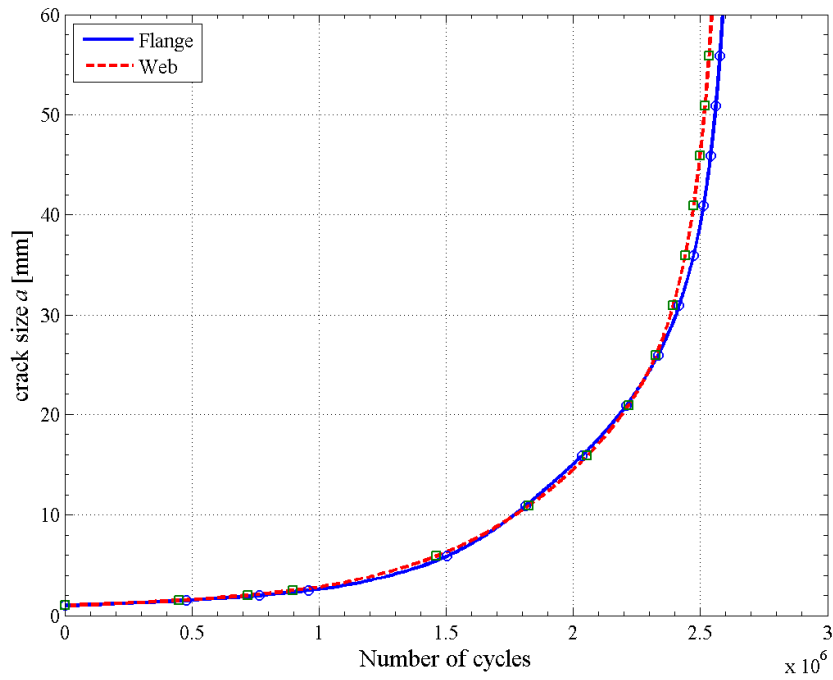


Figure A.13 Comparison of cycle counting during crack propagation for flange and web plates (No.2 case).

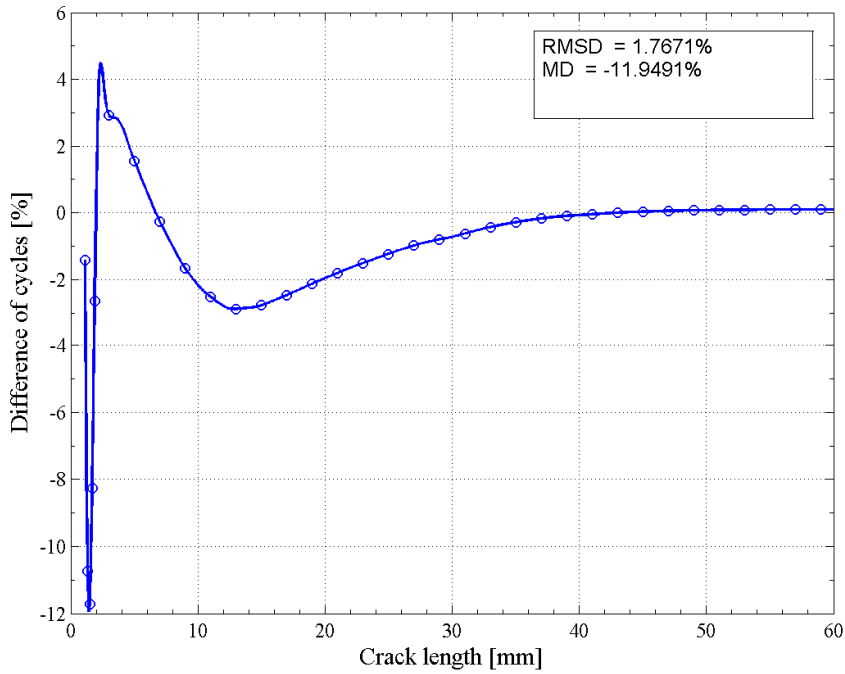


Figure A.14 Difference of cycles counting number between flange and web plates. (No.1 case).

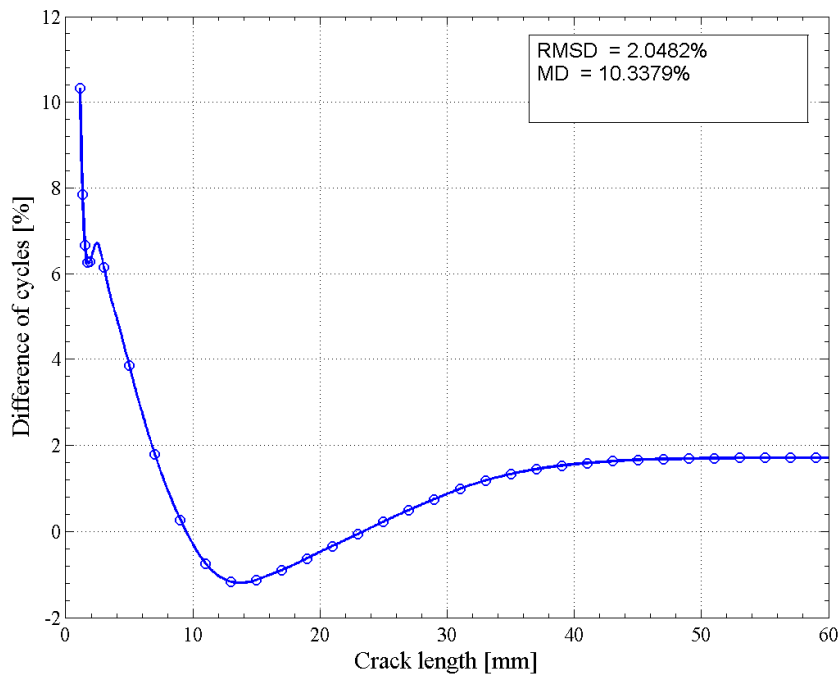


Figure A.15 Difference of cycles counting number between flange and web plates (No.2 case).

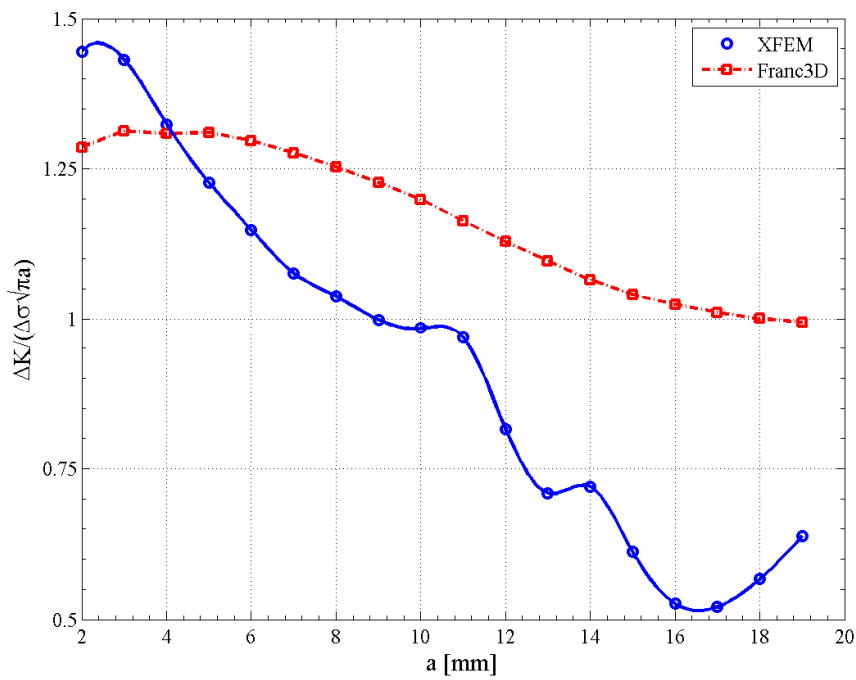


Figure A.16 Comparison of geometry factors, $F(a)$, during the crack propagation on flange plate (No.2 case).

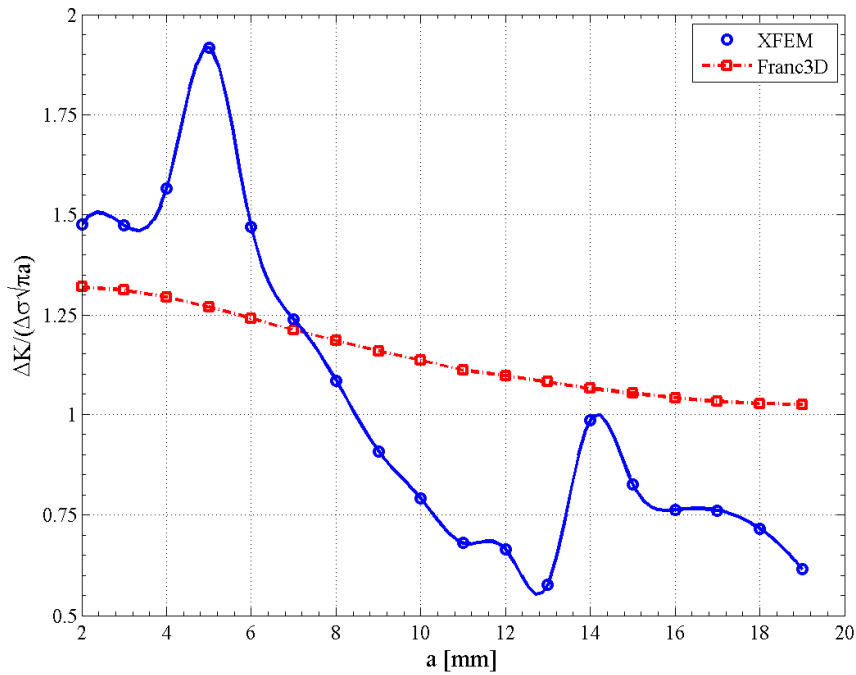


Figure A.17 Comparison of geometry factors, $F(a)$, during the crack propagation on web plate (No.2 case).

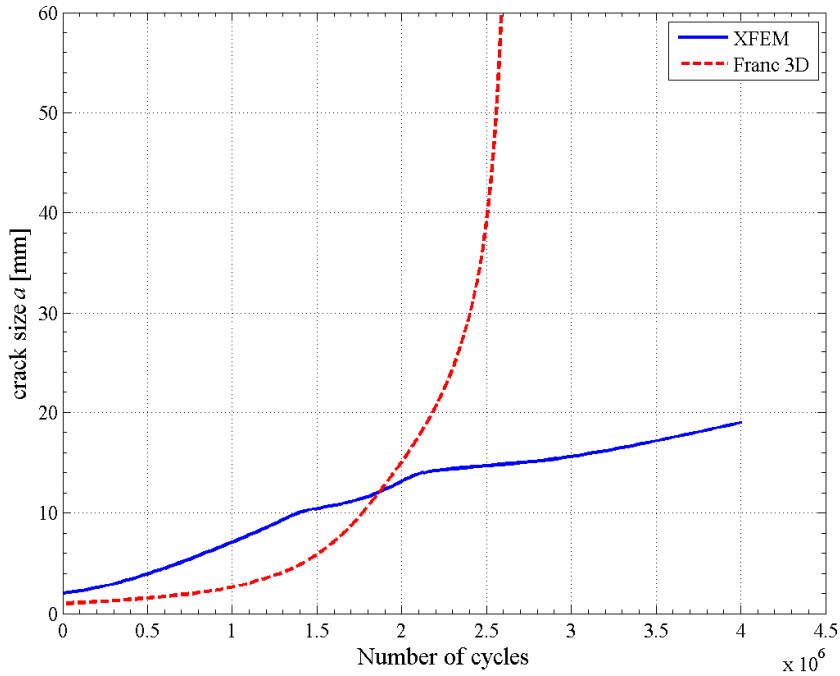


Figure A.18 Comparison of cycle counting during crack propagation for XFEM and FRANC3D analysis on flange plate (No.2 case).

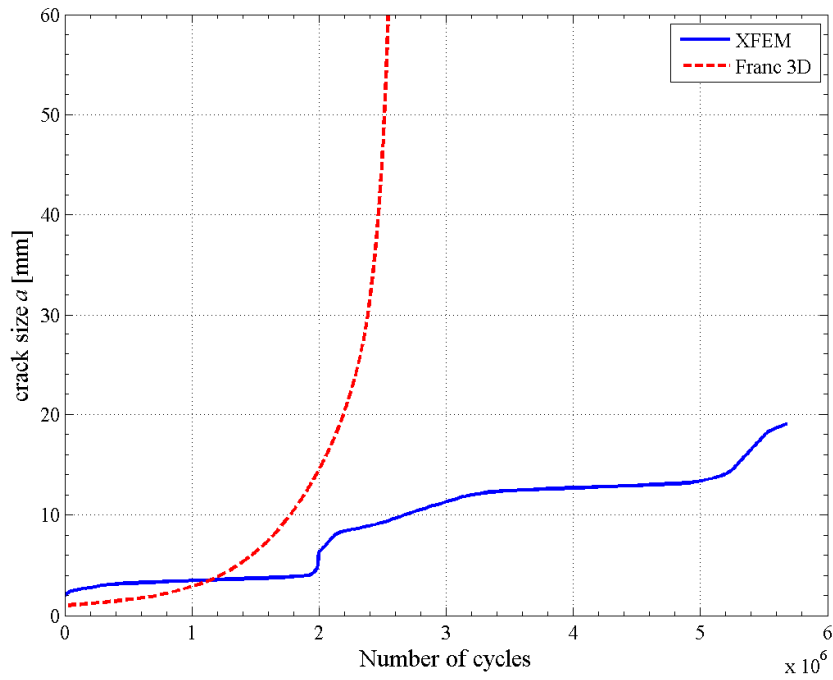


Figure A.19 Comparison of cycle counting during crack propagation for XFEM and FRANC3D analysis on web plate (No.2 case)

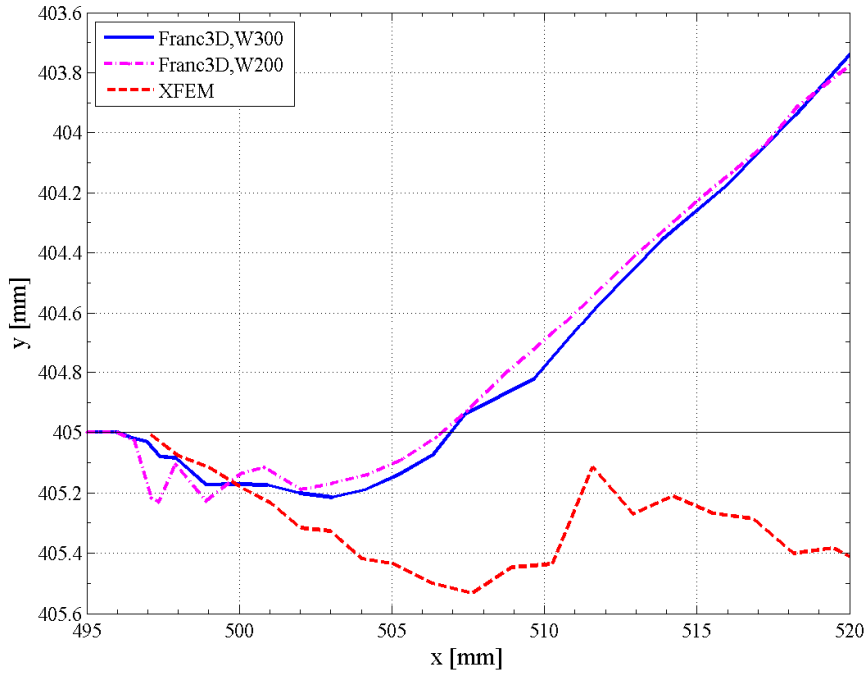


Figure A.20 Comparison of crack path on flange plate for results from FRANC3D and XFEM.

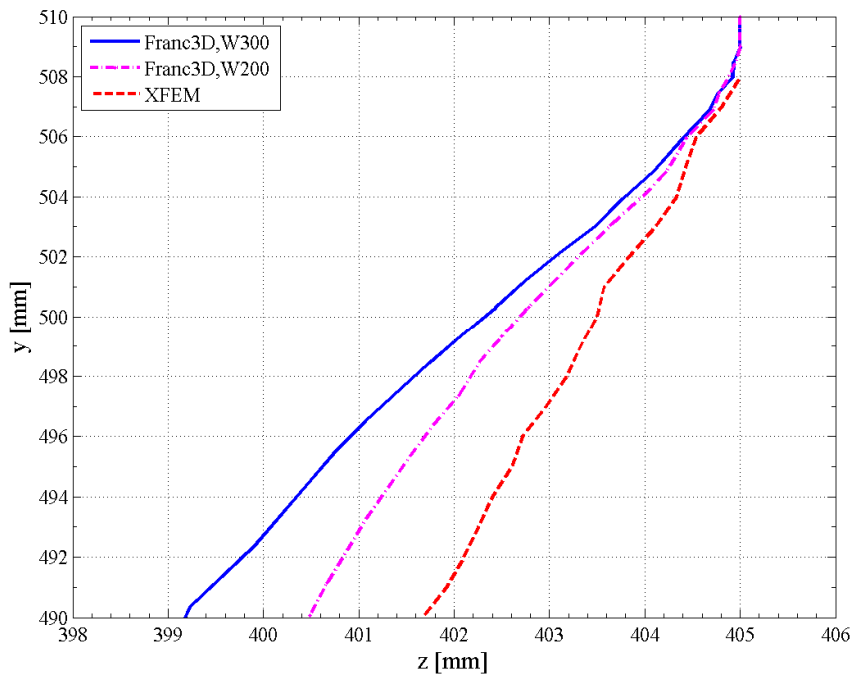


Figure A.21 Comparison of crack path on web plate for results from FRANC3D and XFEM

Appendix B

This appendix is the collection of codes. The MATLAB codes (with the file extension “*m*”) were developed in version 2013b; while the PYTHON codes (with the file extension “*py*”) were completed in version 2.7.

curvature2sigma.m

```

% curvature2sigma.m - The main function for stiffened elements stress
% calculation in Incremental Iterative Approach calculation.
% Authors: Qiaojian Ye (qiaojian@student.chalmers.se).
% June 2015, Department of Shipping and Marine Technology,
% Chalmers University of Technology.
% This file is part of the Master Thesis work:
% Consequence of cracks presence on ship structures.
% The codes are used for the evaluation of
% ship hull girder ultimate strength.

% ----- %
%           Incremental Iterative Approach calculation           %
%           Function for stiffened elements                     %
% ----- %

function sigma=curvature2sigma(epsilon_bar, sigma_0, s, t, E, n, nu, P_r, l, ...
    A_stiff, I_e, b_f, t_f, d_w, t_w, y_0, z_0, I_y, I_z, A_s)

for a=1:1:113
    if epsilon_bar(a)>0
        if epsilon_bar(a)>1           % Yielding in tension
            sigma(a)=sigma_0;
        else
            sigma(a)=sigma_0*epsilon_bar(a);
        end
    else
        %% Beam-column buckling
        beta_E=s(a)/t(a)*sqrt(epsilon_bar(a)^n*sigma_0/E);
        if beta_E>1
            C_E=2/beta_E-1/beta_E^2;
        else
            C_E=1;
        end
        s_E_e=C_E*s(a);
        r_e=sqrt(I_e(a)/A_stiff(a));
        sigma_EC=pi^2*E*r_e^2/(1)^2; % sigma_E(C)
        if sigma_EC<=P_r*sigma_0 % sigma_CA
            sigma_CA=sigma_EC;
        else
            sigma_CA=sigma_0*(1-P_r*(1-P_r)*sigma_0/sigma_EC);
        end
        if sigma_EC<=P_r*sigma_0*epsilon_bar(a)^n % sigma_E_CA
            sigma_E_CA=sigma_EC/epsilon_bar(a)^n;
        else
            sigma_E_CA=sigma_0*(1-P_r*(1-P_r)*...
                sigma_0*epsilon_bar(a)^n/sigma_EC);
        end
        if -epsilon_bar(a)<=sigma_CA/sigma_0 % sigma_C1
            sigma_C1=sigma_0*epsilon_bar(a);
        else
            sigma_C1=-sigma_E_CA*(A_s(a)+s_E_e*t(a))/(A_s(a)+s(a)*t(a));
        end
    end
end

```

```

end
%% Torsion buckling
beta=s(a)/t(a)*(sigma_0/E);
if beta>1
    C_x=2/beta-1/beta^2;
else
    C_x=1;
end
sigma_Ux=C_x*sigma_0;
beta_E=s(a)/t(a)*sqrt(epsilon_bar(a)^n*sigma_0/E);

if beta_E>1
    C_E=2/beta_E-1/beta_E^2;
else
    C_E=1;
end
alpha=1/s(a);
if -epsilon_bar(a)<=sigma_Ux/sigma_0
    sigma_E_UP=sigma_0*epsilon_bar(a);
else
    if alpha>=1
        sigma_E_UP=C_E*sigma_0;
    else
        sigma_E_UP=(C_E*s(a)/1(a)+0.1*(1-s(a)/1(a))*...
            (1+1/beta_E^2)^2)*sigma_0;
    end

end

b1=b_f(a)/2;
u=1-2*b1/b_f(a);
m=1-u*(0.7-0.1*d_w(a)/b_f(a));
C_0=E*(t(a))^3/3/(s(a));
I_zf=t_f(a)*(b_f(a))^3/12;
Gamma=m*I_zf*(d_w(a))^2+(d_w(a))^3*(t_w(a))^3/36;
p=2;
q=100;
sigma_cL=pi^2*E*(p/alpha+alpha/p)^2*(t(a)/s(a))^2/12/(1-nu^2);
I_0=I_y(a)+m*I_z(a)+A_s(a)*(y_0(a)^2+z_0(a)^2);
K=(b_f(a)*(t_f(a))^3+d_w(a)*(t_w(a))^3)/3;
sigma_ET=(K/2.6+(q*pi/(1))^2*Gamma+C_0/E*(1/q/pi)^2)/...
    (I_0+C_0/sigma_cL*(1/(q*pi))^2)*E;
if sigma_ET<=P_r*sigma_0*epsilon_bar(a)^n % sigma_E_CT
    sigma_E_CT=sigma_ET/epsilon_bar(a)^n;
else
    sigma_E_CT=sigma_0*(1-P_r*(1-P_r)*...
        sigma_0*epsilon_bar(a)^n/sigma_ET);
end
if sigma_ET<=P_r*sigma_0 % sigma_CT
    sigma_CT=sigma_ET;
else
    sigma_CT=sigma_0*(1-P_r*(1-P_r)*sigma_0/sigma_ET);
end

```

```

end
if -epsilon_bar(a) <= sigma_CT/sigma_0 % sigma_C2
    sigma_C2=sigma_0*epsilon_bar(a);
else
    sigma_C2=- (sigma_E_CT*A_s(a)+sigma_E_UP*s(a)*t(a))/...
        (A_s(a)+s(a)*t(a));
end
%% Local Buckling
if -epsilon_bar(a) <= sigma_Ux/sigma_0
    sigma_E_UP=sigma_0*epsilon_bar(a);
else
    if alpha >= 1
        sigma_E_UP=C_E*sigma_0;
    else
        sigma_E_UP=(C_E*s(a)/l(a)+0.1*(1-s(a)/l(a))*...
            (1+1/beta_E^2)^2)*sigma_0;
    end
end
C_s=1;% for angle or tee bar
k_s=4*C_s;
sigma_EW=k_s*pi^2*E/12/(1-nu^2)*(t_w(a)/d_w(a))^2;
sigma_EF=0.44*pi^2*E/12/(1-nu^2)*(t_f(a)/0.5/b_f(a))^2;
sigma_EL=sigma_EW; % = sigma_EF
if sigma_EL <= P_r*sigma_0*epsilon_bar(a)^n % sigma_E_CT
    sigma_E_CL=sigma_EL/epsilon_bar(a)^n;
else
    sigma_E_CL=sigma_0*(1-P_r*(1-P_r))*...
        sigma_0*epsilon_bar(a)^n/sigma_EL;
end
sigma_CL=sigma_EW;

if -epsilon_bar(a) <= sigma_CL/sigma_0 % sigma_C3
    sigma_C3=sigma_0*epsilon_bar(a);
else
    sigma_C3=- (sigma_E_CL*A_s(a)+sigma_E_UP*s(a)*t(a))/...
        (A_s(a)+s(a)*t(a));
end
sigma(a)=min(sigma_C1, sigma_C2, sigma_C3); % Choose the min value
end
end
end

```

```

% IIA_hogging_sagging.m - The main function for Incremental Iterative Approach calculation
% Authors: Qiaojian Ye (qiaojian@student.chalmers.se).
% June 2015, Department of Shipping and Marine Technology,
% Chalmers University of Technology.
% This file is part of the Master Thesis work:
% Consequence of cracks presence on ship structures.
% The codes are used for the evaluation of
% ship hull girder ultimate strength.

% ----- %
%           Incremental Iterative Approach calculation code           %
% ----- %

clc
clear all
close all

E=206000;           %MPa
sigma_0=355;       %MPa
epsilon_0=sigma_0/E;
n=2;
nu=0.3;
P_r=0.6;
l=5250;
z_stiff=xlsread('C:\Users\pc\Desktop\data', 1, 'T3:T115');
A_stiff=xlsread('C:\Users\pc\Desktop\data', 1, 'N3:N115');
n_stiff=xlsread('C:\Users\pc\Desktop\data', 1, 'M3:M115');
s=xlsread('C:\Users\pc\Desktop\data', 1, 'G3:G115');
t=xlsread('C:\Users\pc\Desktop\data', 1, 'H3:H115');
I_e=xlsread('C:\Users\pc\Desktop\data', 1, 'X3:X115');
b_f=xlsread('C:\Users\pc\Desktop\data', 1, 'K3:K115');
t_f=xlsread('C:\Users\pc\Desktop\data', 1, 'L3:L115');
d_w=xlsread('C:\Users\pc\Desktop\data', 1, 'I3:I115');
t_w=xlsread('C:\Users\pc\Desktop\data', 1, 'J3:J115');
y_0=xlsread('C:\Users\pc\Desktop\data', 2, 'J2:J114');
z_0=xlsread('C:\Users\pc\Desktop\data', 2, 'K2:K114');
I_y=xlsread('C:\Users\pc\Desktop\data', 2, 'L2:L114');
I_z=xlsread('C:\Users\pc\Desktop\data', 2, 'M2:M114');
z_cor=xlsread('C:\Users\pc\Desktop\data', 1, 'T116:T127');
A_cor=xlsread('C:\Users\pc\Desktop\data', 1, 'O116:O127');
I_red=646.5*2;
z_dk_mean=30.525;
z_NA_red=12.9893;
Z_red=I_red/(z_dk_mean-z_NA_red);
M_U_sagging=-Z_red*sigma_0*10^3;
M_U_hogging=I_red/z_NA_red*sigma_0*10^3;
M_yd=M_U_hogging;
k_F=3*M_yd/(E*I_red)*10^-3;
delta_k=k_F/30;
A_s=A_stiff-s.*t;
%% Sagging condition
i=1;

```

```

for chi=0:-delta_k:-k_F;

    epsilon_stiff=chi.*z_stiff;
    epsilon_bar=epsilon_stiff/epsilon_0;
    sigma=curvature2sigma3(epsilon_bar, sigma_0, s, t, E, n, nu, P_r, l, ...
        A_stiff, I_e, b_f, t_f, d_w, t_w, y_0, ...
        z_0, I_y, I_z, A_s); %stress for stiffened elements
    epsilon_cor=chi*z_cor;
    epsilon_bar2=epsilon_cor/epsilon_0;
    if epsilon_bar2<-1
        sigma_cor=-sigma_0;
    elseif epsilon_bar2>1
        sigma_cor=sigma_0;
    else
        sigma_cor=sigma_0*epsilon_bar2; %Stress in cornered elements
    end
    F1=sigma'.*A_stiff.*n_stiff; %Force for stiffened elements
    F2=sigma_cor.*A_cor; % Force for cornered elements
    F=(sum(F1(:))+sum(F2(:)))/10000;
    if abs(F)>10
        while abs(F)>10
            if F>0 %Adjust NA
                z_stiff=z_stiff+0.0001*ones(113, 1);
                z_cor=z_cor+0.0001*ones(12, 1);
                z_NA_red=z_NA_red-0.0001;
            else
                z_stiff=z_stiff-0.0001*ones(113, 1);
                z_cor=z_cor-0.0001*ones(12, 1);
                z_NA_red=z_NA_red+0.0001;
            end
            epsilon_stiff=chi.*z_stiff;
            epsilon_bar=epsilon_stiff/epsilon_0;
            sigma=curvature2sigma3(epsilon_bar, sigma_0, s, t, E, n, nu, ...
                P_r, l, A_stiff, I_e, b_f, t_f, ...
                d_w, t_w, y_0, z_0, I_y, I_z, A_s); %stress for stiffened elements
            epsilon_cor=chi*z_cor;
            epsilon_bar2=epsilon_cor/epsilon_0;
            if epsilon_bar2<-1
                sigma_cor=-sigma_0;
            elseif epsilon_bar2>1
                sigma_cor=sigma_0;
            else
                sigma_cor=sigma_0*epsilon_bar2; %Stress in cornered elements
            end
            F1=sigma'.*A_stiff.*n_stiff; %Force for stiffened elements
            F2=sigma_cor.*A_cor; % Force for cornered elements
            F=(sum(F1(:))+sum(F2(:)))/10000; % Sum of force
        end
        m_stiff=F1.*z_stiff/1000;
        m_cor=F2.*z_cor/1000;
    end
end

```

```

        M_sagging(i)=sum(m_stiff(:))+sum(m_cor(:));
        Z_NA_sagging(i)=z_NA_red;
    else
        m_stiff=F1.*z_stiff/1000;
        m_cor=F2.*z_cor/1000;

        M_sagging(i)=sum(m_stiff(:))+sum(m_cor(:));
        Z_NA_sagging(i)=z_NA_red;
    end
    i=i+1;
end

%% Hogging condition
z_NA_red=12.9893;
z_stiff=xlsread('C:\Users\pc\Desktop\data',1,'T3:T115');
z_cor=xlsread('C:\Users\pc\Desktop\data',1,'T116:T127');
i=1;
for chi=0:delta_k:k_F;
    epsilon_stiff=chi.*z_stiff;
    epsilon_bar=epsilon_stiff/epsilon_0;
    sigma=curvature2sigma3(epsilon_bar, sigma_0, s, t, E, ...
        n, nu, P_r, l, A_stiff, I_e, b_f, ...
        t_f, d_w, t_w, y_0, z_0, I_y, I_z, A_s); %stress for stiffened elements
    epsilon_cor=chi*z_cor;
    epsilon_bar2=epsilon_cor/epsilon_0;
    if epsilon_bar2<-1
        sigma_cor=-sigma_0;
    elseif epsilon_bar2>1
        sigma_cor=sigma_0;
    else
        sigma_cor=sigma_0*epsilon_bar2; %Stress in cornered elements
    end

    F1=sigma'.*A_stiff.*n_stiff;%Force for stiffened elements
    F2=sigma_cor.*A_cor; % Force for cornered elements
    F=(sum(F1(:))+sum(F2(:)))/10000; % Sum of force
    if abs(F)>10
        while abs(F)>10
            if F>0 %Adjust NA
                z_stiff=z_stiff-0.0001*ones(113,1);
                z_cor=z_cor-0.0001*ones(12,1);
                z_NA_red=z_NA_red+0.0001;
            else
                z_stiff=z_stiff+0.0001*ones(113,1);
                z_cor=z_cor+0.0001*ones(12,1);
                z_NA_red=z_NA_red-0.0001;
            end

            epsilon_stiff=chi.*z_stiff;
            epsilon_bar=epsilon_stiff/epsilon_0;
            sigma=curvature2sigma3(epsilon_bar, sigma_0, s, t, E, ...

```

```

n, nu, P_r, l, A_stiff, I_e, b_f, ...
t_f, d_w, t_w, y_0, z_0, I_y, I_z, A_s); %stress for stiffened elements
epsilon_cor=chi*z_cor;
epsilon_bar2=epsilon_cor/epsilon_0;
if epsilon_bar2<-1
    sigma_cor=-sigma_0;
elseif epsilon_bar2>1
    sigma_cor=sigma_0;
else
    sigma_cor=sigma_0*epsilon_bar2; %Stress in cornered elements
end

F1=sigma'.*A_stiff.*n_stiff;%Force for stiffened elements
F2=sigma_cor.*A_cor;      % Force for cornered elements
F=(sum(F1(:))+sum(F2(:)))/10000;% Sum of force
end
m_stiff=F1.*z_stiff/1000;
m_cor=F2.*z_cor/1000;

M_hogging(i)=sum(m_stiff(:))+sum(m_cor(:));
Z_NA_hogging(i)=z_NA_red;
else
m_stiff=F1.*z_stiff/1000;
m_cor=F2.*z_cor/1000;

M_hogging(i)=sum(m_stiff(:))+sum(m_cor(:));
Z_NA_hogging(i)=z_NA_red;
end
end
i=i+1;
end

k1=0:-delta_k:-k_F;
k2=0:delta_k:k_F;
figure(1)
plot(k1, M_sagging, 'r*-')
hold on
plot(k2, M_hogging, 'bo-')

figure(2)
plot(k1, Z_NA_sagging, 'r*-')
hold on
plot(k2, Z_NA_hogging, 'bo-')

```

Load-end_shortening_curve_drawing.m

```

% Load-en_shortening_curve.m - The main function load-end shortening
% drawing.
% Authors: Qiaojian Ye (qiaojian@student.chalmers.se).
% June 2015, Department of Shipping and Marine Technology,
% Chalmers University of Technology.
% This file is part of the Master Thesis work:
% Consequence of cracks presence on ship structures.
% The codes are used for the evaluation of
% ship hull girder ultimate strength.

% ----- %
%           Load-end shortening curves           %
% ----- %

clc
clear all
close all
E=206000;
sigma_0=355;
nu=0.3;
epsilon_0=sigma_0/E;
n=2;
s=855;
t=19;
l=5250;
P_r=0.6;
alpha=1/s;
b_f=190; %mm
t_f=22; %mm
d_w=590; %mm
t_w=11; %mm
d_NA=(b_f*t_f*(t/2+d_w+t_f/2)+d_w*t_w*(t/2+d_w/2))/(b_f*t_f+d_w*t_w*s*t);
y_0=0;
z_0=(b_f*t_f*(d_w+t_f/2)+d_w*t_w*d_w/2)/(b_f*t_f+d_w*t_w);
I_y=b_f*t_f^3/12+b_f*t_f*(d_w+t_f/2-z_0)^2+t_w*d_w^3/12+d_w*t_w*(d_w/2-z_0)^2;
I_z=t_f*b_f^3/12+d_w*t_w^3/12;
A_s=b_f*t_f+d_w*t_w;
A_e=A_s+s*t; %total sectional area
s_e=s;
A_e=A_s+s_e*t; %mm2
I_e=b_f*t_f^3/12+b_f*t_f*(t/2+d_w+t_f/2-d_NA)^2+...
    t_w*d_w^3/12+d_w*t_w*(t/2+d_w/2-d_NA)^2+...
    s*t^3/12+s*t*d_NA^2; %moment of inertia of longitudinal or stiffener, accounting for the effective
width

%% Plate element
% Yielding in tension
z=17;
i=1;
for chi=0:0.00001:0.001
    epsilon=chi*z;
    epsilon_bar=epsilon/epsilon_0;

```

```

if epsilon_bar>1
    sigma=sigma_0;
else
    sigma=sigma_0*epsilon_bar;
end
i=i+1;
figure(1)
plot(epsilon_bar, sigma/sigma_0, '*-')
hold on
end

% Buckling in compression
i=1;
for chi=0:0.00001:0.001
    epsilon=chi*z;
    epsilon_bar=epsilon/epsilon_0;
    beta=s/t*(sigma_0/E);
    if beta>1
        C_x=2/beta-1/beta^2;
    else
        C_x=1;
    end
    sigma_Ux=C_x*sigma_0;
    beta_E=s/t*sqrt(epsilon_bar^n*sigma_0/E);
    if beta_E>1
        C_E=2/beta_E-1/beta_E^2;
    else
        C_E=1;
    end
    if epsilon_bar<=sigma_Ux/sigma_0
        sigma_E_UP=sigma_0*epsilon_bar;
    else
        if alpha>=1
            sigma_E_UP=C_E*sigma_0;
        else
            sigma_E_UP=(C_E*s/1+0.1*(1-s/1)*(1+1/beta_E^2)^2)*sigma_0;
        end
    end
    i=i+1;
    figure(1)
    plot(-epsilon_bar, -sigma_E_UP/sigma_0, '*-')
    hold on
end
grid on;
xlabel(' Strain ratio,  $\epsilon$  ');
ylabel(' stress ratio,  $\sigma_{UP}/\sigma_0$  ');
title(' Load-end shortening curve for plate ultimate strength')
print -dpng plate_ultimate_strength

```

```

%% Stiffener element
% Yielding in tension
for chi=0:0.00001:0.001
    epsilon=chi*z;
    epsilon_bar=epsilon/epsilon_0;
    if epsilon_bar>1
        sigma=sigma_0;
    else
        sigma=sigma_0*epsilon_bar;
    end
    figure(2)
    plot(epsilon_bar, sigma/sigma_0, '*-')
    hold on
end
% Beam-column buckling
for chi=0:0.00001:0.001
    epsilon=chi*z;
    epsilon_bar=epsilon/epsilon_0;
    beta_E=s/t*sqrt(epsilon_bar^n*sigma_0/E);
    if beta_E>1
        C_E=2/beta_E-1/beta_E^2;
    else
        C_E=1;
    end
    s_E_e=C_E*s;
    r_e=sqrt(I_e/A_e);
    sigma_EC=pi^2*E*r_e^2/l^2; % sigma_E(C)
    if sigma_EC<=P_r*sigma_0 % sigma_CA
        sigma_CA=sigma_EC;
    else
        sigma_CA=sigma_0*(1-P_r*(1-P_r)*sigma_0/sigma_EC);
    end
    if sigma_EC<=P_r*sigma_0*epsilon_bar^n % sigma_E_CA
        sigma_E_CA=sigma_EC/epsilon_bar^n;
    else
        sigma_E_CA=sigma_0*(1-P_r*(1-P_r)*sigma_0*epsilon_bar^n/sigma_EC);
    end
    if epsilon_bar<=sigma_CA/sigma_0 % sigma_C1
        sigma_C1=sigma_0*epsilon_bar;
    else
        sigma_C1=sigma_E_CA*(A_s+s_E_e*t)/(A_s+s*t);
    end
    figure(2)
    plot(-epsilon_bar, -sigma_C1/sigma_0, '*')
    hold on
end
grid on;
xlabel(' Strain ratio,  $\epsilon$  ');
ylabel(' stress ratio,  $\sigma_{UP}/\sigma_0$  ');
hold on
% Torsional-flexural buckling

```

```

for chi=0:0.00001:0.001
    epsilon=chi*z;
    epsilon_bar=epsilon/epsilon_0;
    if epsilon_bar>1
        sigma=sigma_0;
    else
        sigma=sigma_0*epsilon_bar;
    end
    figure(2)
    plot(epsilon_bar, sigma/sigma_0, 'r.')
    hold on
end
for chi=0:0.00001:0.001
    epsilon=chi*z;
    epsilon_bar=epsilon/epsilon_0;
    beta=s/t*(sigma_0/E);
    if beta>1
        C_x=2/beta-1/beta^2;
    else
        C_x=1;
    end
    sigma_Ux=C_x*sigma_0;
    beta_E=s/t*sqrt(epsilon_bar^n*sigma_0/E);
    if beta_E>1
        C_E=2/beta_E-1/beta_E^2;
    else
        C_E=1;
    end
    if epsilon_bar<=sigma_Ux/sigma_0
        sigma_E_UP=sigma_0*epsilon_bar;
    else
        if alpha>=1
            sigma_E_UP=C_E*sigma_0;
        else
            sigma_E_UP=(C_E*s/1+0.1*(1-s/1)*(1+1/beta_E^2)^2)*sigma_0;
        end
    end
    b1=b_f/2;
    u=1-2*b1/b_f;
    m=1-u*(0.7-0.1*d_w/b_f);
    C_0=E*t^3/3/s;
    I_zf=t_f*b_f^3/12*(1+3*u^2*d_w*t_w/A_s);
    Gamma=m*I_zf*d_w^2+d_w^3*t_w^3/36;
    p=2;
    q=100;
    sigma_cL=pi^2*E*(p/alpha+alpha/p)^2*(t/s)^2/12/(1-nu^2);
    I_0=I_y+m*I_z+A_s*(y_0^2+z_0^2);
    K=(b_f*t_f^3+d_w*t_w^3)/3;
    sigma_ET=(K/2.6+(q*pi/1)^2*Gamma+C_0/E*(1/q/pi)^2)/(I_0+C_0/sigma_cL*(1/(q*pi))^2)*E;
    if sigma_ET<=P_r*sigma_0*epsilon_bar^n % sigma_E_CT
        sigma_E_CT=sigma_ET/epsilon_bar^n;
    end
end

```

```

else
    sigma_E_CT=sigma_0*(1-P_r*(1-P_r)*sigma_0*epsilon_bar^n/sigma_ET);
end
if sigma_ET<=P_r*sigma_0 % sigma_CT
    sigma_CT=sigma_ET;
else
    sigma_CT=sigma_0*(1-P_r*(1-P_r)*sigma_0/sigma_ET);
end
if epsilon_bar<=sigma_CT/sigma_0 % sigma_C2
    sigma_C2=sigma_0*epsilon_bar;
else
    sigma_C2=(sigma_E_CT*A_s+sigma_E_UP*s*t)/(A_s+s*t);
end
figure(2)
plot(-epsilon_bar, -sigma_C2/sigma_0, 'r.')
hold on
end
grid on;
xlabel(' Strain ratio,  $\epsilon$  ');
ylabel(' stress ratio,  $\sigma_{UP}/\sigma_0$  ');
% Local buckling of stiffeners
for chi=0:0.00001:0.001
    epsilon=chi*z;
    epsilon_bar=epsilon/epsilon_0;
    if epsilon_bar>1
        sigma=sigma_0;
    else
        sigma=sigma_0*epsilon_bar;
    end
    figure(2)
    title(' Load-end shortening curve for Siffened element' )
    plot(epsilon_bar, sigma/sigma_0, 'go')
    hold on
end
for chi=0:0.00001:0.001
    epsilon=chi*z;
    epsilon_bar=epsilon/epsilon_0;
    beta=s/t*(sigma_0/E);
    if beta>1
        C_x=2/beta-1/beta^2;
    else
        C_x=1;
    end
    sigma_Ux=C_x*sigma_0;
    beta_E=s/t*sqrt(epsilon_bar^n*sigma_0/E);
    if beta_E>1
        C_E=2/beta_E-1/beta_E^2;
    else
        C_E=1;
    end
    if epsilon_bar<=sigma_Ux/sigma_0

```

```

        sigma_E_UP=sigma_0*epsilon_bar;
    else
        if alpha>=1
            sigma_E_UP=C_E*sigma_0;
        else
            sigma_E_UP=(C_E*s/1+0.1*(1-s/1)*(1+1/beta_E^2)^2)*sigma_0;
        end
    end
    C_s=1;% for angle or tee bar
    k_s=4*C_s;
    sigma_EW=k_s*pi^2*E/12/(1-nu^2)*(t_w/d_w)^2;
    sigma_EF=0.44*pi^2*E/12/(1-nu^2)*(t_f/0.5/b_f)^2;
    sigma_EL=sigma_EW;%=sigma_EF
    if sigma_EL<=P_r*sigma_0*epsilon_bar^n % sigma_E_CT
        sigma_E_CL=sigma_EL/epsilon_bar^n;
    else
        sigma_E_CL=sigma_0*(1-P_r*(1-P_r)*sigma_0*epsilon_bar^n/sigma_EL);
    end
    sigma_CL=sigma_EW;
    if epsilon_bar<=sigma_CL/sigma_0 % sigma_C3
        sigma_C3=sigma_0*epsilon_bar;
    else
        sigma_C3=(sigma_E_CL*A_s+sigma_E_UP*s*t)/(A_s+s*t);
    end
    figure(2)
    plot(-epsilon_bar,-sigma_C3/sigma_0,'go')
    hold on
end
grid on;
xlabel(' Strain ratio,  $\epsilon'$  ');
ylabel(' stress ratio,  $\sigma_{UP}/\sigma_0'$  ');
print -dpng Stiffener_ultimate_strength
%% Corner element
for chi=0.001:0.00001:0.001
    epsilon=chi*z;
    epsilon_bar=epsilon/epsilon_0;
    if epsilon_bar<-1
        sigma=-sigma_0;
    elseif epsilon_bar>1
        sigma=sigma_0;
    else
        sigma=sigma_0*epsilon_bar;
    end
    figure(3)
    plot(epsilon_bar, sigma/sigma_0, '*-')
    hold on
end
grid on;
xlabel(' Strain ratio,  $\epsilon'$  ');
ylabel(' stress ratio,  $\sigma_{UP}/\sigma_0'$  ');
title(' Load-end shortening curve for Corner element')

```

```

1  #-*- coding: utf-8 -*-
2  # odbPrintENRRTXFEM.py - Extract the XFEM crack tip information from ABAQUS ODB file
3  # Authors: Da Wu (dawu@student.chalmers.se)
4  # June 2015, Department of Shipping and Marine Technology, Chalmers University of Technology
5  # This file is part of the Master Thesis work:
6  # Consequence of cracks presence on ship structures.
7  # The codes are used for the evaluation of ship structure elements EDGE crack growth
8
9
10 import sys
11 import os
12 import logging
13 import time
14 from collections import OrderedDict
15
16 from odbAccess import *
17 from abaqusConstants import *
18
19
20 def element_nodes(instance, element_label):
21     """
22     Gte nodes in given elements
23     """
24     element_ind = element_label - 1
25     node_inds = sorted(instance.elements[element_ind].connectivity)
26     node_inds = [n - 1 for n in node_inds]
27     nodes_label = [instance.nodes[ind].label for ind in node_inds]
28     return nodes_label
29
30
31 def odb_prin_enrtrxfem(odb_path, instance_name, part):
32     """
33     Extract crack tip outputs
34     """
35     odb = openOdb(path=odb_path)
36     if part.upper() == 'FLANGE':
37         axes = 0 # means x axis
38         rev = False
39     elif part.upper() == 'WEB':
40         axes = 1 # means y axis
41         rev = True
42     else:
43         logger.error('please define "FLANGE" or "WEB"...\n')
44         sys.exit(1)
45
46     # -----
47     # initialize instance, element set, node set
48     # -----
49     output_file_name = 'crack_length_history_' + part.lower()
50     element_set = part.upper() + '-ELEMENT'
51     node_sets = part.upper() + '-NODE'
52     logger.info('assembly name: ' + str(odb.rootAssembly.name))
53     grout_instance = odb.rootAssembly.instances[instance_name.upper()]
54     elset = odb.rootAssembly.elementSets[element_set.upper()]
55     nset = odb.rootAssembly.nodeSets[node_sets.upper()]
56     logger.info('region name: ' + part + '\n')
57     # -----

```

```

58 # start loop steps
59 # -----
60 for key in odb.steps.keys():
61     # start from cyclic step
62     if key == 'Step-Static':
63         continue
64     step = odb.steps[key]
65     logger.info('step = ' + key)
66     frame_repository = step.frames
67     if len(frame_repository):
68         # labels of nodes for determine the crack tip location
69         phi_node_list = []
70         # store all phi values and relevant node labels
71         phi_dict = {}
72         # store crack instance and relevant time
73         crack_dict = {}
74         # xfem happen element and nodes
75         statxfem_element_list = []
76         # statxfem_node_list = []
77         # -----
78         # extract data at each time
79         # -----
80         for frame in frame_repository:
81             logger.info('Id = %d, Time = %f' % (frame.frameId, frame.frameValue))
82             ENRRT = frame.fieldOutputs['ENRRTXFEM']
83             PHI = frame.fieldOutputs['PHILSM']
84             STAXFEM = frame.fieldOutputs['STAXXFEM']
85             enrrt_grout = ENRRT.getSubset(region=elset)
86             statxfem_grout = STAXFEM.getSubset(region=elset)
87             phi_grout = PHI.getSubset(region=nset)
88             # -----
89             # extract statusxfem value
90             # -----
91             # current frame xfem nodes list
92             statxfem_node_list = []
93             # collect the xfem=1 elements and node labels
94             for value in statxfem_grout.values:
95                 if not value.elementLabel in statxfem_element_list:
96                     if value.data == 1.0:
97                         # add current frame xfem element into list
98                         statxfem_element_list.append(value.elementLabel)
99                         statxfem_node_list = list(set(statxfem_node_list +
100                                                         element_nodes(grout_instance, value.elementLabel)))
101
102             # -----
103             # extract enrrt value
104             # -----
105             # enrrt element list at current time
106             enrrtxfem_dict = {}
107             for value in enrrt_grout.values:
108                 if value.data.any():
109                     nodes_label = element_nodes(grout_instance, value.elementLabel)
110                     if value.elementLabel in enrrtxfem_dict.keys():
111                         logger.info('update enrrt value at element:' + str(value.elementLabel))
112                         # update the maximum enrrt value at this element
113                         if sum([d for d in value.data]) > sum([d for d in enrrtxfem_dict[value.elementLabel][0]]):
114                             # nodes list at this element
115                             enrrtxfem_dict[value.elementLabel] = [
116                                 (value.data[0], value.data[1], value.data[2]).extend(nodes_label)
117                             ]
118                 else:

```

```

118         enrtrxfem_dict.setdefault(value.elementLabel, []).append(
119             (value.data[0], value.data[1], value.data[2]))
120         enrtrxfem_dict.setdefault(value.elementLabel, []).extend(nodes_label)
121
122     logger.info('field output componentLabels: ' + str(ENRRT.componentLabels))
123     logger.info('enrtrxfem: ' + str(OrderedDict(
124         sorted(enrtrxfem_dict.items(), key=lambda t: t[0]).items()))
125     # -----
126     # extract phislm value
127     # -----
128     # store phi node at current list
129     current_phi_node = []
130     for value in phi_grout.values:
131         if abs(value.data) < 1e6:
132             if value.nodeLabel in statxfem_node_list:
133                 phi_dict.setdefault(value.nodeLabel, value.data)
134                 current_phi_node.append(value.nodeLabel)
135
136     # find out the tip end boundary
137     # select 4 nodes touched current xfem element
138     if any(current_phi_node):
139         # find front nodes {key=node label, content=(x or y, z, phi value)}
140         selected_node = {}
141         for node_label in current_phi_node:
142             node = grout_instance.nodes[node_label - 1]
143             coords = [axie for axie in node.coordinates]
144             x_coord = coords[axes]
145             z_coord = coords[2]
146             selected_node.setdefault(node_label, (x_coord, z_coord, phi_dict[node_label]))
147
148     # sort phi nodes according to the coordinates
149     od_selected_node = OrderedDict(
150         sorted(selected_node.items(), key=lambda t: t[1][0], reverse=rev))
151
152     # left the last two items
153     for key in od_selected_node:
154         if len(od_selected_node.items()) > 2:
155             del od_selected_node[key]
156
157     # calculate the corrected phi values
158     if len(od_selected_node.items()) == 2:
159         x_coords = []
160         z_coords = []
161         phis = []
162         for key in od_selected_node.keys():
163             x_coords.append(od_selected_node[key][0])
164             z_coords.append(od_selected_node[key][1])
165             phis.append(od_selected_node[key][2])
166
167     # calculate front edge length
168     element_len = ((x_coords[0] - x_coords[1]) ** 2 +
169                 (z_coords[0] - z_coords[1]) ** 2) ** 0.5
170     # calculate scales
171     scale1 = phis[0] / (abs(phis[0]) + abs(phis[1]))
172     scale2 = phis[1] / (abs(phis[0]) + abs(phis[1]))
173     scales = [scale1, scale2]
174     j = 0
175     # update new phi value into phi dictionary
176     for key in od_selected_node.keys():
177         x = od_selected_node[key][0]

```

```

178         y = od_selected_node[key][1]
179         p = scales[j] * element_len
180         od_selected_node[key] = (x, y, p)
181         phi_dict[key] = p
182         j += 1
183
184         # select a phi node into the phi_node_list (closest to front tip)
185         if abs(od_selected_node.items()[0][1][2]) < abs(od_selected_node.items()[-1][1][2]):
186             if not od_selected_node.items()[0][0] in phi_node_list:
187                 phi_node_list.append(od_selected_node.items()[0][0])
188             else:
189                 if not od_selected_node.items()[-1][0] in phi_node_list:
190                     phi_node_list.append(od_selected_node.items()[-1][0])
191
192     else:
193         logger.error('cannot find phism values...\n')
194         sys.exit(1)
195     #-----
196     # calculate crack tip coordinates
197     #-----
198     # the node picked for determine crack front coordinates
199     node = grout_instance.nodes[phi_node_list[-1] - 1]
200     phi_corrdinates = [axie for axie in node.coordinates]
201     # crack location coordinates
202     tip_corrdinates = (
203         phi_corrdinates[0], phi_corrdinates[1], phi_corrdinates[2] - phi_dict[phi_node_list[-1]])
204
205     # find the enrrt element label
206     selected_enrrtxfem_key = None
207     # judge if the enrrt is at the crack front
208     for key in enrrtxfem_dict.keys():
209         enrrt_nodes = element_nodes(grout_instance, key)
210         # if the given enrrt element touches crack front edge
211         # if so, select its enrrt value as crack tip enrrt
212         if node.label in enrrt_nodes:
213             selected_enrrtxfem_key = key
214
215     if not selected_enrrtxfem_key:
216         logger.error('cannot find enrrt values...\n')
217         continue
218
219     # creat a crack instance
220     crack = Crack(time=frame.frameValue, coordinates=tip_corrdinates,
221                  enrrt=enrrtxfem_dict[selected_enrrtxfem_key][0])
222     # add this crack into the dictionary {key=time, content=crack}
223     crack_dict.setdefault(frame.frameValue, crack)
224     # logging messages
225     logger.info('field output name: ' + PHI.name)
226     logger.info('field output componentLabels: ' + str(PHI.componentLabels))
227     logger.info('phi node list: ' + str(phi_node_list))
228     logger.info('phism: @' + str(phi_node_list[-1]) + ': ' + str(phi_dict[phi_node_list[-1]]))
229     logger.info('selected node: ' + str(phi_corrdinates) + '@' + str(node.label))
230     logger.info('selected enrrtxfem: ' + str(enrrtxfem_dict[selected_enrrtxfem_key][0]))
231     logger.info('crack instance: ' + str(crack) + '\n')
232
233     #-----
234     # calculate crack length
235     #-----
236     # sort crack dictionary as time increase
237     od_cracks = OrderedDict(sorted(crack_dict.items(), key=lambda t: t[0]))

```

```

238     # pick the first crack
239     before_last_crack = None
240     last_crack = None
241     # initialize crack length as zero
242     crack_length_list = []
243     for key in od_cracks.keys():
244         # if it's the first crack, then
245         # use the initial crack length
246         if key == od_cracks.keys()[0]:
247             last_crack = od_cracks[key]
248             crack_length_list.append(od_cracks[key].length)
249             continue
250
251         # if it's not the first crack, then
252         # calculate crack length
253         if not cmp(od_cracks[key].coordinates, last_crack.coordinates):
254             del od_cracks[key]
255             continue
256         elif od_cracks[key].coordinates[axes] == last_crack.coordinates[axes]:
257             if before_last_crack:
258                 del od_cracks[last_crack.time]
259                 last_crack = before_last_crack
260                 crack_length_list.pop()
261
262             crack_length = crack_length_list[-1]
263             crack_length += ((od_cracks[key].coordinates[0] - last_crack.coordinates[0]) ** 2 +
264                             (od_cracks[key].coordinates[1] - last_crack.coordinates[1]) ** 2 +
265                             (od_cracks[key].coordinates[2] - last_crack.coordinates[2]) ** 2) ** 0.5
266
267             od_cracks[key].length = crack_length
268             before_last_crack = last_crack
269             last_crack = od_cracks[key]
270             crack_length_list.append(crack_length)
271
272     # -----
273     # write to output file
274     # -----
275     writer(output_file_name, od_cracks)
276     odb.close()
277
278
279 def writer(filename, tips):
280     """
281     write output file
282     """
283     output_file_name = filename + '.csv'
284     try:
285         output_file = open(output_file_name, "w")
286     except IOError as e:
287         print 'I/O error({0}:{1})'.format(e.errno, e.strerror)
288         sys.exit(1)
289
290     output_format = "{0},{1},{2},{3},{4},{5},{6},{7},{8},{9},{10},{11}"
291     output_text = list()
292     output_text.append(
293         output_format.format('index', 'time', 'tip_x', 'tip_y', 'tip_z', 'length', 'enrrt11', 'enrrt22', 'enrrt33',
294                               'k11', 'k22',
295                               'k33'))
296
297     ind = 0

```

```

298 for key in tips.keys():
299     output_line = output_format.format(ind, key, tips[key].coordinates[0], tips[key].coordinates[1],
300                                     tips[key].coordinates[2], tips[key].length, tips[key].enrrt[0],
301                                     tips[key].enrrt[1], tips[key].enrrt[2], tips[key].enrrt2k()[0],
302                                     tips[key].enrrt2k()[1], tips[key].enrrt2k()[2])
303     output_text.append(output_line)
304     ind += 1
305
306 for l in range(len(output_text)):
307     try:
308         # print output_text[l]
309         output_file.write(output_text[l])
310         output_file.write('\n')
311     except IOError as e:
312         print 'I/O error({0}:{1})'.format(e.erno, e.strerror)
313         sys.exit(1)
314
315
316 def new_logger():
317     """
318     create a logger
319     """
320     # -----
321     # create now_logger
322     log_name = time.strftime('%y%m%d%H%M%S', time.localtime(time.time()))
323     logging.basicConfig(filename=log_name + '.log', level=logging.DEBUG)
324     now_logger = logging.getLogger('-')
325     # create console handler and set level to debug
326     ch = logging.StreamHandler()
327     ch.setLevel(logging.DEBUG)
328     # create formatter
329     formatter = logging.Formatter('%(asctime)s - %(name)s - %(levelname)s - %(message)s')
330     # add formatter to ch
331     ch.setFormatter(formatter)
332     # add ch to now_logger
333     now_logger.addHandler(ch)
334     return now_logger
335     # -----
336
337
338 class Crack:
339     """class of crack"""
340
341     def __init__(self, time=0, coordinates=(0.0, 0.0, 0.0), enrrt=(0.0, 0.0, 0.0), length=2):
342         self.time = time
343         self.coordinates = coordinates
344         self.enrrt = enrrt
345         self.length = length
346
347     def __str__(self):
348         strings = [self.time, self.coordinates, self.enrrt]
349         return str(strings)
350
351     def enrrt2k(self, e=210000):
352         k11 = (self.enrrt[0] * e) ** 0.5
353         k22 = (self.enrrt[1] * e) ** 0.5
354         k33 = (self.enrrt[2] * e) ** 0.5
355         return (k11, k22, k33)
356
357

```

```
358 if __name__ == '__main__':
359     logger = new_logger()
360     JobID = r'd:\SIMULIA\Abaqus\Temp\00_ia_xfem_lcf_c12_0_422_50map'
361     odbPath = JobID + r'.odb'
362     logger.info(odbPath)
363     if not os.path.exists(odbPath):
364         print "odb %s does not exist!" % odbPath
365         sys.exit(1)
366     odb_prin_enrrtxfem(odbPath, 'GEO-IA-1', 'FLANGE')
```

main.m

```
% main.m - The main function of the codes used to process SIF data and plot
% cycle numbers versus crack length curve based on Paris law.
% Authors: Da Wu (dawu@student.chalmers.se).
% June 2015, Department of Shipping and Marine Technology,
% Chalmers University of Technology.
% This file is part of the Master Thesis work:
% Consequence of cracks presence on ship structures.
% The codes are used for the evaluation of
% ship structure elements EDGE crack growth.

clear all
close all

%% INDATA
% Add subfolder into system
addpath(genpath(pwd));
% Give the definition of variables
initializeStr;
s = struct([]);
% select a case as : infoW200Web, infoW200Flange, infoW300Web
% infoW300Flange, infoW200F2d, infoW300F2d
% infoW300F2d3d
% Give a input below
ss = [infoW200Web, infoW200Flange, infoW300Web, ...
      infoW300Flange, infoW200F2d, infoW300F2d, ...
      infoW300F2d3d, info2dNoStiff];
s = ss(1);

%%
% Processing
process(s.sampleName, ...
       s.spTitleName, ...
       s.titleName, ...
       s.spPngName, ...
       s.pngName, ...
       s.saveFile);

% Resampling
% Initial strings
outputDataFilePath = 'outputData';
file = [s.saveFile, '.mat'];
saveFile = [file(1:end-4), '_resamp.mat'];
saveFile = fullfile('.', outputDataFilePath, saveFile);
% titleName = [s.pngName, '_resamp'];

% Load selected variables.
vars = {'cycles', 'a_vec', 'DK_vec'};
X = load(file, vars{:});
cycles = X.cycles;
a_vec = X.a_vec;
DK_vec = X.DK_vec;

% Interpolate data with 3rd order spline
S_a_c = csapi(a_vec, cycles);
```

```

S_a_k = csapi(a_vec, DK_vec);
% divide the crack length with space of 0.1 mm
X_p_600 = [a_vec(1):0.1:60];
X_p_60 = [a_vec(1):1:60];
% interpolate SIF value
Y_p = fnval(S_a_c, X_p_600);
Z_p = fnval(S_a_k, X_p_60);

% Exchange axes
cycles = Y_p;
a_vec = X_p_600;
a_vec_60 = X_p_60;
DK_vec = Z_p;
save(saveFile, 'cycles', 'a_vec', 'a_vec_60', 'DK_vec');

```

initializeStr.m

```
% initializeStr.m - The function used to initialize the strings.
% Authors: Da Wu (dawu@student.chalmers.se).
% June 2015, Department of Shipping and Marine Technology,
% Chalmers University of Technology.
% This file is part of the Master Thesis work:
% Consequence of cracks presence on ship structures.
% The codes are used for the evaluation of
% ship structure elements EDGE crack growth.
```

```
clear all
close all
```

```
%% w200, web
% infoW200Web
```

```
infoW200Web = struct('sampleName', '', ...
                    'spTitleName', '', ...
                    'titleName', '', ...
                    'spPngName', '', ...
                    'pngName', '', ...
                    'saveFile', '');
infoW200Web.sampleName = 'w200_web.txt';
infoW200Web.spTitleName = 'W=200 WEB SIF';
infoW200Web.titleName = 'W=200 WEB CRACK GROWTH SPEED';
infoW200Web.spPngName = 'W=200_WEB_SIF';
infoW200Web.pngName = 'W=200_WEB_CRACK_GROWTH_SPEED';
infoW200Web.saveFile = 'f3d_w200_web';
```

```
%% w200, flange
% infoW200Flange
```

```
infoW200Flange = struct('sampleName', '', ...
                       'spTitleName', '', ...
                       'titleName', '', ...
                       'spPngName', '', ...
                       'pngName', '', ...
                       'saveFile', '');
infoW200Flange.sampleName = 'w200_flange.txt';
infoW200Flange.spTitleName = 'W=200 Flange SIF';
infoW200Flange.titleName = 'W=200 Flange CRACK GROWTH SPEED';
infoW200Flange.spPngName = 'W=200_FLANGE_SIF';
infoW200Flange.pngName = 'W=200_FLANGE_CRACK_GROWTH_SPEED';
infoW200Flange.saveFile = 'f3d_w200_flange';
```

```
%% w300, flange
% infoW300Flange
```

```
infoW300Flange = struct('sampleName', '', ...
                       'spTitleName', '', ...
                       'titleName', '', ...
                       'spPngName', '', ...
                       'pngName', '', ...
                       'saveFile', '');
infoW300Flange.sampleName = 'w300_flange.txt';
infoW300Flange.spTitleName = 'W=300 Flange SIF';
```

```

infoW300Flange.titleName = 'W=300 Flange CRACK GROWTH SPEED' ;
infoW300Flange.spPngName = 'W=300_FLANGE_SIF' ;
infoW300Flange.pngName = 'W=300_FLANGE_CRACK_GROWTH_SPEED' ;
infoW300Flange.saveFile = 'f3d_w300_flange' ;

```

```
%% w300, web
```

```
% infoW300Web
```

```

infoW300Web = struct('sampleName', '', ...
                    'spTitleName', '', ...
                    'titleName', '', ...
                    'spPngName', '', ...
                    'pngName', '', ...
                    'saveFile', '');
infoW300Web.sampleName = 'w300_web.txt' ;
infoW300Web.spTitleName = 'W=300 WEB SIF' ;
infoW300Web.titleName = 'W=300 WEB CRACK GROWTH SPEED' ;
infoW300Web.spPngName = 'W=300_WEB_SIF' ;
infoW300Web.pngName = 'W=300_WEB_CRACK_GROWTH_SPEED' ;
infoW300Web.saveFile = 'f3d_w300_web' ;

```

```
%% Case 2D, w200
```

```
% infoW200F2d
```

```

infoW200F2d = struct('sampleName', '', ...
                    'spTitleName', '', ...
                    'titleName', '', ...
                    'spPngName', '', ...
                    'pngName', '', ...
                    'saveFile', '');
infoW200F2d.sampleName = 'f2d_w200.txt' ;
infoW200F2d.spTitleName = 'W=200 SIF' ;
infoW200F2d.titleName = 'W=200 CRACK GROWTH' ;
infoW200F2d.spPngName = 'W=200_SIF' ;
infoW200F2d.pngName = 'W=200_CRACK_GROWTH_F2D' ;
infoW200F2d.saveFile = 'f2d_w200' ;

```

```
%% Case 2D, w300
```

```
% infoW300F2d
```

```

infoW300F2d = struct('sampleName', '', ...
                    'spTitleName', '', ...
                    'titleName', '', ...
                    'spPngName', '', ...
                    'pngName', '', ...
                    'saveFile', '');
infoW300F2d.sampleName = 'f2d_w300.txt' ;
infoW300F2d.spTitleName = 'W=300 SIF' ;
infoW300F2d.titleName = 'W=300 CRACK GROWTH' ;
infoW300F2d.spPngName = 'W=300_SIF' ;
infoW300F2d.pngName = 'W=300_CRACK_GROWTH_F2D' ;
infoW300F2d.saveFile = 'f2d_w300' ;

```

```

%% Case 2D&3D, w300
% infoW300F2d3d
infoW300F2d3d = struct('sampleName', '', ...
                      'spTitleName', '', ...
                      'titleName', '', ...
                      'spPngName', '', ...
                      'pngName', '', ...
                      'saveFile', '');

infoW300F2d3d.sampleName = 'f2d3d_w300.txt';
infoW300F2d3d.spTitleName = 'W=300 SIF F2D3D';
infoW300F2d3d.titleName = 'W=300 CRACK GROWTH F2D3D';
infoW300F2d3d.spPngName = 'W=300_SIF_F2D3D';
infoW300F2d3d.pngName = 'W=300_CRACK_GROWTH_F2D3D';
infoW300F2d3d.saveFile = 'f2d3d_w300';

%% Reference
% info2dNoStiff
info2dNoStiff = struct('sampleName', '', ...
                      'spTitleName', '', ...
                      'titleName', '', ...
                      'spPngName', '', ...
                      'pngName', '', ...
                      'saveFile', '');

info2dNoStiff.sampleName = '2d_no_stiff.txt';
info2dNoStiff.spTitleName = 'W=0 SIF F2D';
info2dNoStiff.titleName = 'W=0 CRACK GROWTH F2D';
info2dNoStiff.spPngName = 'W=0_SIF_F2';
info2dNoStiff.pngName = 'W=0_CRACK_GROWTH_F2D';
info2dNoStiff.saveFile = '2d_no_stiff';

```

process.m

```
function process(sampleName, spTitleName, titleName, spPngName, pngName, saveFile)
%PROCESS Implement the cycle by cycle crack growth
% sampleName: the SIF data sample
% spTitleName: the SIF curve title name
% titleName: the crack growth curve title name
% spPngName: the SIF curve file name
% pngName: the crack growth curve file name
% saveFile: the data collection file name

% process.m - The function used to process SIF data and plot
% cycle numbers versus crack length curve based on Paris law.
% Authors: Da Wu (dawu@student.chalmers.se).
% June 2015, Department of Shipping and Marine Technology,
% Chalmers University of Technology.
% This file is part of the Master Thesis work:
% Consequence of cracks presence on ship structures.
% The codes are used for the evaluation of
% ship structure elements EDGE crack growth.

% INDATA
% material parameters
C = 5.21e-13; % crack growth parameter (mm/cycle, DK in MPa*mm0.5)
n = 3; % crack growth exponent
KIc = 2084.91; % Fracture toughness [MPa*sqrt(mm)]

% Format file path
inputDataFilePath = 'inputData';
sampleName = fullfile('.', inputDataFilePath, sampleName);
outputDataFilePath = 'outputData';
spPngName = fullfile('.', outputDataFilePath, spPngName);
pngName = fullfile('.', outputDataFilePath, pngName);
saveFile = fullfile('.', outputDataFilePath, saveFile);

% Interpolation
nums = textReader(sampleName);
crackLen = nums(1,:);
crackDeltK = nums(2,:);

% Crack sizes
a_ini = crackLen(1); % initial crack size [mm]
a = a_ini; % current crack size [mm]
a_vec = [a]; % vector with crack sizes

% generate a 3rd spline base on crack length and delta K
sp = csapi(crackLen, crackDeltK);
% set the figure handle
h = figure();
fnplt(sp, ':');
cax = gca; % newplot returns handle of current axes
% set(gca, 'XTick', [0:5:65])
set(cax, 'FontName', 'Times', 'FontSize', 12)
xlabel(strcat('Length of crack'), 'FontSize', 14, 'Fontname', 'Times');
ylabel('SIF: \it{K}I \rm[MPa\sqrt{mm}]', 'FontSize', 14, 'Fontname', 'Times');
title(spTitleName);
```

```

grid:
% plot the SIF curve
print(h, '-dpng', spPngName);

% do a cycle by cycle crack growth interation
cycles = [0];
DK_vec = [fnval(sp, a)];
% start loop
k = 1;
tic:
while 1
    if a > 60
        disp (strcat(' End at a=', num2str(a)))
        disp (strcat(' DK=', num2str(DK_vec(end))))
        break
    end
    DK = fnval(sp, a);
%     if DK > KIc
%         disp (strcat(' FRACTURE at a=', num2str(a)))
%         break
%     end
    da = C * DK ^ n; % Crack growth in mm per cycle
    a = a + da; % Updated crack length [mm]
    a_vec(end + 1) = a; % Add to vector of crack lengths
    cycles(end + 1) = k; % Add to vector of cycles
    DK_vec(end + 1) = DK; % Add to vector of Delta K values
    k = k + 1;
end
% end the loop
toc:

save(saveFile, 'cycles', 'a_vec', 'DK_vec');
% plot new figure
h = figure();
plot(cycles, a_vec, 'LineWidth', 2)
cax = gca; % newplot returns handle of current axes
set(cax, 'FontName', 'Times', 'FontSize', 12)
xlabel(strcat('Number of cycles'), 'FontSize', 14, 'Fontname', 'Times');
ylabel('crack size \it{a} \rm[mm]', 'FontSize', 14, 'Fontname', 'Times');
title(titleName)
legend('Cycle-by-cycle evaluation', 'Location', 'NorthWest')
grid
print(h, '-dpng', pngName);
end

```

textReader.m

```
function [ nums ] = textReader(fileName)
%TEXTREADER read the SIF, Crack length data from txt file
% fileName: data file name

% textReader.m - The function used to read the input data from txt file.
% Authors: Da Wu (dawu@student.chalmers.se).
% June 2015, Department of Shipping and Marine Technology,
% Chalmers University of Technology.
% This file is part of the Master Thesis work:
% Consequence of cracks presence on ship structures.
% The codes are used for the evaluation of
% ship structure elements EDGE crack growth.

fileID = fopen(fileName, 'r');
C = textscan(fileID, '%', ...
    'Delimiter', ',', 'EmptyValue', -Inf);
fclose(fileID);
nums = [C{:}];
end
```